平成 29 年度博士学位論文

Highly sensitive terarylenes:

Synthesis, switching, and scanning tunneling microscopy studies

奈良先端科学技術大学院大学

物質創成科学研究科

Jan Patrick Dela Cruz Calupitan

Université de Toulouse

THESE

En vue de l'obtention du

DOCTORAT DE L'UNIVERSITÉ DE TOULOUSE

Délivré par *l'Université Toulouse III – Paul Sabatier*

Présentée et soutenue le 25 Janvier 2018

Jan Patrick Dela Cruz Calupitan

Térarylènes photo réactifs : Synthèse et études par microscopie à effet tunnel.

JURY

Eléna ISHOW	Professeur, Université de Nantes	Rapporteur
Michel SLIWA	Chargé de recherches, CNRS Lille	Rapporteur
Kenji MATSUDA	Professeur, Université de Kyoto	Examinateur
Hisao YANAGI	Professeur, NAIST	Examinateur
Eric BENOIST	Professeur, Université de Toulouse	Examinateur
Takuya NAKASHIMA	Professeur Associé, NAIST	invité
Gwénaël RAPENNE	Professeur, Université de Toulouse	Co-Directeur de thèse, invité
Tsuyoshi KAWAI	Professeur, NAIST	Directeur de thèse

Ecole doctorale et spécialité
SDM : Chimie moléculaire – CO 046
Unité de recherche
Centre d'Elaboration de Matériaux et d'Etudes Structurales CEMES-CNRS UPR 8011
Directeur de thèse
Professeur Tsuyoshi KAWAI
Co-directeur de thèse
Professeur Gwénaël RAPENNE

"...kapag nasabi na ang lahat ng masasabi, ang pinakamahalaga ay hindi masasabi."

(...when all things that can be said have already been said, the most significant is what cannot.)

Roque Ferriols, S.J.

para kay Nanay

Contents

Preface

Chemistry is a particular way of looking at the world. We understand phenomena in our everyday lives, i.e. the macroscale, by coming up with models consistent with the molecular level understanding of matter: intermolecular forces, bonding, reactivity, and many others.

It is powerful as it is flexible: depending on the phenomena, whether physical or chemical, one can choose at what level they may be explained. Physical changes? Fine with intermolecular forces. Chemical reactions? Let's look at the molecular orbitals, bonds broken, bonds made. It is powerful as it has depth and breadth: depending on the aspect one wants to explore, they may use different tools and perspectives from different subfields. Reaction is failing? Check the free energy of reactants and products or look at the substrate nucleophilicity. It is powerful as it has predictive power: depending on the properties/performance/process we want to observe in the macroscale, we intervene at the molecular level. Material is not performing well? Tweak a certain functional group or change how molecules rearrange in the solid material.

This is what lured me into the field. It amazes me how such esoteric ideas about atoms and molecules, invisible to the naked eye, could have such power to explain things all around us. What amazement and excitement I had, when, 4 months before starting my PhD, I learned that I could be working with a microscope so powerful it could image individual molecules. I could finally "see" atoms and molecules! Whereas before, I would content myself with looking at how my design of the molecule affects the macroscale, this work allowed me to directly address actual individual molecules.

This is an interdisciplinary work (which is an academic way of saying I covered many fields). Albeit touching on various topics of organic synthesis, photochemistry, and surface science, this study revolves around one theme: molecular design. Building upon previous molecular design principles, we synthesized compounds which we expected to perform in certain ways in bulk (in solution) and on a 2D surface and addressed them accordingly. It is thus my humble hope that this study could contribute to new engineering and molecular design principles not only in the macroscale but in the nanoscale as well.

I keep this perspective working in the field: chemistry is a certain way, one of the many possible ways, of making order out of this disordered world. In chemistry, we try to break things down to the molecular level to understand them—an act of deconstruction in the mind in order to construct something in the material world. Chemistry allows us to say something about the world, to see the world around us a certain way. The most valuable will still be left unsaid, but it is nonetheless important to say something explicitly, even just from a certain angle or perspective, even just a small slice of understanding.

It is with humility and honor that I am able to take part in this endeavor of attempting to speak about the world. With the same humility and honor am I amazed with the many questions chemistry continues to pose. This journey humbled me in showing me the kinds of questions I can answer. If that which is of most significance evades utterance, it is of great honor that I could speak of it, even just a tiny parcel of it.

J.P.D.C. Calupitan
Takayama, Ikoma, Nara, Japan
2 November 2017

Abstract

Photoswitching diarylethenes, and their terarylene derivatives, are promising for the next generation optoelectronic devices because of their excellent photochemical properties. To make them viable for miniaturized electronic devices, it is necessary to study this class of molecules at the single molecular level by scanning tunneling microscopy under ultra-high vacuum (UHV STM). This thesis has three parts: 1) development of terarylenes highly sensitive to switching; (2) their modification for STM studies; and 3) results of STM investigations.

To be studied at the single molecular level by STM, terarylenes with high switching sensitivity have been selected. These compounds display high quantum yields of up to 100 %. However, the cycloreversion reaction remains low so an alternative route, through a chain-reaction oxidative mechanism, has been sought. In the first part, we show that the efficiency and speed of this reaction may be controlled by attachment of aromatic groups on the reactive carbons. In the second part, we functionalized these molecules for STM studies by attaching *tert*-butyl and chloride groups. These substituents preserve their excellent photochemical and switching properties while *tert*-butyl groups show bright contrast in STM images, minimize aggregation of these molecules on the surface, and slightly decouple the molecule from the surface. The chlorine group has been introduced to direct their surface assembly on insulating substrates composed of crystalline NaCl bilayer previously grown over a metallic substrate.

In the third part, results of STM are presented. We developed a new bottom-up approach for forming reproducible nanoassemblies of the unmodified terarylene at 77 K. Meanwhile, at 5 K, the terarylene functionalized with *tert*-butyl groups present different forms on the Ag(111) surface. From the positioning of the high-contrast *tert*-butyl groups and with the aid of DFT calculations, we assign different conformations of the molecule on the surface. On NaCl/Ag(111), direct visualization of the occupied and unoccupied states could be achieved.

This illustrates that for these applications, molecules with appropriate properties can be interesting candidates for STM studies to obtain information at the single molecular level. Such molecules may be redesigned with a consideration of the surface as its mere presence may induce behavior previously unobserved or neglected if they were studied in solution. This thesis opens terarylenes to future applications which require a solid surface.

Résumé

Les diaryléthènes et leurs dérivés terrylènes sont prometteurs pour la prochaine génération de dispositifs optoélectroniques en raison de leurs excellentes propriétés photochimiques. Pour les rendre viables pour les appareils électroniques miniaturisés, il est nécessaire d'étudier cette classe de molécules au niveau unimoléculaire avec le microscope à tunnel sous vide ultra-élevé (UHV STM). Cette thèse comporte trois parties: 1) développement de terarylènes hautement sensibles à la commutation; (2) leur modification pour les études STM; et 3) les résultats de ces études STM.

Pour être étudié à l'échelle de la molécule unique par STM, des terarylènes ayant une sensibilité de commutation élevée ont été sélectionnés. Ces composés présentent des rendements quantiques élevés allant jusqu'à 100%. Cependant, la réaction de cycloréversion reste faible, de sorte qu'une voie alternative, grâce à un mécanisme oxydatif à réaction en chaîne, a été recherchée. Dans une première partie, nous montrons que l'efficacité et la vitesse de cette réaction peuvent être contrôlées par la fixation de groupes aromatiques sur les carbones réactifs. Dans la deuxième partie, nous avons fonctionnalisé ces molécules afin de les étudier par STM en introduisant des groupes tert-butyle et chlorure. Tout en préservant leurs excellentes propriétés photochimiques, les groupes *tert*-butyle présentent un excellent contraste lumineux dans les images STM, ils minimisent aussi l'agrégation de ces molécules sur la surface et découplent légèrement les molécules de la surface. Les atomes de chlore permettent de contrôler les assemblages moléculaires sur des substrats isolants de type bicouche de NaCl cristalline précédemment déposés sur un substrat métallique.

Dans la troisième partie, les résultats de STM sont présentés. Nous avons développé une nouvelle approche ascendante pour la formation reproductible de nano-assemblages du terarylène non modifié à 77 K. Quant au terarylène modifié par les groupes *tert*-butyle, il présente à 5 K sur une surface d'Ag (111) différentes formes qui, grâce à la position des groupes *tert*-butyles à contraste élevé et à l'aide de calculs DFT, ont pu être assignées comme étant différentes conformations de surface de la molécule. Sur NaCl / Ag (111), il a été possible de visualiser les états occupés et inoccupés de la molécule.

Cela illustre que, pour ces applications, des molécules avec des propriétés appropriées peuvent être des candidates intéressantes pour des études STM afin d'obtenir des informations sur leurs propriétés à l'échelle de la molécule unique. De telles molécules peuvent être optimisées pour tenir compte de la surface, car sa simple présence peut induire un comportement bien différent de celui obtenu en solution. Cette thèse ouvre les terarylènes à des applications futures nécessitant une surface solide.

Chapter 1

Introduction: Photoresponsive materials on surfaces

The fundamental understanding of light-matter interactions is one of the hallmarks of 20th century science. From Einstein's elucidation of the photoelectric effect[1] to Bohr's explication of line spectra by atomic energy levels,[2] the interaction between energy, in the form of photons, and matter at the atomic level led us to the foundations of quantum mechanics. From the resulting quantum molecular conception of atoms[3] originated our understanding of molecules: chemical bonding[4-5] and molecular orbital theory[6] led to more systematic studies on structure-property relationships and chemical reactions – the very foundations of chemistry. Modern understanding of matter was built upon atoms interacting with and reacting to light, so that when they are built into molecules, it is only natural that these more complex systems are explored with respect to how they interact with and react to light as well.

Whereas individual atoms may respond to light excitation by releasing heat, electrons, or photons, once held together in a molecule by chemical bonds, they present a new possible response: isomerization or rearrangement of such bonds.[7-8] The manipulation of chemical bonds by light is exciting especially in the context of nanosciences because it allows for macro-level control of molecular level properties; miniatiurization is an ultimate goal for next generation technologies.[9] Therefore, building upon foundations set by seminal early 20th century works on light-atom interactions that gave us a deeper understanding of the material world, pushing towards 21st century technologies demands the study and development of molecules that could be controlled and manipulated by light.

Of particular interest are photoswitching molecules having isomers with hugely different properties: light irradiation allows access to control properties at the molecular level. One family of compounds recognized for their excellent photoswitching properties is the diarylethenes and their derivative terarylenes. Upon exposure to photons of appropriate energy, these molecules switch between two stable states with large differences in their electronic structures. As molecular properties could be fine-tuned, they promise applications for miniaturized electronics such as molecular switches and optical memory devices.

Their macroscale properties in solution and in the solid state are rather well-understood, but given that a large aspect of these materials are focused on the molecular scale (both switching properties and possible applications are at the nanoscale), they must be studied at that level as well. Further, applications sought require that these molecules perform on two-dimensions (2D). For this, scanning tunneling microscopy (STM) under ultra-high vacuum conditions (UHV) provides a technique and a tool to access properties not when they are dissolved in solution nor when in the crystalline state but on a 2D surface from the nanoscale down to the single molecular level.

It is therefore in this context that this dissertation explores the design of new terarylenes with excellent switching properties and their studies at the nanoscale by STM.

This opening chapter will provide a brief review of photoresponsive molecules before focusing a discussion on a particular family, diarylethenes and their extension to terarylenes. Main structure-property relations will be highlighted, along with possible future applications. Then, the power of the

STM technique will be illustrated by outlining a brief history of its major technical and technological developments. The literature background will then end with a review of related works of STM done on diarylethenes/terarylenes. Proceeding from this background, we will specify specific areas of the field yet unexplored and therefore our attempts to contribute to those by stating the objectives and scope of the study.

1.1 Photoswitching molecular materials: from azobenzene to diarylethenes

Photoconversion lighted the way towards the isolation of the elusive *cis* isomer of azobenzene (Scheme 1.1). Gortner and Gortner reported in 1910 that during the preparation of azobenzene (hitherto synthesized and isolated as the *trans* isomer) from the reduction of azoxybenzene, a red liquid in small quantities consistently remained as a residue. In one instance, they succeeded to prepare a crystal from this red liquid and used it to seed other batches. This crystal was characterized as long thin needles, which melted at ~25 °C, and were more soluble in polar solvents than azobenzene. These were grossly different from the then-known properties of azobenzene (rectangular crystals, T_m = 68 °C, less soluble) but elemental analysis showed similar nitrogen content, leading them to interpret this as the isolation of the *cis* isomer of azobenzene. *Cis*-azobenzene had been predicted to be less stable and more polar, which conveniently explained the disparity in properties observed.[10] Four years later, Hartley and Stuart dismissed these crystals as mixed crystals: they showed that azobenzene and its precursor azoxybenzene can be immiscible in the solid state and provided phase diagrams showing that the melting point observed by Gortner and Gortner was a eutectic melting temperature for a solid mixture of these two compounds.[11]

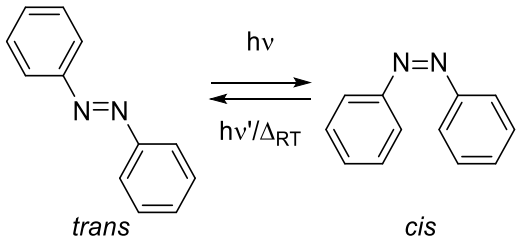

Scheme 1.1. *cis-trans* isomerism of azobenzene.

It took 23 more years before Hartley, realizing that the erratic solubility measurements of azobenzene could be due to the formation of an isomer, took advantage of these fluctuations upon light exposure to isolate and crystallize this second isomer. The changes in absorbance, increased solubility, and higher dipole moment upon crystallization of the same sample followed by recovery of original properties upon reillumination undoubtedly proved that the isomerization of *cis* to *trans* azobenzene could be induced by light.[12] After just one year, the photochemically-induced *trans-cis* isomerism of azobenzene was well-established and further studies on the thermal stability of the *cis* form started to come out.[13] Light therefore played a key role to access this rather unstable N=N bond of azobenzene that placed the aromatic rings in a *cis* conformation. Since then, further details into the photochemistry and switching mechanism of azobenzene were further elucidated.[14]

Over the decades, with the advent and commercialization of absorption spectrophotometers, the molecular property change seen most evidently upon *cis-trans* isomerization was the change in absorbance properties. Thus, azobenzene was considered to be one of the first *photochromic* molecules. The name comes from Greek: *φωτός* (photos) for light and *χρῶμα* (khrôma) for color which refer to reversible color changes exposed to light irradiation.

This access to molecular geometry (*cis* / *trans*) and molecular electronic properties (change in molecular orbitals and thus in color/absorbance spectra) is one of the main fronts of miniaturization, as dreamed by Feynman,[9] so that azobenzenes are now finding applications to control functional changes in nanoscale environments from biological[15] to smart material applications.[16]

Since then, other photochromic compounds started to emerge. Spiropyrans (Scheme 1.2a) were known since the 1900s and were shown to respond to heat stimulus by isomerization in the 1920s but only in 1952 was their photochromism established.[17-18] Different derivatives of fulgides synthesized in the 1960s-70s (Scheme 1.2b) had established thermal reactions but it was in 1981 when a derivative with reversible photochromism between two stable states was reported.[19]

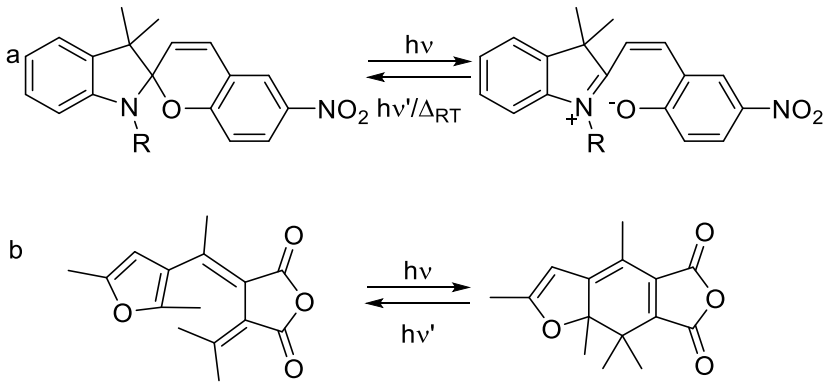

Scheme 1.2. Structure and photochromism of (a) spiropyrans and (b) fulgides.

1988 saw the first report on the synthesis and photochromism of diarylethenes.[20] In a recent review, Irie recounted how they designed 2,3-dimesitylbutadiene as a derivative of stilbene which could avoid H_2-elimination and phenanthrene formation upon cyclization (Scheme 1.3a). The synthesis failed due to steric hindrance on the mesitylene groups which led them to redesign their target compounds to harbor the smaller 2,3-dimethylthiophene instead. The synthesized compound did form the expected cyclization product upon UV light irradiation, but, in a serendipitous moment, the compound did not display thermal reversion but was found to be stable up to 100 °C; only illumination under visible light could switch the compound back to the original isomer (Scheme 1.3b).[21] From then, the synthesis and photochromism of these compounds expanded so that molecular design principles were established to improve the photoswitching properties.[21-22]

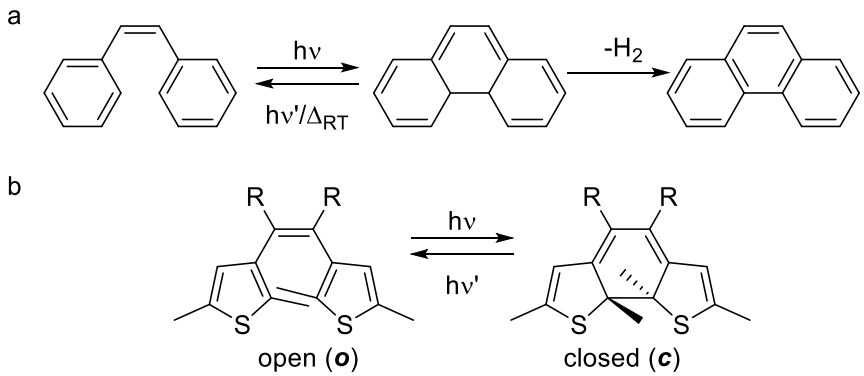

Scheme 1.3. a) Irie's initially attempted to prevent this irreversible H_2 elimination by synthesizing 2,3-dimesitylbutadiene. b) Synthesis failed due to steric hindrance so they replaced the compound with a smaller thiophene derivative which surprisingly did not show thermal reversion but could be reverted back by visible light instead.[20]

The name diarylethene is due to its structure having two aromatic rings connected by an ethene bridge (Scheme 1.3b). The label open (***o***) form comes from the central hexatriene moiety. In solution at ambient conditions, the single bonds of this hexatriene moiety may rotate so that no π-conjugation is present among the rings. The electronic structure of the ***o*** form is therefore determined by the electronic structure of these aromatic rings. Due to this, they absorb light in the UV but not in the visible region of the light spectrum resulting to clear transparent solutions. Upon photoexcitation with UV, the ***o*** form undergoes bond rearrangement to the closed (***c***) form, referring to the cyclized cyclohexadiene moiety of the compound. This central moiety presents the double bonds in a planar configuration so that the electronic structure is mainly influenced by π-conjugation. A band appears in the visible region, presenting a strong color when in solution. The ***c*** form was found to be thermally stable, with lifetimes in the scale of months, and only visible irradiation could turn it back to the ***o*** form.

The immense difference in electronic structures between the two isomers makes this class of compounds promising for molecular electronic devices.[21] In addition to these, diarylethenes satisfy requirements such as the thermal bistability of the ***c*** form, high sensitivities, fast reactions, high fatigue resistance, and reactivity in the solid state.[20-22] The stability of the ***c*** form is attributed to the low aromatic stabilization energy of aromatic rings in the ***o*** forms so that there is no driving force for the former to spontaneously revert back to the latter. Derivatives with aromatic rings having high aromatic stabilization energy such as phenyls and indoles simultaneously revert back to their ***o*** forms. Experimental measurements and theoretical calculations show that the photoreaction is completed in the scale of nanoseconds. The high sensitivities are attributed to the fact that due to this fast dynamics, most successful excitations result in successful reactions as long as the atoms and bonds concerned are within a certain distance.[20-22] Since their initial syntheses in 1988, several substitutions of and functionalizations around aromatic rings and the ethene bridge were reported for different purposes.[21-23]

1.2 Beyond diarylethenes: terarylenes

A higher level of complexity is achieved when the ethenyl bond is a part of another aromatic ring, so that three aromatic rings, each one contributing a double bond to the hexatriene moiety, are arranged in a triangular configuration. These class of compounds are thus called terarylenes. The first

of such compounds was reported in 2004 by Kawai *et al*. and was proposed as a molecular current rerouter.[24] Scheme 1.4 shows terarylenes **1.1**-**1.3** and their closed forms in which the two side-thiophene units are connected by an ethenyl bridge which is part of another thiophene unit. By showing that the ***c*** forms of these compounds have very similar adsorption bands in the visible region and that the ***o*** forms have λ_{max} red-shifting as the π-conjugation from **1.1** to **1.3** extended, they proved that the incorporation of the central thiophene ring presents different electronic paths for π electrons in the ***o*** and ***c*** forms, thus forming a molecular rerouter.[24] The incorporation of aromatic rings was then expanded to new terarylene derivatives which interestingly maintained high thermal stabilities of the ***c*** forms despite the increased loss of aromaticity (of three aromatic rings) upon cyclization. Some compounds displayed thermal stabilities in the scale of months and even years.[25]

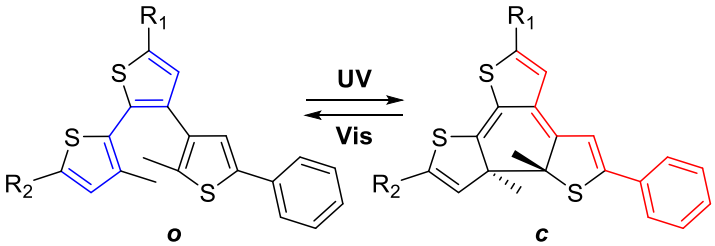

1.1: $R_1 = R_2 = H$
1.2: $R_1 = Ph$, $R_2 = H$
1.3: $R_1 = R_2 = Ph$

Scheme 1.4. Switching of π electron pathways in two isomers due to the incorporation of aromatic rings on the bridge.[24]

The effect of extending the π-conjugation to the central ring were investigated in subsequent works.[26-28] Further tuning of photocyclization quantum yield was shown to be possible by modulation of the highest occupied molecular orbital (HOMO) and lowest unoccupied molecular orbital (LUMO) in systems having push-pull systems such as thiophene in compound **1.4** (Scheme 1.5).[26] Both **1.4** and **1.5** also have thiazole groups which could present S and N to the side aryl rings to take part in H-bonding interactions that could control their geometric conformation (Scheme 1.5).[27] These compounds were also shown to preserve the reactivity of diarylethenes in the crystalline and amorphous states.[26,28]

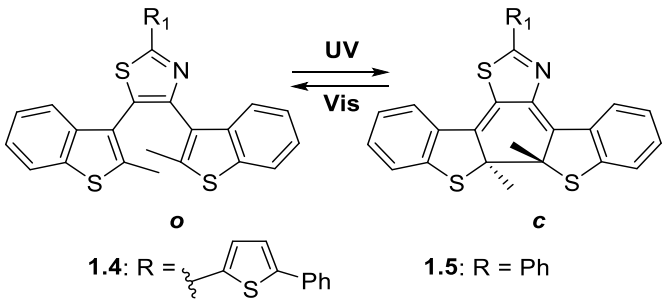

Scheme 1.5. Structure and photochromism of terarylenes derivatives having push-pull systems from ref. 26-27.

This aromatic central ring also allowed for more sites of functionalization whilst preserving the central moieties responsible for ***o-c*** photoisomerization. For example, in **1.6** where cationic aromatic moieties were functionalized on the central ring, light irradiation switches the π-conjugation structure so that the central moiety switches between imidazolium and imidazolinium (Scheme 1.6a).[29] This novel function allowed the switching of the ionic charge between a delocalized heteroaromatic imidazolium and a localized cationic N-C-N moiety in the imidazolinium ring. This essentially uses light to reversibly localize and delocalize charges down to the submolecular scale, i.e. inside aromatic rings. In a recent work on **1.7**, this functional switching was incorporated with a push-pull thienothiophene system. A greater level of complexity above that of the classical ***o-c*** switching (which was preserved) due to possible protonation, quaternization, and twist-turn switching on the central bridge was achieved (Scheme 1.6b).[30]

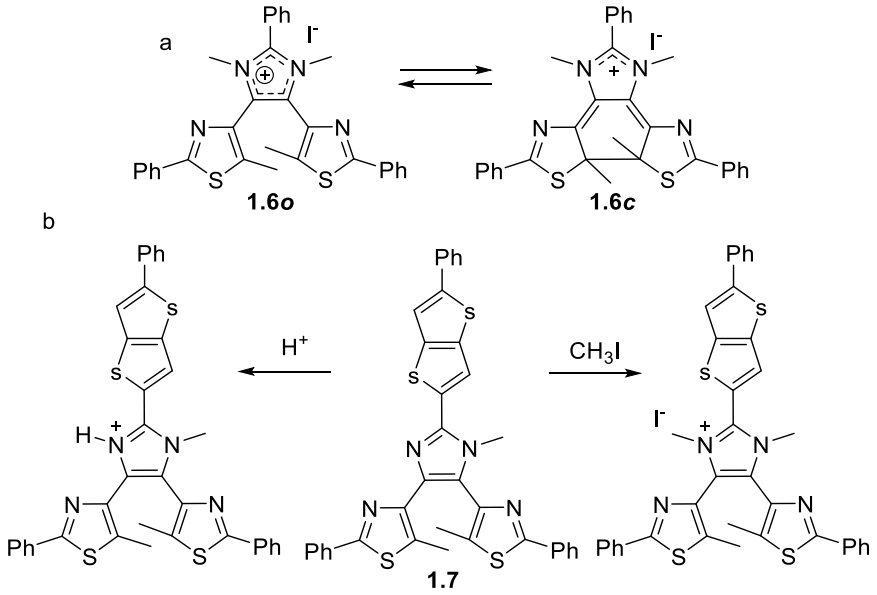

Scheme 1.6. a) Photochromism of **1.6** allowing control of localization of cationic charge[29] and b) functional modification of imidazole ring leading to central moieties whilst keeping the isomerizing unit.[30]

For some cases, fine tuning of photosensitivity was achieved by using the central aromatic ring to lock the side-chains in their reactive conformations.[31-34] In **1.8**, benzothiophene was used for the central ring flanked by thiazole rings so that S-N and N-H interactions were present as shown in Scheme 1.7. The photocyclization quantum yield was found to be 98 ± 2 % or almost photon-quantitative in hexane.[31] These studies were then expanded to other moieties for applications in polar solvents.[33-34] Elucidation of these intramolecular interactions and how the solvent affects them also led to compounds with photoreactivities which could be gated by solvents.[34]

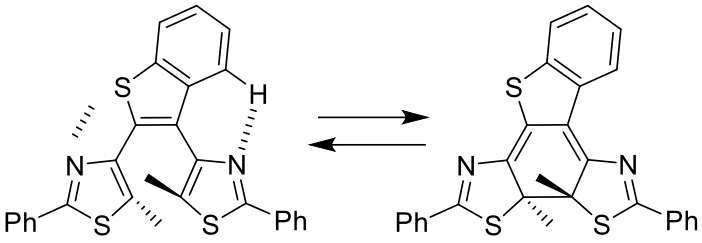

Scheme 1.7. Photochromism of **1.8** showing S-N and N-H interactions.[31]

The expansion of flat central rings also paved way toward subsequent release of organic species upon cyclization. In **1.9** which has proton and methoxy groups on their reactive carbons, the stability afforded due to the wide aromaticity made the photorelease of methanol thermodynamically favorable (Scheme 1.8a).[35-36] The high photocyclization quantum yields and the immense stability of the reaction product led the way to the development of efficient photoacid generators.[37-39] Further, with the understanding of intramolecular interactions between the central ring and side aromatic rings and how solvent systems could affect the relative strengths of these interactions, the design of compounds which could present different leaving groups was also achieved (Scheme 1.8b, **1.10**).[40]

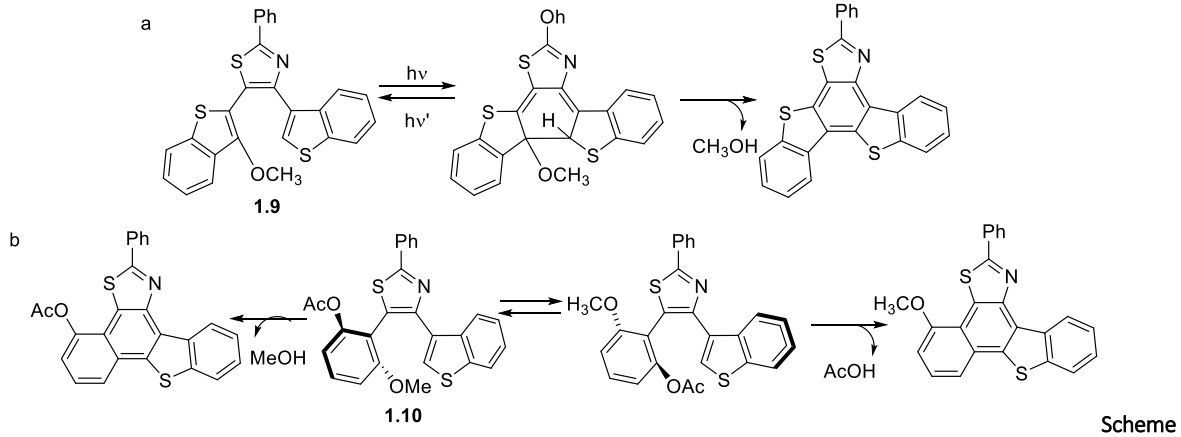

Scheme 1.8. a) The stability of the elimination product of **1.9**[35] led to photoacid generators and (b) selective release of organic fragments.[40]

Other than hydrogen bonding and atom-atom interactions, the additional aromatic ring also allowedπ-π interactions in extended derivatives with four or more 2-phenyl-thiazole derivatives for novel helical oligo-aromatic compounds.[41] With this, a new dimension—chirality—was added to these derivatives so that "folding-states" were observed[42] and functional switching of circularly polarized luminescence (CPL) was developed (Scheme 1.9).[43] The central ring could also be functionalized so that the open form is chiral. Due to steric effects upon cyclization, stereoselectivity of photoreaction could be observed.[44]

Lastly, the central aromatic ring also seems to play a major role for reactions of terarylenes in the cationic state. When oxidized to the cationic +1 state, the ***o*** and ***c*** form could spontaneously interconvert due to the thermal kinetic energy at room temperature. The equilibrium of this interconversion is highly dependent on the relative stabilities of the cationic states.[45] With an additional aromatic ring to stabilize the charge, the equilibrium was consistently against the side of the ***o*** forms so that efficient oxidative cycloreversion processes were developed for these compounds.[46] This equilibrium was further controlled on the side of the ***o*** forms so that the kinetics of oxidative cycloreversion could be improved 1000x and the efficiency 100x.[47] This will further be elucidated in Chapter 2.

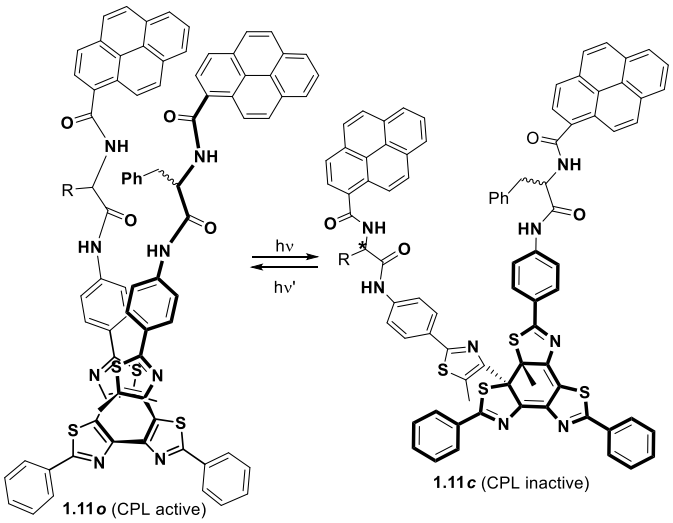

Scheme 1.9. CPL switching of **1.11**.[43]

1.3 Scanning tunneling microscopy (STM)

Rohrer and Binning first demonstrated electron tunneling in vacuum in 1981. They were able to isolate the system from mechanical vibrations which allowed for a very sensitive demonstration of the exponential dependence of tunneling current to the tip-surface distance (Figure 1.1a) under ultra high vacuum (UHV).[48] It was exactly this exponential dependence that made tunneling phenomena a highly sensitive imaging technique of surfaces in real space, without the need for indirect methods such as scattering and diffraction. They first showed that the technique can have lateral resolution of 1 nm and vertical resolution down to 0.2 Å in order to image monoatomic steps on the surface reconstruction of $CaIrSn_4$(111) and Au(111).[49] What captured the attention of the scientific community back then was the resolution of one the biggest problems in surface science that time, that of the Si(111) surface (Figure 1.1b), which hitherto was only investigated by indirect diffraction and theoretical methods.[50] In 1986, the power of the technique was asserted, when Rohrer and Binnig were awarded the Nobel Prize in Physics for their work which started only 5 years prior.[51]

STM paved the way for the first observation of molecules in real space. Until then, it was used to study surfaces but in 1988 Ohtani and co-workers imaged the first molecules, assemblies of benzene on Rh(111), under UHV (Figure 1.1c). For the first time, the threefold symmetry of benzene was seen in

real space.[52] This was then followed by manipulation of single molecules: Foster, Frommer, and Arnett showed direct evidence of the STM tip being able to move, pin, and effect chemical transformations on individual molecules.[53] In the same year, Foster and Frommer showed that an interface between a solid substrate and a liquid crystal, could also support electron tunneling and thus imaging of molecular assemblies (Figure 1.1d).[54] This was followed by imaging not under UHV but at the so-called solid-liquid interface of other liquid crystals[55-56] and assemblies of hydrocarbons.[57-58]

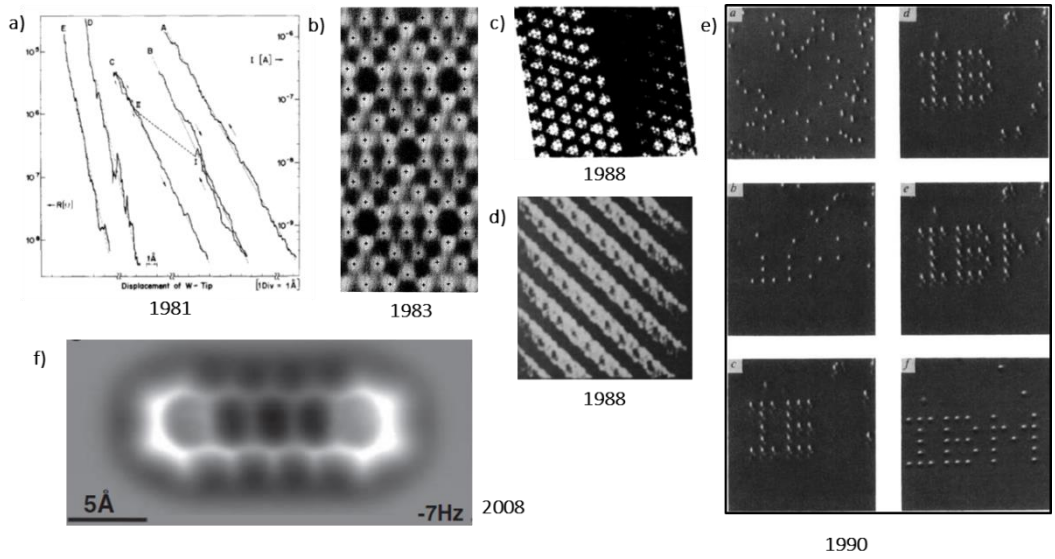

Figure 1.1. A brief history of STM in images. a) The exponential dependence of tunneling current vs tip-surface distance is the basis of why STM is such a powerful imaging technique, b) allowing it to solve the most enigmatic problems of surface science of the time: the atomic structure of the Si (7 x 7) reconstruction. c) The technique was then developed to image not only surfaces but also molecules under UHV and d) liquid crystals on the solid-liquid interface. e) One of the most iconic images of nanotechnology is the logo of IBM written by atomic manipulation. f) Years later, submolecular resolution was reached to image bonds and atoms in a pentacene molecule by functionalization of the tip by CO. Images for a, b, c, d, e, f, are lifted from references 48, 50, 52, 54, 59, and 60, respectively.

STM was hailed as one of the most important tools for nanotechnology when, in 1990, Eigler showed the incredible power of STM to manipulate the most fundamental units of matter. Equipped with an STM in the IBM labs in California, he showed that individual xenon atoms could be picked up and moved on top of a nickel surface, spelling their company acronym on the scale of nanometers, to produce one of the most iconic photos of nanotechnology.[59] (Figure 1.1e)

The next summit was reached in 2009 with the development of tip functionalization technique to image molecules with submolecular resolution (Figure 1.1f). The tunneling current, and thus the images, are highly dependent on the electronic and geometric structure of the tip. Even the sharpest tips would have several hundred metallic atoms on its apex. By functionalizing the tip with CO molecules, the electronic structure was "determined" and the tip was ensured to have one and only one atom on its apex so that bonds between individual carbon atoms in pentacene and HOMO-LUMO states could be "imaged". [60] For the first time, atoms within molecules could be "seen".[61] The origin of contrast remained a controversy at first but the technique resulted in remarkable advancements to resolve the structure of natural compounds, intermolecular interactions, reversible bond formations;[62]

submolecular monitoring of bond breaking and formation in chemical reactions;[62-63] and even the synthesis of the elusive triangulene.[64]

STM is a powerful tool to image not only surfaces but atoms and molecules as well. The STM tip could be useful for mechanical (pushing, stretching, etc.) and chemical manipulations. Thus, STM developed not only as a tool but as a field in surface science, solid state chemistry, and nanotechnology, so much so that the first nanocar race was held in 2017 not only to promote the field to the general public but advance it as well.[65]

1.4 STM studies on diarylethenes/terarylenes

With the promise of photoswitching diarylethenes/terarylenes for applications to miniaturized electronics such as molecular switches and memory, several groups started to study the interactions of diarylethenes with a solid surface, which is a requirement for the said applications. The past ten years saw studies either at the single molecular level or at the scale of supramolecular assemblies in the solid-liquid interface, ambient conditions, and UHV.

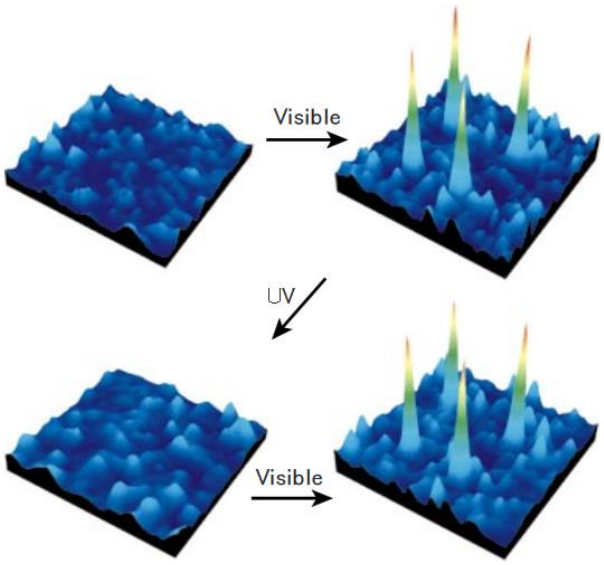

Figure 1.2. Switching of a fluorescent diarylethene derivative under fluorescence microscopy. From ref. 66.

Diarylethenes were first observed at the single molecular level by fluorescence microscopy. A derivative functionalized with a fluorescence unit, whose fluorescence intensity is reversibly quenched following the reversible isomerization of the ***o*** and ***c*** forms (Figure 1.2).[66] Years later, diarylethenes without fluorescence units were observed to undergo uncontrolled switching under the STM.[67-68] Thereafter, the difference in conductance between open and closed forms led to studies on using these molecules as switches in conductance switching experiments.[69-70] These studies cemented their promise for next generation molecular electronics and memories as it was shown that they could be addressed, i.e. “written” and “read”, at the single molecular level.

In this part, we will review STM studies on diarylethenes/terarylenes in the past decade. This section is divided into three parts: diarylethenes imaged by STM in the solid-liquid interface;

diarylethenes imaged under ultra-high vacuum conditions and self-assembled monolayers of diarylethenes/terarylenes studied by STM under ambient conditions.

1.4.1 Diarylethenes in the solid-liquid interface. As demonstrated by Rabe and Buchholz in a seminal paper in 1991,[58] the adsorption-desorption process on the solid-liquid interface as probed by STM may give insight on the strength of surface-molecule and molecule-molecule interactions due to the high molecular resolution of images. Even if the surface interface has one fewer dimension than the (3D) bulk or solution phase in which intermolecular forces of attraction are fairly well-understood, the mere existence of the surface could affect, disrupt, or reinforce such interactions.[71-72]

Since the bistable isomerization diarylethenes is the root of their promise for molecular electronics, which in itself requires an understanding of surface interactions,[21-23] a further understanding of how this dynamics affects molecule-molecule and surface-molecule interactions is also important. Matsuda *et al*. first reported a study of diarylethene derivatives (Figure 1.3a) self-assembled and imaged by STM on the interface between highly-oriented pyrolytic graphite (HOPG) and liquid solvents.[73] Compounds **1.13** and **1.14** were both designed for such studies. The pyrene moiety was expected to interact with HOPG by π-π interactions to stabilize the 2D assembly while long alkyl chains were designed to allow for flexibility. This flexible chain could have interactions with the octanoic acid solvent so that there were competing driving forces for the equilibrium between molecules in solution and those adsorbed on the surface by π-π interactions. Both ***o*** and ***c*** forms of compound **1.13** assembled neatly on the surface with those of the ***o*** form having unit cell parameters similar to those in the crystalline phase. In the ***o*** forms, the pyrene unit was found to be parallel to the surface, satisfying the hypothesis that these could interact with the surface while in the ***c*** forms, the pyrene units were found to be perpendicular to the surface and parallel to the photoswitching unit (Figure 1.3b). The destabilization from loss of the pyrene-HOPG interaction seemed to be offset by π-π interactions in the denser of the core of the ***c*** forms. When an assembly of ***o*** forms were illuminated by UV *in situ*, the assembly disappeared which were interpreted to mean two things: (1) photocyclization happened in solution and (2) the existence of ***c*** forms seemed to disrupt the assembly of ***o*** forms by interfering with the adsorption-desorption process of the ***o*** forms.

Meanwhile, the assembly of ***o-o*** and ***c-c*** forms (in which both of the two diarylethene moieties are in the ***o*** and ***c*** forms respectively) of **1.14** also showed long-range order but in this case the images and molecular mechanics calculations showed that in both forms, the pyrene moieties are always parallel to the surface with the alkyl chain allowing for rotation (Figure 1.3c). π-π stacking between pyrene and HOPG seemed to be the stronger interactions that stabilized 2D assemblies. It is noteworthy that illumination of the ***o-o*** assemblies *in situ* did not lead to its disappearance as in **1.13**, but instead, the ***c-c*** assembly was formed. Subsequent illumination of the ***c-c*** assemblies for about 10 minutes formed the ***o-o*** assemblies.[73]

Matsuda and his team remarked that the alkyl chains could also help in the stabilization of the 2D networks as a derivative sans alkyl chain did not form assemblies. However, it seemed to be insufficient for such stabilization as the assembly of **1.13*o*** was destabilized in the presence of **1.13*c***.[73] This was further confirmed in a subsequent study of diarylethene derivatives **1.15**-**1.17** (Figure 1.3d) on an HOPG-octanoic acid interface. Only **1.15** was found to form assemblies (Figure 1.3e). The methyl groups in **1.16** seemed to disrupt effective tethering on the surface by steric effects while the absence of the amide groups in **1.17** made van der Waals interactions the sole intermolecular forces which could have stabilized the assemblies. Both H-bonding interactions and van der Waals interactions were

necessary to stabilize the assemblies of **1.15**, which placed the alkyl chains in the same direction so that **1.15** adopted a non-reactive conformation on the surface. Upon *in situ* UV irradiation for 5 min, the assemblies disappeared as in **1.13** which implies that this parallel conformation, absent in the geometry of the ***c*** form, was an important stabilizing force for the assemblies. This also implied that photocyclization happened in the liquid phase where the molecule had freedom to adopt the reactive anti-parallel conformation. The assembly could be reversibly formed upon subsequent visible light irradiation at the same time scale. Another implication of photocyclization/cycloreversion happening in the liquid phase is that illumination to produce either ***o*** or ***c*** isomer was in the minutes timescale similar to usual photochemical measurements in solutions. [74]

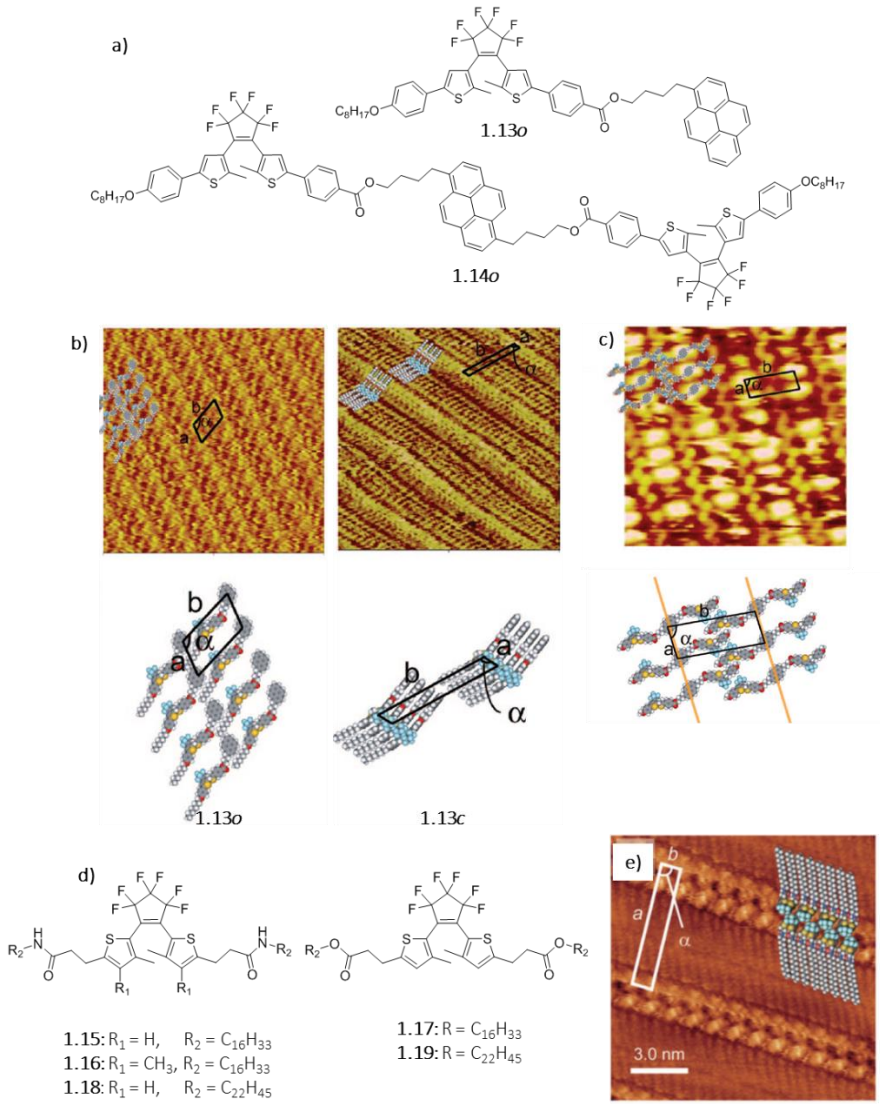

Figure 1.3. a) Structures of **1.13** and **1.14**. b) STM images of open and closed forms of **1.13** (***o***, ***c*** respectively). For **1.13*o***, the stacking parameters are: *a* = 1.4 ± 0.1 nm, *b* = 2.6 ± 0.1 nm, α = 115 ± 2°. For **1.13*c***, the stacking parameters are: *a* = 0.5 ± 0.04 nm, *b* = 4.9 ± 0.1 nm, α = 109 ± 6°. Both images have sizes 50 x 50 nm^2. c) 25 x 25 nm^2 image of assemblies of **1.14*o*-*o***, *a* = 2.4 ± 0.2 nm, *b* = 6.3 ± 0.2 nm, α = 87 ± 2°. Data and images for b-c are from reference 73. d) Structures of compounds **1.15**-**1.19**. e) STM images of **1.15**, *a* = 6.3 ± 0.2 nm, *b* = 1.04 ± 0.04 nm, α = 88.6 ± 0.9° from ref. 74.

These findings were further expanded to more derivatives of **1.15** and **1.17** having various alkyl chain lengths on HOPG-octanoic acid interface.[75] By showing that the critical concentration for full surface coverage decreases as alkyl chain length increases, Matsuda's team illustrated that these alkyl chains also contribute to the stabilization of the 2D assemblies, albeit not as strong as H-bonding. (For brevity, we just showed the derivatives having 22 carbon chains **1.18** and **1.19**, see Figure 1.3d.) Full surface coverage, i.e. an equilibrium between molecules in solution and those adsorbed on the surface, were assumed to be achieved within the timescale of STM experiments (5 mins). This timescale were similarly assumed for other studies. Alkyl chain lengths of up to 22 carbon atoms were necessary for the derivative without amide groups, **1.19**, to form assemblies, and even then, a critical concentration of 25 times higher than that of **1.18** was necessary for full surface coverage. The closed form of **1.18** also formed assemblies in which the alkyl chains are pointing to opposite directions in contrast to that of the ***o*** forms. By looking at the concentration dependence of surface coverage, Matsuda *et al.* remarked that the nucleation process for **1.18*c*** assemblies was more thermodynamically favorable than that of the ***o*** form.[75]

In ***c*** forms which force the alkyl chains in an anti-parallel direction, the photochromic core seems to contribute to the stabilization of the 2D networks. This was demonstrated in a subsequent work on comparison between compound **1.20** (Figure 1.4a) and **1.15**. STM showed that the ***c*** forms of **1.20** formed new assemblies upon UV irradiation unlike that of the case of **1.15** in ref. 74. Molecular mechanics simulations showed that in **1.20*c***, the photochromic core has more contact with the surface than that of **1.15*c***. With the large sulfur atoms presented to the surface, the planar photochromic core could interact with the surface more and contribute to the stabilization of the assemblies.[76]

Switching applications depend on reliable isomerization between ***o*-*c*** forms so that fatigue resistance, consecutive switching without significant loss of function due to side reactions, is also an important consideration. The general degradation reaction for diarylethenes is shown on Scheme 1.10. Prolonged exposure of the ***c*** form could lead to the irreversible formation of the annulated form.[20-23] This was first observed by STM for compound **1.21** (Figure 1.5a).[77] STM imaging of the as-synthesized ***o*** form of **1.21** showed ordering labelled as α which was stabilized by van der Waals and H-bonding interaction similar to other studies.[73-76] The phenyl rings seemed to make the alkyl chains point to anti-parallel directions so that the photochromic core is in the reactive conformation. Deposition of the ***c*** form resulted in a different ordering labelled as β. When a solution of ***o*** was illuminated overnight, both ***o***, ***c***, and annulated isomer were formed. The annulated isomer was then isolated by HPLC and then imaged by STM at the HOPG-octanoic acid interface (Figure 1.5d).[77]

a)

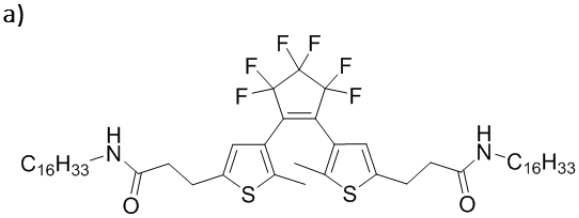

1.20

b)

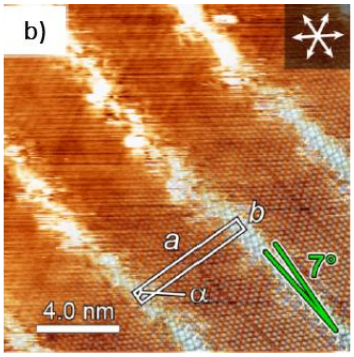

Figure 1.4. a) Structure of **1.20**. b) STM images of **1.20*c*** : a = 5.65 ± 0.0.03 nm, b = 0.52 ± 0.03 nm, α = 89 ± 1°. From ref. 76.

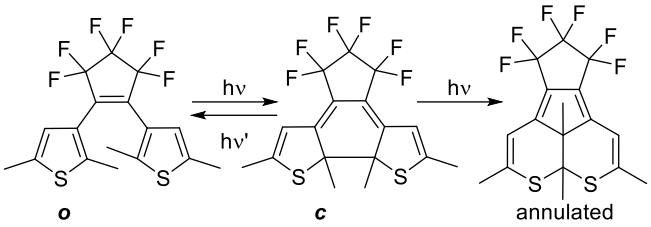

o ***c***

Scheme 1.10. Formation of annulated isomer.

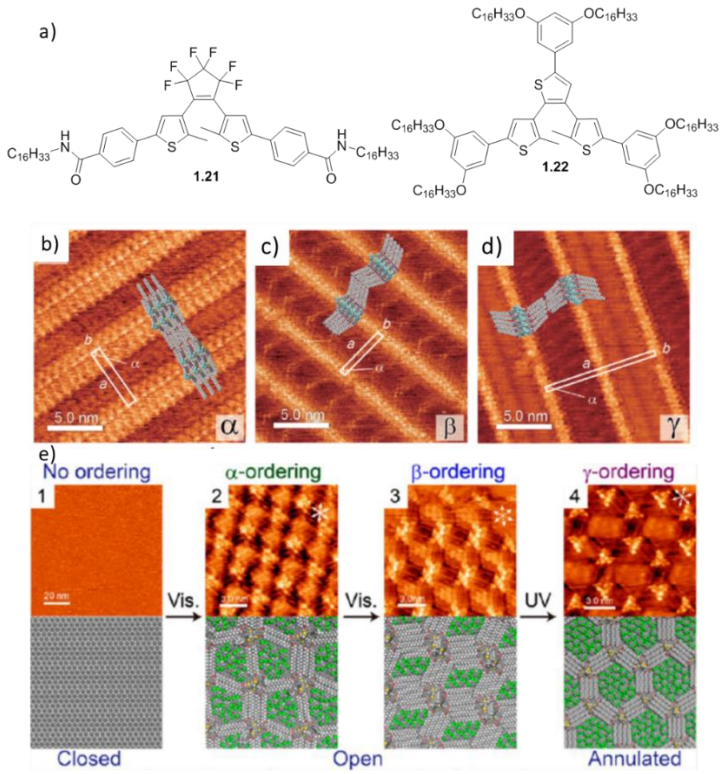

Figure1.5. a) Structures of **1.21** and **1.22**. b-d) assemblies of the ***o***, ***c***, and annulated form of **1.21**. Packing parameters for b) a = 5.71 nm, b = 0.89 nm, α = 88°; c) a = 4.82 nm, b = 0.56 nm, α = 85°; d) a = 10.2 nm, b = 0.48 nm, α = 87°; data from ref. 77. e) Four state switching of compound **1.22** from the ***c*** form, two concentration-dependent orderings of the ***o*** forms, and that of the annulated form. From ref. 81.

A subsequent report showed that the annulated isomer has a high affinity to the surface, so that it could disproportionately dominate STM images even if it was produced in small quantities only. By a careful examination of the effect of ***c*** concentration to the assembly formation of ***o***, they showed that the former could increase the cooperativity for the assembly of the latter.[78] Another report showed (by molecular mechanics calculations) that the annulated isomer has a denser packing than that of the ***c*** form, which explains its strong surface adsorption and disproportionate dominance on STM images.[79] The irreversibility of the annulated form could make it an unwanted side-reaction from the viewpoints of rewritable optical memories or switches but it could be useful for permanent memories (non-rewritable or write-once memories) similar to applications sought for diarylethenes with very low cycloreversion quantum yields.[80] In a subsequent report, Matsuda's team found that the ***o*** form of **1.22** (Figure 1.5a) can have two packing patterns depending on the concentration of the solution. Together with the ***c*** form and the annulated isomer formed by UV-illumination in a timescale

of 10-30 minutes,[77] these four possible orderings were developed to show four states under the STM as shown in Figure 1.5e.[81]

Finally, the solid-liquid interface also afforded a medium to resolve the chiral isomers of the ***c*** forms (Scheme 1.11). Whereas in bulk solution, they are indistinguishable as they both have the same photophysical and switching properties, STM affords molecular-level resolution and a 2D plane that could resolve these two isomers. The 2D plane lacks some symmetry elements so that molecules which are achiral in 3D (in solution, crystal, or gas phase) could (1) be chiral on the surface or (2) make the resolution of enantiomeric forms easier.[82-83] This was shown for the closed form of **1.15**. STM imaging of the previously synthesized and separated ***c*** forms of **1.15** showed domains which have bright lines rotated either +7° or -7° relative to the main axis of the graphitic surface, which is a clear indication of the chirality of the assemblies (Figure 1.8).[84]

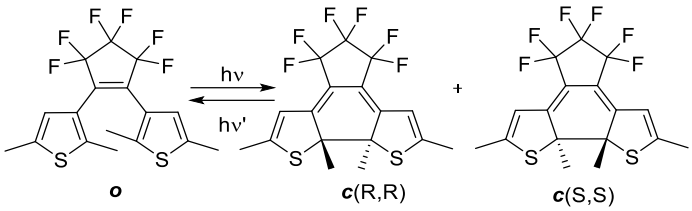

Scheme 1.11. Photoconversion of diarylethene showing the chiral isomers of the ***c*** forms.

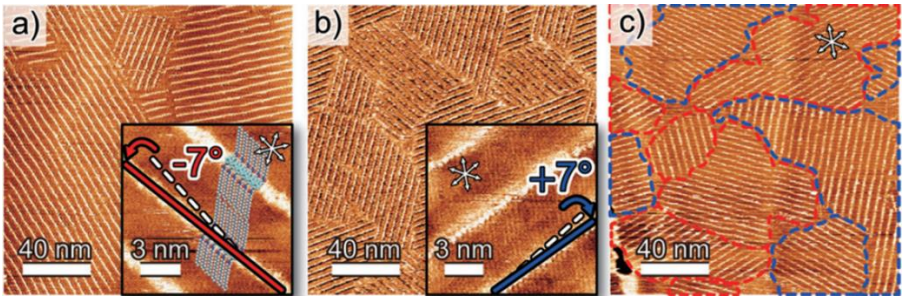

Figure 1.6. STM images of the (a) (R,R) isomer, (b) (S,S) isomer, and a (c) racemic mixture of **1.15*c***. Adapted from ref. 84.

1.4.2 Diarylethenes under UHV. As shown above, STM on the solid-liquid interface provides significant insight about surface-molecule and molecule-molecule interactions. The images are a result of a dynamic equilibrium between adsorption-desorption of molecules on the surface. If surface-molecule interactions are weak, the desorption process is favored and no ordered assemblies on the surface may be observed as all of them are in the liquid phase. Multi-component assemblies could also compete for assembly formation on the surface. Species with low concentrations with respect to the bulk could seem to have a significant concentration if they could be observed on STM images, i.e. if they have strong interactions with the surface as seen in the annulated forms.

To extend studies in the solid-liquid interface, STM studies of molecules without a solvent, under UHV conditions are also important. The UHV also ensures the absence of contamination and could potentially improve the contrast of STM images.

Initial STM studies of diarylethenes under UHV involved the deposition either of the as-synthesized ***o*** forms or a pre-irradiated mixture that contains ***o*** and ***c*** forms. Deposition of a solution of **1.23*o*** and ***c*** (Figure 1.7a) did result in the observation of two forms (Figure 1.7b) on Si(001), which, with the aid of calculations, could be assigned to their respective forms (Figure 1.7b and 1.7c). They proposed a possible scenario in which the adsorption configuration is heavily influenced by the surface through the formation of a Si-S bond that forces the two thiophene rings in different configurations.[85] Meanwhile, adsorption of **1.24*o*** led to the observation of the reactive anti-parallel conformation and of the compound (Figure 1.7). It seems that the molecule has high enough interactions with the reactive Cu(111) surface so that long alkyl chains like those of previous works in the solid-liquid interface were not necessary anymore. Indeed, the adsorption of the molecule on Cu(111) causes the appearance of standing waves which are indicative of the formation of a copper complex. Calculations and analyses showed that these are due to interactions between the cyclopentene moiety and a Cu atom on the surface. They were strong enough for charge transfer between the metal and the ethenyl bond that effectively quenched the switching; this was shown by analyses of the images, calculations, and electrochemical experiments.[86]

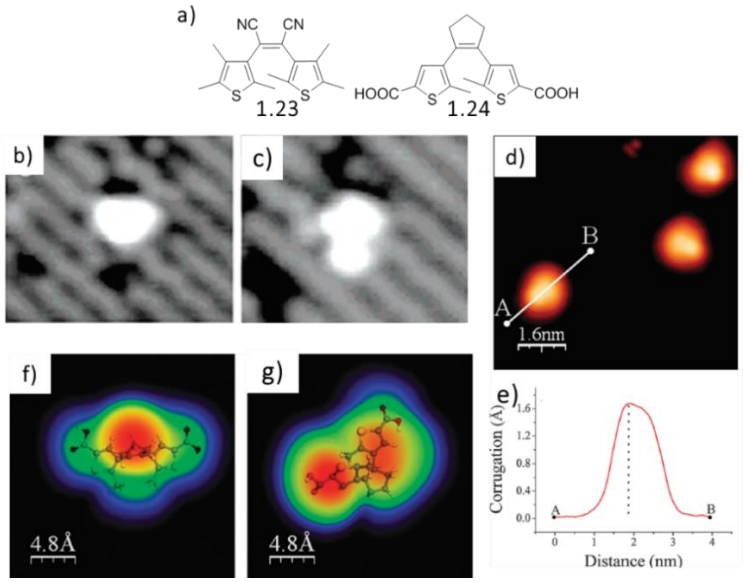

Figure 1.7. a) Structure of **1.23** and **1.24**. b) and c) are STM images of the ***o*** and ***c*** forms of **1.23** from ref. 85. d) Deposition of **1.24** results an assymetric one which is highlighted by the line scan in (e). By ESQC calculations on the parallel (f) and anti-parallel (g) conformation of **1.24**, the experimental images were assigned to the anti-parallel conformation.

Charge transfer between the surface and molecules is also important in the context of bistable compounds because the equilibrium and potential energy curve between the ***o*** and ***c*** in their charged radical states could be drastically different from those of the neutral states.[46-47] Kim's group clearly demonstrated this when they showed that the ***c*** form is more stable than the ***o*** form in STM studies of **1.25** (Figure 1.8a) on metallic surfaces. Deposition and subsequent imaging of the as-synthesized ***o*** forms resulted in the observation of both ***o*** and ***c*** forms, seen as extended and triangular lobes respectively, on Cu(111) at room temperature (Figure 1.8b). Subsequent annealing to 80 ^{o}C converted the remaining ***o*** forms to the ***c*** forms, which indicates that a rather low kinetic barrier separates the

two so that some ***o*** were converted to the ***c*** forms. Upon thermal activation the more stable ***c*** isomer is formed (Figure 1.8b,c). Although evidence pointed to strong charge transfer interactions on Cu(111), similar observation of stability reversal was also found in the more intert Au(111). [87]

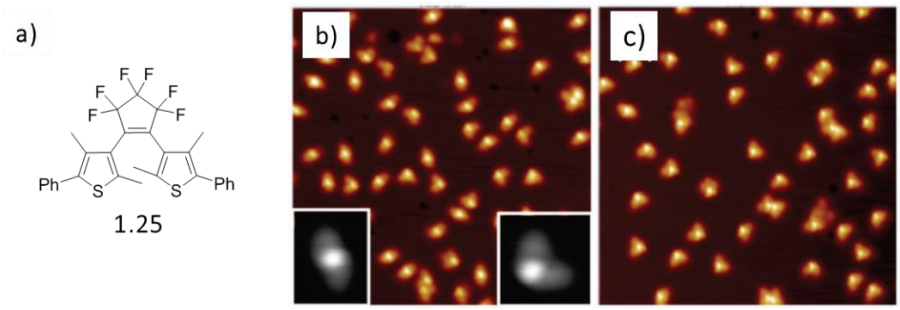

Figure 1.8. a) Structure of **1.25**. (b)Deposition of **1.25** on Cu(111) showed two shapes corresponding to the ***o*** and ***c*** forms (c) which transformed to 100 % ***c*** forms upon heating. From ref. 87.

Kim's group also reported on using ion-dipole interactions to assemble diarylethenes on the surface even under UHV. As there are no solvents involved, deposition of molecules on the substrates usually proceeds by sublimating them from a Knudsen cell directly on a path to the substrate. As these are all in the gas phase, no condensed phase could serve as the medium for the molecules to interact. Kim's group however showed that by co-depositing NaCl on a substrate held at 5 K, which could easily nucleate on the surface with a diarylethene having a perfluorocyclopentene core, the ions could interact with the F atoms to form assemblies. The molecule was calculated to have a high dipole moment (5.83 D) to interact with NaCl and deposit as assemblies on Cu(111).[88]

Only one group so far succeeded to use the STM tip to switch diarylethene molecules adsorbed on a surface using the STM tip under UHV. In a 2015 report, Franke and co-workers investigated the diarylethene **1.26** whose structure is shown on Figure 1.9a. **1.26** was found to form assemblies on surfaces due to strong hydrogen bonds between the aryl protons neighboring F and N from cyclopentafluoro and pyridine moieties of neighboring compounds (Figure 1.9b). Contrary to previous studies, these were performed on the more inert Ag(111) surface. They observed switching upon application of bias pulses >1.5 V as evidenced by a subtle change in contrast in one of the spots (Figure 1.9c-d). There is only a small difference in geometry between the open and closed forms but the change in contrast is evidence of a considerable change in the electronic structure.[89] It is well-known that in solution the ***c*** forms have a lower HOMO-LUMO gap than the ***o*** form. This is the fundamental basis for the promise of diarylethenes for molecular electronics applications.[20-23] Under UHV, this was illustrated with the change in scanning tunneling spectra with a lowering of resonance in the region above the Fermi level (Figure 1.9e-f).[89] By a combination of DFT calculations and analyses of STM spectra, they showed that the closing reaction is induced by hot electrons from the tip, so that the ***c*** form observed is actually the thermal disrotatory *cis*-product instead of the photochemical conrotatory product[89] in accordance with Woodward-Hoffman rules.[90]

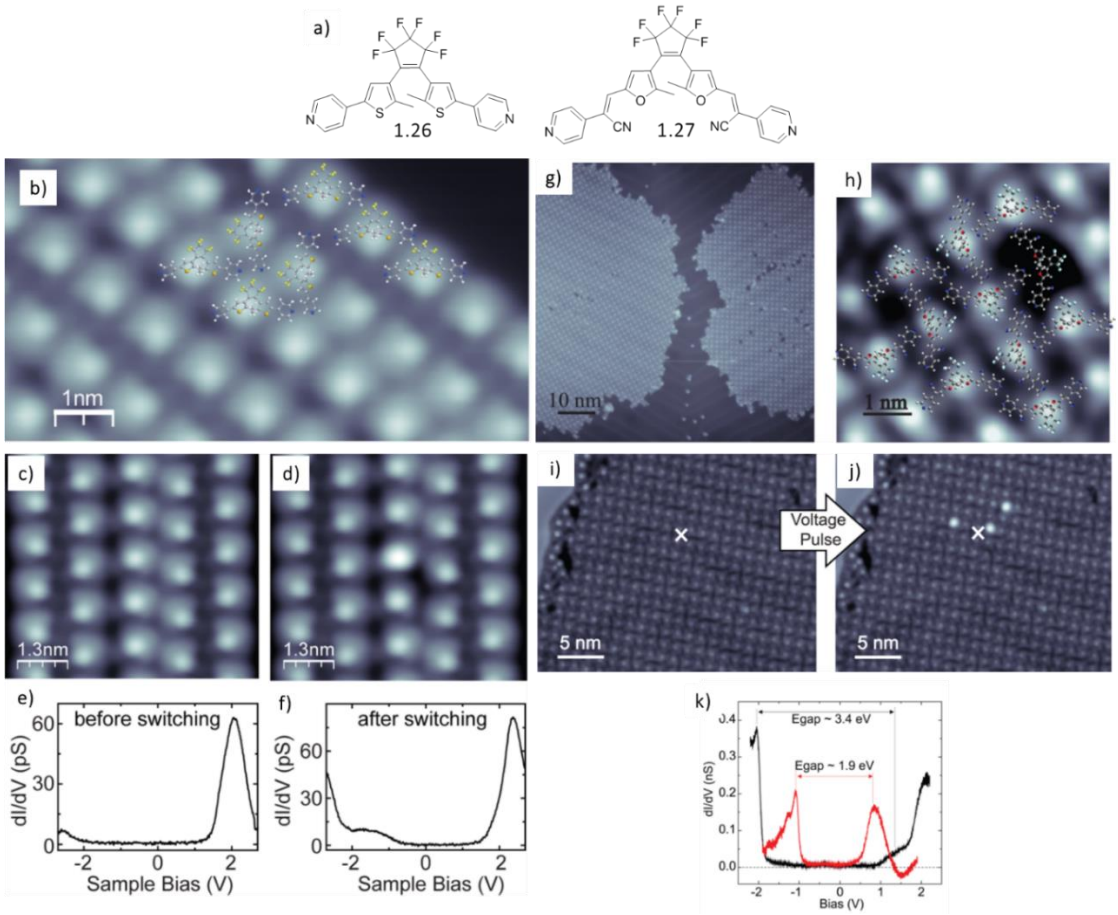

Figure 1.9. a) Structure of 1.26 and 1.27. (b)Deposition of 1.26 showed assemblies of the compound stabilized by H-bonding interactions. c) and d) show the same area before and after a switch-inducing bias pulse was applied. e) and f) show STS spectra before and after the switching event. Data from ref. 89. g) and h) show large-scale and zoom-in images on assemblies of 1.27. A higher contrast was seen upon switching (i and j). k) STS spectrum of the unswitched (dark) and switched (red) molecules. Data from ref. 91.

This was followed by a second study on compound **1.27**, (Figure 1.9a) intentionally devoid of any sulfur heteroatom to prevent strong interactions with the surface.[91] The compound similarly assembled on the Au(111). They did observe a stronger difference in contrast between ***o*** and ***c*** forms, performed conductance switching experiments, and imaged dI/dV maps (Figure 1.9i-j, k).[91] In a subsequent report on the same compound, the authors showed that the switching could be induced by the electric field between tip and surface as well.[92] It seems that the more inert Au or Ag surfaces are more suited for successful switching by the STM tip. Meanwhile, if strong interactions with the surface were desired, the Cu(111) surface were more suitable.

1.4.3 Diarylethenes/Terarylenes in SAMS. As cited above, initial STM studies on uncontrolled switching of diarylethenes were done on their self-assembled monolayers under ambient conditions.[67-68] van Wees first compared the number of molecules in the ***o*** and ***c*** forms before and after illumination.[67] They did not have a molecular level control of switching individual molecules. Dumas and co-workers on the other hand noted some diarylethenes "flickering" (i.e. displaying uncontrolled switching) when

imaged. [68] In a later report, van Wees and co-workers followed up on measuring the conductance of the compounds before and after reversible switching by light. [70]

For terarylenes, only one team reported two studies on STM of SAMs of **1.28** (Figure 1.10a). The switching unit was a terthiazole derivative previously functionalized with a long alkyl chain terminated by a thiol group to anchor the molecule on the Au surface.[93-94] In a preliminary letter, Lacaze and co-workers showed that the ***o*** and ***c*** forms could be distinguished on the Au surface by a subtle difference in contrast of the STM images and more compact packing parameters for the ***c*** forms (Figure 1.10b).[93] This was followed by a full paper on the switching between the two isomers by the STM tip and by light.[94]

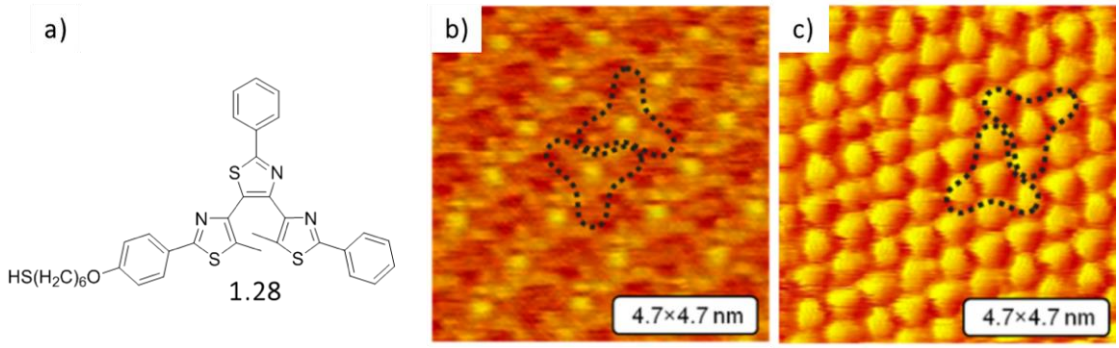

Figure 1.0. a) Structure of **1.28**. Self-assemblies of the b) ***o*** form and the c) ***c*** forms. From ref. 94.

1.5 Objectives and scope of the thesis

This chapter has thus reviewed significant advances on STM studies on diarylethenes containing an ethene bridge in their central hexatriene structure.[73-80, 84-89, 91-92] Given the significant opportunities for molecular design and functional tuning of properties afforded by the extra aromatic ring in terarylenes[24-43], it is imperative that their surface properties be elucidated by STM as well. In fact, most studies in the solid-liquid interface that elucidated molecule-molecule and surface-molecule interactions utilized the non-functional perfluoro head on top of the photochromic core which usually does not interact with the surface in a way that would show contrast in the STM images.[73-80] When Matsuda's team used a terarylene derivative having 2-phenylthiophene moieties instead of perfluorocyclopentene, they were able to develop switching involving four states beyond the usual photochromic switching of the compound (Figure 1.5).[81] Under UHV, the strong dipole of perfluorocyclopentene group was shown to aid in assembly formation[88] but the electronic switching remained mainly dependent on the rearrangement around the aromatic rings.[91-92] Only two studies from one team reported on the STM of self-assembled monolayers of terarylene under ambient conditions.[91-92] Nevertheless, as the 2D solid surface could induce new phenomena previously unobserved in solution or in the solid state,[71-72] breakthroughs were uncovered such as chiral resolution of the closed forms,[84] inelastic electron induced switching that goes through thermal routes,[89] and stability reversal of the open and closed isomers on the metallic surface.[87] Given the additional functions that terarylenes afford to diarylethenes, as discussed in section 1.2, it is imperative that they be studied under UHV conditions as well. This study therefore aims to contribute to this field

by performing STM studies of terarylenes under UHV conditions. The thesis aims to (1) choose and, if necessary, develop terarylenes highly sensitive to switching stimuli; (2) develop them for surface deposition; and (3) study them by STM under UHV.

The thesis therefore proceeds first with a discussion of highly sensitive terarylenes in the second chapter. Photochemical and physical considerations are taken into account to develop them so that they could be switched in both directions, with high sensitivity, by different stimuli. A short discussion on how a careful engineering of intramolecular forces of attraction between aromatic side-chains can be instrumental in pushing the sensitivities of photocylization near 1 is first presented. Then, we developed a method to make cycloreversion 1000 x faster and 100 x more efficient. Then, in chapter 3, they are functionalized with appropriate functional groups to allow well-resolved STM studies; we show in this chapter, by a combination of theoretical calculations and experimental photochemical and spectroscopic measurements, that such groups preserve their excellent switching capabilities.

Chapters 4 and 5 showcase the first STM studies of terarylenes under UHV. Chapter 4 concerns a study on assemblies of terarylenes formed under UHV through alignment to the induced electric field between the tip and the surface. This is a new bottom-up approach to make supramolecular networks on surfaces. On the other hand, Chapter 5 is the first single molecular level study of the adsorption of terarylenes on metallic and non-conducting surfaces. These are followed by conclusions and future prospects and details of experimental procedures.

1.6 Notes and References

[1] A. Einstein, On a heuristic viewpoint concerning the production and transformation of light, *Ann. Phys.* 1905, *17*, 132-148; an English translation could be found in *Einstein's Miraculous Year,* J. Stachel (Ed.), Princeton University Press, Princeton, 1998.

[2] N. Bohr, *The Theory of Spectra and Atomic Constitution*, Cambridge University Press, Cambridge, 1922.

[3] For a compilation of landmark papers in quantum mechanics translated in English, see B.L. van der Waerden, *Sources of Quantum Mechanics*, Dover, New York, 2007.

[4] L. Pauling, The nature of the chemical bond. Application of results obtained from the quantum mechanics and from a theory of paramagnetic susceptibility to the structure of molecules, *J. Am. Chem. Soc.*, 1931, *53*, 1367-1400.

[5] L. Pauling, The nature of the chemical bond. II. The one-electron bond and the three-electron bond, *J. Am. Chem. Soc.*, 1931, *53*, 3225-3237.

[6] Robert S. Mulliken - Nobel Lecture: Spectroscopy, Molecular Orbitals, and Chemical Bonding". *Nobelprize.org.* Nobel Media AB 2014. Web. 12 Oct 2017. http://www.nobelprize.org/nobel_prizes/chemistry/laureates/1966/mulliken-lecture.html

[7] N. J. Turro, V. Ramamurthy, J. C. Scaiano, *Principles of Molecular Photochemistry: An Introduction*, University Science Books, 2009.

[8] B. Valeur, M. N. Berberan-Santos, *Molecular Fluorescence : Principles and Applications*, Wiley-VCH, Weinheim, 2013.

[9] R. Feynman, There's Plenty of Room at the Bottom in *The Pleasure of Finding Things Out: The Best Short Works of Richard Feynman,* J. Robins (Ed.), Perseus, Cambridge, 1999, 117-140.

[10] C. V. Gortner, R. A. Gortner, The stereomeric azobenzenes, *J. Am. Chem. Soc.* 1910, *32*, 1294-1296.

[11] H. Hartley, J. M. Stuart, The miscibility of azobenzene and azoxybenzene in the solid state and the supposed existence of a stereoisomeride of azobenzene, *J. Chem. Soc. Trans.* 1914, *105*, 309-312.

[12] G. S. Hartley, The *cis*-form of azobenzene, *Nature,* 1937, *140*, 281.

[13] G. S. Hartley, The cis-form of azobenzene and the velocity of the thermal cis⟶trans-conversion of azobenzene and some derivatives, *J. Chem. Soc.* 1938, *0*, 633-642.

[14] For a recent review, see H. M. D. Bandara, S. C. Burdette, Photoisomerization in different classes of azobenzene, *Chem. Soc. Rev.* 2012*, 41*, 1809-1825.

[15] A. A. Beharry, G. A. Woolley, Azobenzene photoswitches for biomolecules, *Chem. Soc. Rev.* 2011, *40*, 4422-4437.

[16] *Smart Light-Responsive Materials,* Y. Zhao, I. Ikeda (Eds.) John Wiley & Sons, Hoboken, New Jersey, 2009.

[17] B. S. Lukyanov, M. B. Lukyanova, Spiropyrans: synthesis, properties, and application, *Chem. Hetrocycl. Compd.* 2005, *42*, 281-311.

[18] For a recent review on spiropyran chemistry and applications, see R. Klajn, Spiropyran-based dynamic materials, *Chem. Soc. Rev.* 2014, *43,* 148.

[19] Y. Yokoyama, Fulgides for memories and switches, *Chem. Rev.* 2000, *100*, 1717-1740.

[20] M. Irie, M. Mohri, Thermally irreversible photochromic systems. Reversible photocyclization of diarylethene derivatives. *J. Org. Chem.*, 1988, *53*, 803-808.

[21] M. Irie, T. Fukaminato, K. Matsuda, S. Kobatake, Photochromism of diarylethene molecules and crystals: memories, switches, and actuators, *Chem. Rev.* 2014, *114*, 12174-12277.

[22] M. Irie, Diarylethenes for memories and switches, *Chem. Rev.* 2000, *100*, 1685-1716.

[23] *New Frontiers in Photochromism*, M. Irie, Y. Yokoyama, T. Seki (Eds.) Springer, Tokyo, 2013.

[24] T. Kawai, T. Iseda, M. Irie, Photochromism of triangle terthiophene derivatives as molecular re-router, *Chem. Commun.* 2004, 72-73.

[25] T. Nakashima, K. Atsumi, S. Kawai, T. Nakagawa, Y. Hasegawa, T. Kawai, Photochromism of thiazole-containing triangle terarylenes, *Eur. J. Org. Chem.* 2007, *19*, 3212-3218.

[26] Y. Kutsunugi, S. Kawai, T. Nakashima, T. Kawai, Photochromic properties of terarylene derivatives having a π-conjugation unit on central aromatic ring, *New J. Chem.* 2009, *33*, 1638-1373.

[27] S. Kawai, T. Nakashima, Y. Kutsunugi, H. Nakagawa, H. Nakano, T. Kawai, Photochromic amorphous molecular materials based on dibenzothienylthiazole structure, *J. Mater. Chem.* 2009*, 19,* 3606-3611.

[28] S. Fukumoto, T. Nakagawa, S. Kawai, T. Nakashima, T. Kawai, Syntheses and photochromic properties of diaryl acenaphthylene derivatives, *Dyes and Pigments,* 2011, *89*, 297-304.

[29] T. Nakashima, M. Goto, S. Kawai, T. Kawai, Photomodulation of ionic interaction and reactivity: reversible photoconversion between imidazolium and imidazolinium, *J. Am. Chem. Soc.* 2008, *130*, 14570-14575.

[30] R. Kanazawa, T. Nakashima, T. Kawai, Photophysical properties of a terarylene photoswitch with a donor-acceptor conjugated bridging unit, *J. Phys. Chem. A*, 2017, *121*, 1638-1646.

[31] S. Fukumoto, T. Nakashima, T. Kawai, Photon-quantitative reaction of a dithiazolylarylene in solution, *Angew. Chem. Int. Ed.* 2011, *50*, 1565-1568.

[32] S. Fukumoto, T. Nakashima, T. Kawai, Intramolecular hydrogen bonding in a triangle dithiazolyl-azaindole for efficient photoreactivity in polar and non-polar solvents, *Eur. J. Org. Chem,* 2011, *92*, 5047-5053.

[33] R. Li, T. Nakashima, O. Galangau, S. Iijima, R. Kanazawa, T. Kawai, Photon-quantitative 6π-electrocyclization of a diarylbenzo[b]thiophene in polar medium, *Chem. Asian. J.* 2015, *10*, 1725-1730.

[34] T. Nakashima, R. Fujii, T. Kawai, Regulation of folding and photochromic reactivity of terarylenes through a host-guest interaction, *Chem. Eur. J.* 2011, *17*, 10951-10957.

[35] H. Nakagawa, S. Kawai, T. Nakashima, T. Kawai, Synthesis and photochemical reactions of photochromic terarylene having leaving methoxy group, *Org. Lett.* 2009, *11*, 1475-1478.

[36] H. Nakagawa, T. Nakashima, T. Kawai, Subsequent chemical reaction of photochromic 4,5-dibenzothienylthiazoles, *Eur. J. Org. Chem.* 2012, 4493-4500.

[37] T. Nakashima, K. Tsuchie, R. Kanazawa, R. Li, S. Iijima, O. Galangau, H. Nakagawa, K. Mutoh, Y. Kobayashi, J. Abe, T. Kawai, Self-Contained Photoacid Generator Triggered by Photocyclization of Triangle Terarylene Backbone, *J. Am. Chem. Soc.* 2015, *137*, 7023-7026.

[38] R. Li, T. Nakashima, R. Kanazawa, O. Galangau, T. Kawai, Efficient self-contained photoacid generator system based on photochromic terarylenes, *Chem. Eur. J.* 2016, *22*, 16250-16257.

[39] R. Li, T. Nakashima, T. Kawai, Self-contained photoacid generator for super acid based on photochromic terayle, *Chem. Commun.* 2017, 4339-4341.

[40] O. Galangau, S. Delbaere, N. Ratel-Ramond, G. Rapenne, R. Li, J. P. D. C. Calupitan, T. Nakashima, T. Kawai, Dual photochemical bond cleavage for a diarylethene-based phototrigger containing both methanolic and acetic sources, *J. Org. Chem.* 2016, *81*, 11282-11290.

[41] T. Nakashima, K. Imamura, K. Yamamoto, Y. Kimura, S. Katao, Y. Hashimoto, T. Kawai, Synthesis, structure and properties of α,β-linked oligothiazoles with controlled sequence, *Chem. Eur. J.* 2014, *20*, 13722-13729.

[42] T. Nakashima, K. Yamamoto, Y. Kimura, T. Kawai, Chiral photoresponsive tetrathiazoles giving snapshots of folding states, *Chem. Eur. J.* 2013, *19*, 16972-16980.

[43] Y. Hashimoto, T. Nakashima, D. Shimizu, T. Kawai, Photoswitching of an intramolecular chiral stack in a helical tetrathiazole, *Chem. Commun.* 2016, 52, 5171-5174.

[44] S. Iijima, T. Nakashima, T. Kawai, Stereoselective Photoreaction in P-Stereogenic dithiazolylbenzo[b]phosphole chalcogenides, *New J. Chem.*, 2016, *40*, 10048-10055.

[45] Y. Moriyama, K. Matsuda, N. Tanifuji, S. Irie, M. Irie, Electrochemical cyclization/cycloreversion reactions of diarylethenes, *Org. Lett.* 2005, *7*, 3315-3318.

[46] T. Nakashima, Y. Kajiki, S. Fukumoto, M. Taguchi, S. Nagao, S. Hirota, T. Kawai, Efficient oxidative cycloreversion reaction of photochromic dithiazolylthiazole, *J. Am. Chem. Soc.* 2012, *134*, 19877-19883.

[47] J.P. Calupitan, T. Nakashima, Y. Hashimoto, T. Kawai, fast and efficient oxidative cycloreversion reaction of a π-extended photochromic terarylene, *Chem. Eur. J.* 2016, *22*, 10002-10008.

[48] G. Binnig, H. Rohrer, Ch. Gerber, E. Weibel, Tunneling through a controllable vacuum gap, *Appl. Phys. Lett.* 1982, *40*, 178-180.

[49] G. Binnig, H. Rohrer, Ch. Gerber, E. Weibel, Surface studies by scanning tunneling microscopy, *Phys. Rev. Lett.* 1982, *49*, 57-61.

[50] G. Binnig, H. Rohrer, Ch. Gerber, E. Weibel, 7 x 7 Reconstruction on Si(111) resolved in real space, *Phys. Rev. Lett.* 1982, *50*, 120-123.

[51] The incredible story of how fast the technique developed was told by Rohrer and Binnig in their Nobel lecture which could be found in G. Binnig, H. Rohrer, *Rev. Mod. Phys.* 1987, *59*, 615-625.

[52] H. Ohtani, R. J. Wilson, S. Chiang, C. M. Mate, Scanning tunneling microscopy observations of benzene molecules on the Rh(111)-(3 × 3) (C_6H_6 + 2CO) surface, *Phys. Rev. Lett.* 1988, *60*, 2398-2401.

[53] J. S. Foster, J. E. Frommer, P. C. Arnett, Molecular manipulation using a tunneling microscope, *Nature*, 1988, *331*, 324-326.

[54] J. S. Foster, J. E. Frommer, Imaging of liquid crystals using a tunneling microscope, *Nature,* 1988, *333*, 542-545.

[55] D. P. E. Smith, H. Horber, Ch. Gerber, G. Binnig, Smectic liquid crystal monolayers on graphite observed by scanning tunneling microscopy, *Science*, 1989, *245*, 43-45.

[56] D. P. E. Smith, H. Horber, Ch. Gerber, G. Binnig, Structure, registry and imaging mechanism of alkylcyanobiphenyl molecules by tunnelling microscopy, *Nature*, 1990, *344*, 631-644.

[57] G. C. McGonigal, R. H. Bernhardt, D. J. Thomson, Imaging alkane layers at the liquid/graphite interface with the scanning tunneling microscope, *Appl. Phys. Lett.* 1990, *57*, 28.

[58] J. P. Rabe, S. Buchholz, Direct observation of molecular structure and dynamics at the interface between a solid wall and an organic solution by scanning tunneling microscopy, *Phys. Rev. Lett.* 1991, *66*, 2096-2099.

[59] D. M. Eigler, E. K. Schweizer, Positioning single atoms with a scanning tunneling microscope, *Nature*, 1990, *344*, 524-526.

[60] L. Gross, F. Mohn, N. Moll, P. Liljeroth, G. Meyer, The chemical structure of a molecule resolved by atomic force microscopy, *Science*, 2009, *325*, 1110-1114.

[61] One has to be careful with using the term “imaging” or “observing” molecular orbitals, see B. Q. Phan, M. S. Gordon, Can orbitals really be observed in scanning tunneling microscopy experiments? *J. Phys. Chem. A,* 2017, *121*, 4851-4852.

[62] L. Gross, Recent advances in submolecular resolution with scanning probe microscopy, *Nature Chemistry*, 2011, *3*, 273-278; and references therein.

[63] B. Schuler, S. Fatayer, F. Mohn, N. Moll, N. Pavliček, G. Meyer, D. Peña, L. Gross, Reversible Bergman cyclization by atomic manipulation, *Nature Chemistry*, 2016, *8*, 220-224.

[64] N. Pavliček, A. Mistry, Z. Majszk, N. Moll, G. Meyer, D. J. Fox, L. Gross, Synthesis and characterization of triangulene, *Nature Nanotech.* 2017, *12*, 308-311.

[65] G. Rapenne, C. Joachim, The first nanocar race, *Nat. Rev. Mat.* 2017, *2*, 17040.

[66] M. Irie, T. Fukaminato, T. Sasaki, N. Tamai, T. Kawai, Organic chemistry: a digital fluorescent molecular photoswitch, *Nature* 2002, *420*, 759-760.

[67] S. J. van der Molen, H. van der Vegte, T. Kudernac, I. Amin, B. L. Feringa, B. L., M. van Wees, Stochastic and photochromic switching of diarylethenes studied by scanning tunnelling microscopy, *Nanotechnology* 2006, *17*, 310−314.

[68] N. Battaglini, H. Klein, C. Hortholary, C. Coudret, F. Maurel, P. Dumas, STM observation of single diarylethene flickering, *Ultramicroscopy* 2007, *107*, 958-962.

[69] K. Uchida, Y. Yamanoi, T. Yonezawa, H. Nishihara, Reversible on/off conductance switching of single diarylethene immobilized on a silicon surface, *J. Am. Chem. Soc.* 2011, *133*, 9239-9241.

[70] T. C. P. Arramel, T. Kudernac, N. Katsonis, M. van der Maas, B. L. Feringa, B. J. van Wees, Reversible light induced conductance switching of asymmetric diarylethenes on gold: surface and electronic studies, *Nanoscale* 2013, *5*, 9277-9282.

[71] K. S. Mali, N. Pearce, S. De Feyter, N. R. Champness, Frontiers of supramolecular chemistry at solid surfaces. *Chem. Soc. Rev.* 2017, *46*, 2520-2542.

[72] X. Bouju, C. Mattioli, G. Franc, A. Pujol, A. Gourdon, Bicomponent supramolecular architectures at the vacuum–solid interface, *Chem. Rev.* 2017, *117*, 1407-1444.

[73] R. Arai, S. Uemura, M. Irie, K. Matsuda, Reversible photoinduced change in molecular ordering of diarylethene derivatives at a solution-HOPG interface, *J. Am. Chem. Soc.* 2008, *130*, 9371-9379.

[74] S. Yokoyama, T. Hirose, K. Matuda, Phototriggered formation and disappearance of surface-confined self-assembly composed of photochromic 2-thienyl-type diarylethene: a cooperative model at the liquid/solid interface, *Chem. Commun.* 2014, 5964-5966.

[75] S. Yokoyama, T. Hirose, K. Matsuda, Effects of alkyl chain length and hydrogen bonds on the cooperative self-assembly of 2-thienyl-type diarylethenes at a liquid/highly oriented pyrolytic graphite interface, *Chem. Eur. J.* 2015, *21*, 13569-13576.

[76] N. Maeda, T. Hirose, S. Yokoyama, K. Matsuda, Rational design of highly photoresponsive surface-confined self-assembly of diarylethenes: reversible three-state photoswitching at the liquid/solid interface, *J. Phys. Chem. C* 2016, *120*, 9317-9325.

[77] T. Sakano, Y. Imaizumi, T. Hirose, K. Matsuda, Formation of two-dimensionally ordered diarylethene annulated isomer at the liquid/HOPG interface upon in situ UV irradiation, *Chem. Lett.* 2013, *42*, 1537-1539.

[78] D. Frath, T. Sakano, Y. Imaizumi, S. Yokoyama, T. Hirose, K. Matsuda, Diarylethene self-assembled monolayers: cocrystallization and mixing-induced cooperativity highlighted by scanning tunnelling microscopy at the liquid/solid interface, *Chem. Eur. J.* 2015, *21*, 11350-11358.

[79] S. Bonacchi, M. El Garah, A. Ciesielski, M. Herder, S. Conti, M. Cecchini, S. Hecht, P. Samori, Surface-induced selection during in situ photoswitching at the solid/liquid interface, *Angew. Chem. Int. Ed.* 2015, *54*, 4865-4869.

[80] S. Takami, T. Kawai, Photochromism of dithiazolylethenes having methoxy groups at the reaction centers, *Eur. J. Org. Chem.* 2002, *22*, 3796-3800.

[81] S. Yokoyama, T. Hirose, K. Matsuda, Photoinduced four-state three-step ordering transformation of photochromic terthiophene at a liquid/solid interface based on two principles: photochromism and polymorphism, *Langmuir,* 2015, *31*, 6404-6414.

[82] S. De Feyter, P. Iavicoli, H. Xu, Expression of chirality in physisorbed monolayers observed by scanning tunneling microscopy in *Chirality at the Nanoscale*, D. Amabilino (Ed.), Wiley-VCH, Weinheim, 2009, 215-245.

[83] K.-H. Ernst, Supramolecular surface chirality in *Supramolecular Chirality*. M. Crego-Calama, D.N. Reinhoudt (Eds.), Springer, Heidelberg, 2006, 209-252.

[84] N. Maeda, T. Hirose, K. Matsuda, Discrimination between conglomerates and pseudoracemates using surface coverage plots in 2d self-assemblies at the liquid-graphite interface, *Angew. Chem. Int. Ed.* 2017, *56*, 2371-2375.

[85] A. Bellec, M. Cranney, Y. Chalopin, A. J. Mayne, G. Comtet, G. Dujardin, Distinguishing different isomers of the photochromic CMTE molecule on the Si(100) surface studied by STM, *J. Phys. Chem.* 2007, *111*, 14818-14822.

[86] C. Coudret, G. Guirado, N. Estrampes, R. Coratger, Adsorption of a single molecule of a diarylethene photochromic dye on Cu(111), *Phys. Chem. Chem. Phys.* 2011, *13*, 20946-20953.

[87] T. K. Shimizu, J. Jung, H. Imada, Y. Kim, Adsorption-induced stability reversal of photochromic diarylethene on metal surfaces, *Chem. Commun.* 2013, 8710-8712.

[88] T. K. Shimizu, J. Jung, H. Imada, Y. Kim, Supramolecular assembly through interactions between molecular dipoles and alkali metal ions, *Angew. Chem. Int. Ed.* 2014, *53*, 13729-13733.

[89] J. Wirth, N. Hatter, R. Drost, T. R. Umbach, S. Barja, M. Zastrow, R. Rück-Braun, J. I. Pascual, P. Saalfrank, K. J. Franke, Diarylethene molecules on a Ag(111) surface: stability and electron-induced switching, *J. Phys. Chem. C,* 2015, *119*, 4874-4883.

[90] R. B. Woodwards, R. Hoffmann, The conservation of orbital symmetry, *Angew. Chem., Int. Ed.* 1969, *8*, 781-853.

[91] G. Reecht, C. Lotze, D Sysoiev, T. Huhn, K. J. Franke, Visualizing the role of molecular orbitals in charge transport through individual diarylethene isomers, *ACS Nano*, 2016, *10*, 10555-10562.

[92] G. Reecht, C. Lotze, D Sysoiev, T. Huhn, K. J. Franke, Disentangling electron- and electric field-induced ring-closing reactions in a diarylethene derivative on Ag(111), *J. Phys. Condens. Matter* 2017, *29*, 294001.

[93] S. V. Snegir, A. Marchenko, P. Yu, F. Maurel, O. Kapitanchuk, S. Mazerat, S. M. Lepeltier, A. Léaustic, E. Lacaze, STM observation of open- and closed-ring forms of functionalized diarylethene molecules self-assembled on a Au(111) surface, *J. Phys. Chem. Lett.* 2011, *2*, 2433-2436.

[94] S. V. Snegir, P. Yu, F. Maurel, O. Kapitanchuk, A. Marchenko, E. Lacaze, Switching at the nanoscale : light- and STM-tip-induced switch of a thiolated diarylethene self-assembly on Au(111), *Langmuir* 2014, *30*, 13556-13563.

Chapter 2
Highly sensitive terarylenes

The bistability of diarylethenes/terarylenes gives these compounds promise in applications for molecular electronics.[1-4] Specifically, they are sought for applications in switching and memory storage devices due to the difference in electronic structure of their two isomers. Thus, derivatives most sensitive to switching stimuli must be prioritized for development in STM studies.

Depending on the switching direction and structure of a particular derivative, there are various stimuli available for switching. These include light, heat, and redox agents (by chemical redox agents, electrochemistry, or inelastic tunneling electrons). Given this variety, the chapter opens with theoretical considerations on reaction kinetics and dynamics to develop appropriate switching molecules. (Section 2.1) Then, the discussion proceeds to the design of molecules for highly sensitive photocyclization and cycloreversion. For photocyclization, molecular design principles to achieve quantum yields up to 98 % is provided. (Section 2.2) Meanwhile, an alternative route for cycloreversion is sought and developed in Section 2.3. Results provided in this Section 2.3 are published in the article:

> *Fast and efficient oxidative cycloreversion reaction of a π-extended photochromic terarylene,* by J.P. Calupitan, T. Nakashima, Y. Hashimoto, T. Kawai, in *Chem. Eur. J.* 2016*, 22,* 10002-10008.

2.1 The conical intersection and switching stimuli

Isomerization of diarylethenes/terarylenes proceeds through the potential energy surface on Figure 2.1. The two isomers, the open (***o***) and closed (***c***) forms, refer to the open hexatriene and closed cyclohexadiene moieties in the central part of their respective structures.[4] The ***o*** form loses aromaticity upon isomerization to the ***c*** form so that the former is more stable than the latter. However, the high kinetic barrier separating the two prevents instantaneous cycloreversion, making this class of photoswitches stable under dark conditions.[4]

Photoexcitation of ***o*** raises it to the S_1 state. Excitation to higher states happens but fast thermal relaxation causes most other excitations to relax to the S_1 state. S_1 has a potential minimum slightly biased to the side of closed form at the S_0 state (Figure 2.1). Therefore, as long as the ground state ***o*** form is oriented so that the reactive carbons are within reasonable bond formation distance and there is sufficient electron density, most excitations may lead to successful photocyclization. The excited state conformation hence plays a big role in controlling the sensitivity of ***o*** to photons. Due to the fast dynamics of this excitation, this excited state conformation heavily relies on the ground state conformation. Thus, controlling the ground state conformation provides a simplified way to maximize the number of photocyclization events from a single burst of photons i.e. maximize the photocyclization quantum yield.[4] (This of course assumes that no other events happen in the excited state.)

Excitation and subsequent relaxation of the closed form in S_0 leads to the same local minimum in the S_1 state, which is biased to return back to the closed form (Figure 2.1) so that majority of excitations do not lead to opening/cycloreversion. Therefore, it seems difficult to simultaneously

achieve high quantum yields for both the photo-cyclization and the cycloreversion reaction. Photochromic molecules showing high photocyclization efficiencies indeed exhibit suppressed reactivity in photocycloreversion reaction with quantum yield less than 1%.[4] An alternative route to cycloreversion is sought, namely oxidative processes. In this route, the closed form is oxidized to the radical cationic state (Figure 2.1, dotted potential energy curve). In this charged state, cycloreversion goes through a different potential energy surface having a lower activation energy. Cycloreversion activation energies are low so that they proceed at room temperature; the charged closed form is thermally unstable. Strategies to control this cycloreversion route are further elucidated in section 2.3.

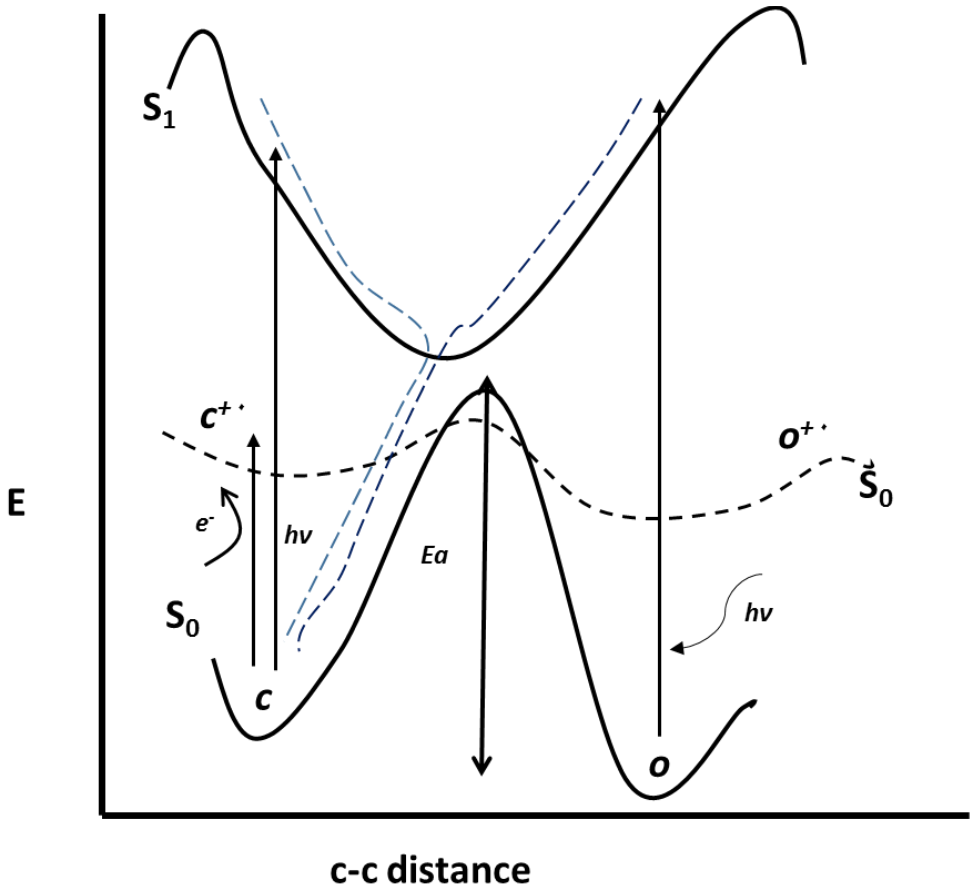

Figure 2.1. Approximate potential energy diagram of the S_0 and S_1 states of the open (***o***) and closed (***c***) isomers of diarylethenes. Photoexcitation of the ***o*** form to the S_1 state and subsequent relaxation to the conical intersection (broken dark blue lines) causes cyclization to the c form. The intersection is biased towards the ***c*** form so that virtually all successful excitations lead to cyclization but this bias causes most excitation of the ***c*** form to just return to the ***c*** form (broken blue lines). So that for cycloreversion, this was bypassed by going through an alternative potential energy curve (S_0 broken lines) of the radical states.

2.2 Photon-quantitative cyclization

As mentioned, it is enough to control the ground state conformation of terarylenes in order to control their photocyclization sensitivity. In solution, diarylethenes oscillate between two conformers: the non-reactive parallel conformation and the reactive anti-parallel conformation (Scheme 2.1).[4] Pushing the photocyclization quantum yield towards unity therefore involved shifting the equilibrium

between these two conformations. Strategies for these mostly include introducing bulky groups or bridging the two side rings to prevent the rotation of the side moieties to the parallel conformation.[5-8] These strategies were perfected in the design and synthesis of the molecule on Scheme 2.2a, which harbor multiple non-covalent interactions to lock the molecule in the reactive conformation.[9]

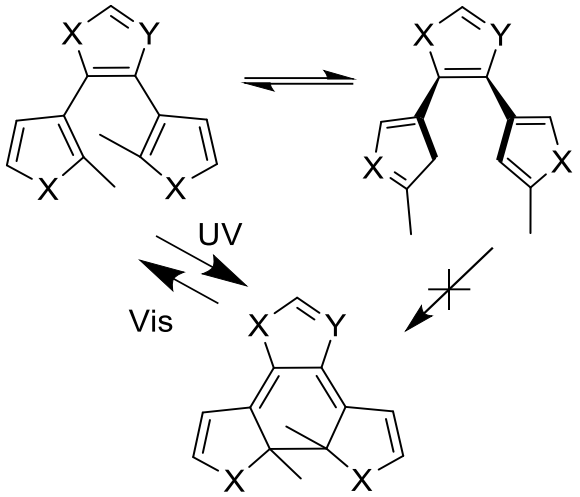

Scheme 2.1. The reactive and non-reactive conformation of diarylethenes/terarylenes.

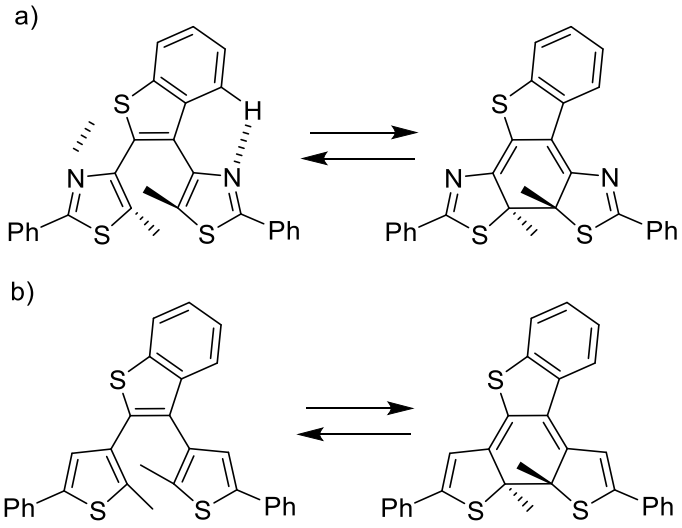

Scheme 2.2. a) Structure and reaction of molecule displaying photon-quantitative reaction. b) Structure of diarylethene/terarylene with no intramolecular forces strong enough to keep the reactive conformation. Adapted from ref. 9.

In hexane, the photocyclization quantum yield was found to be 98 ± 2 %. Photon-quantitative reaction was achieved. DFT, NMR, and X-ray crystallography studies showed that the intramolecular forces responsible for these are H-bonding, S-N, and C-H-π interactions as depicted in Scheme 2.2a. In methanol, a solvent that disrupts H-bonding, the quantum yield was found to be 52 %.[9] In a derivative where the nitrogen atoms (which participate in the two stronger interactions) were replaced by carbon atoms, quantum yield went down to 49 % under the same conditions (Scheme 2.2b).

However, the dependence on intramolecular forces limits this photon-quantitative reaction to nonpolar solvents only. Further designs were therefore put forward to maintain these interactions even in polar solvents.[10] This variety of designs allowed the development of new applications not limited by solvent polarity such as photoacid generators.[11,12]

2.3 Highly efficient oxidative cycloreversion

As explained above, reaching photocyclization quantum yields of up to 100 % comes at the cost of low cycloreversion quantum yields. The photochromic terarylenes discussed and other derivatives did display cycloreversion quantum yields of around 1%.[4-10] Alternative stimuli were therefore sought for cycloreversion. These include multiphoton excitation,[13-14] heat,[15] or electric potential. Chemical and electrochemical oxidation have attracted attention as an alternative route for the ring-opening reaction of diarylethenes because they offer high efficiency in an (electro)catalytic manner.[16-26] The efficiency of the electrocatalytic cycloreversion reaction for **2.3*o*** (Figure 2.2, R_1 = R_2 = methyl) was first quantitatively estimated to be more than 900% as net efficiency while the instantaneous current efficiency reached over 2000% involving the chain reaction shown in Scheme 2.3.[16] The one-electron oxidation of ***c*** form readily produces the radical cation $\boldsymbol{c}^{\cdot+}$, which is spontaneously converted to the radical cation $\boldsymbol{o}^{\cdot+}$ through the non-photochemical cycloreversion reaction with the rate constant of k_2 = (3.3 ± 0.06) × 10^{-1} s^{-1}. This cycloreversion rate constant is far larger than that of neutral ***c*** form by 7-orders of magnitude,[27] which clearly suggests that the activation energy of thermal cycloreversion reaction is greatly reduced for the radical cation state.[13,28] A radical cation $\boldsymbol{o}^{\cdot+}$ form oxidizes a neutral ***c*** form to give a pair of $\boldsymbol{c}^{\cdot+}$ form and ***o*** form in the chain reaction. Since the diffusion-controlled intermolecular charge transfer process takes place very quickly in a solution with the rate constant of k_4 >> 10^4 s^{-1},[16] the isomerization of $\boldsymbol{c}^{\cdot+}$ form to $\boldsymbol{o}^{\cdot+}$ form (τ_2 = 3.0 s) is the rate-limiting step. The long lifetime of radical cation $\boldsymbol{c}^{\cdot+}$ form, which is inactive in the chain reaction, may increase the chance of the backward formation of neutral ***c*** upon reduction by co-existing reductants in the environment and suppress the formation of active species ($\boldsymbol{o}^{\cdot+}$).

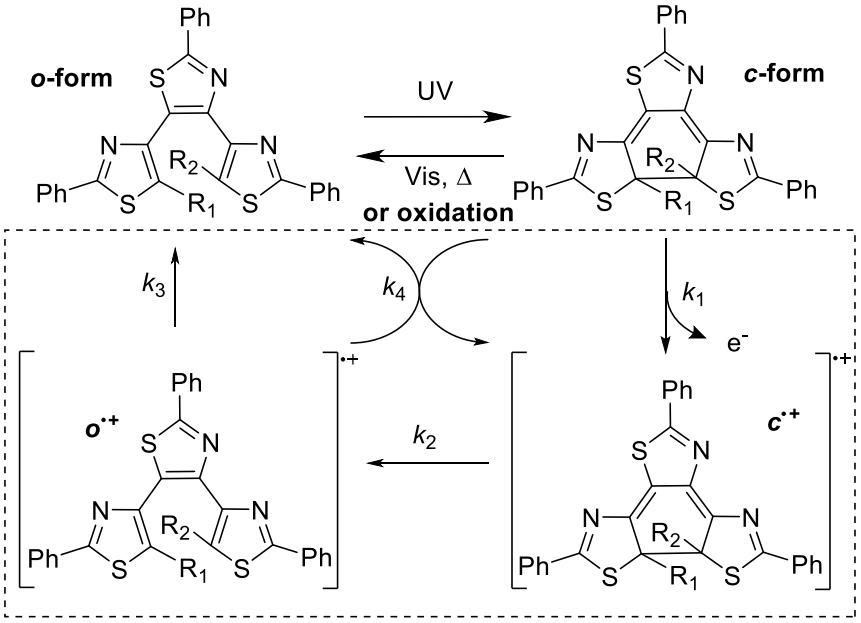

Scheme 2.3. Mechanism of alternative oxidative cycloreversion.

2.3.1 Molecular design for faster oxidative cycloreversion. To further explore this, we show that controlling the rate-determining step, i.e. conversion from $c^{\cdot+}$ to $o^{\cdot+}$ form (k_2), can hasten the overall chain reaction by focusing on the substituents at the reactive carbon atoms (R_1 and R_2 in Scheme 2.3). The introduction of bulky substituents at these positions was reported to increase the thermal cycloreversion rate for diarylethenes in the neutral state.[18-19,29] We expect a similar effect in the radical cationic state. Bulky phenyl groups are introduced in **2.1*o*** (Figure 2.2). In addition to the destabilization of $c^{\cdot+}$ by the steric effects of bulky phenyl groups on the planar fused ring, the extended π-system may stabilize the radical cation state in the $o^{\cdot+}$ form but not the $c^{\cdot+}$ form. Overall, the destabilized $c^{\cdot+}$ and the stabilized $o^{\cdot+}$ are expected to accelerate the rate-limiting non-photochemical cycloreversion step from $c^{\cdot+}$ to $o^{\cdot+}$.[30] A tetrathiazole-based photochromic molecule **2.2*o***[28,31] was also investigated. The extension of an aryl unit from the terthiazole (**2.3*o***) led to the stabilization of the photochromic-active conformation with a one-turn helix,[32] which may also stabilize the radical cationic $o^{\cdot+}$.

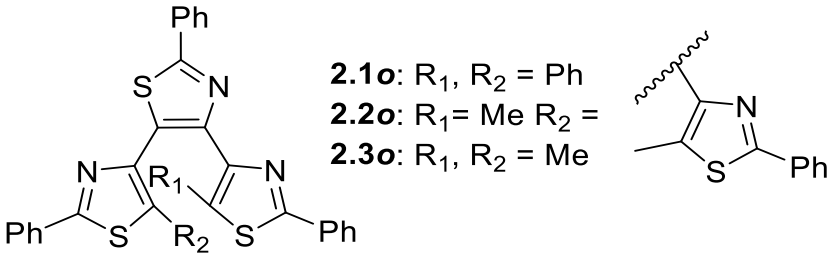

Figure 2.2. Structures of molecules for oxidative cycloreversion.

2.3.2 Synthesis, optical, and electrochemical properties. Scheme 2.4 shows the synthesis route for **2.1*o***. **2.2*o***[31] and **2.3*o***[27] were synthesized by previously reported methods. Detailed syntheses procedure may be found in section 7.1. Table 2.1 summarizes the experimental results on optical, photochemical, and electrochemical properties of **2.1*o***-**2.3*o*** while Figure 2.3 shows their UV-Vis absorption spectra upon UV-illumination. Although the absorption bands were similar to each other, the absorption onset shifted to longer wavelengths in order of **2.3*o***, **2.2*o***, and **2.1*o***. Irradiation with UV light induced the emergence of a new absorption band at around 600 nm for these molecules, showing the photochromic capability and the formation of ***c*** forms. These ***c*** forms exhibited absorption bands with bimodal peaks at almost identical positions as well as absorption coefficients, indicating that the substituents at the R_1 and R_2 positions have little impact on the absorption property of ***c*** forms. Their photochemical properties are mainly defined by the identical π-electronic structures of the molecules. The colored solutions could be completely bleached upon irradiation with visible light, producing absorption spectra identical to those of the initial solutions. The coloration and decoloration cycles could be repeated at least twenty times without any photodegradation.

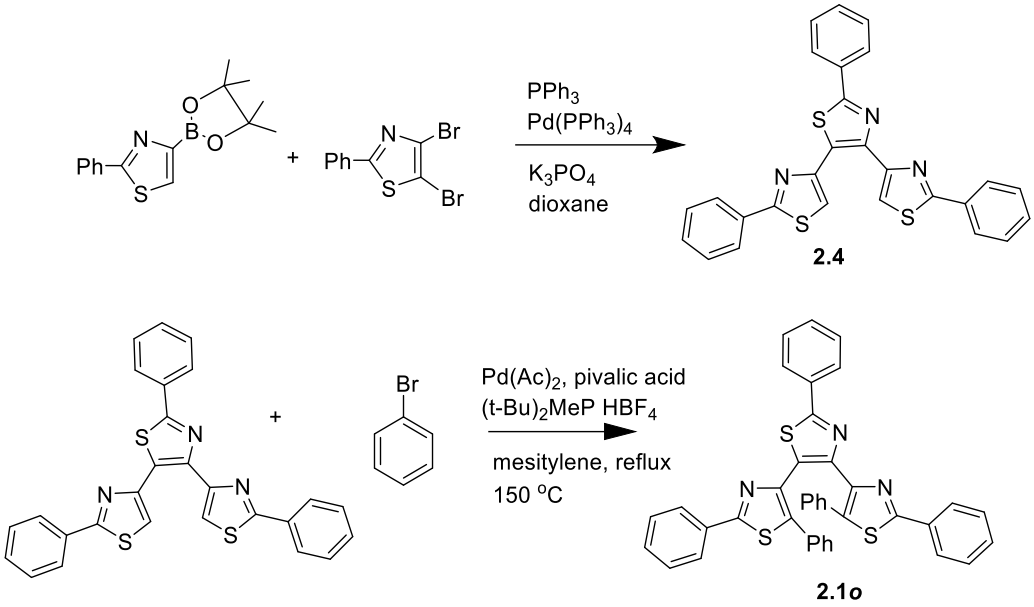

Scheme 2.4. Synthesis route for **2.1*o***. See Section 7.1.2 for details.

Table 2.1. Optical, photochemical and electrochemical properties of compounds **2.1**-**2.3**.

	λ_{max} (ε)[a]	$\varphi_{o\text{-}c}$	$\varphi_{c\text{-}o}$	α at PSS[b]	$E_{ox,onset}$/ V[c]
2.1*o*	327(3.40)	0.12	–	22	1.12
2.1*c*	605(1.30)	–	0.03	–	0.5
2.2*o*	324(4.20)	0.6[d]	–	82[d]	1.16
2.2*c*	621(1.39)	–	0.03[d]	–	0.45
2.3*o*	327(3.21)	0.4[e]	–	93[e]	1.26
2.3*c*	591(1.32)	–	0.03[e]	–	0.65

[a] Solvent: dichloromethane, λ_{max} in nm, ε in x 10^4 $(M\text{-}cm)^{-1}$; [b] Conversion (α) at photostationary state (PSS) in %; [c] vs Ag/Ag^+, 50 mV/s in dichloromethane with tetrabutylammonium hexafluorophosphate (0.1 M) as electrolyte; [d] from ref. 31; [e] from ref. 27. All values reported within the number of significant digits from measurements of triplicate measurements.

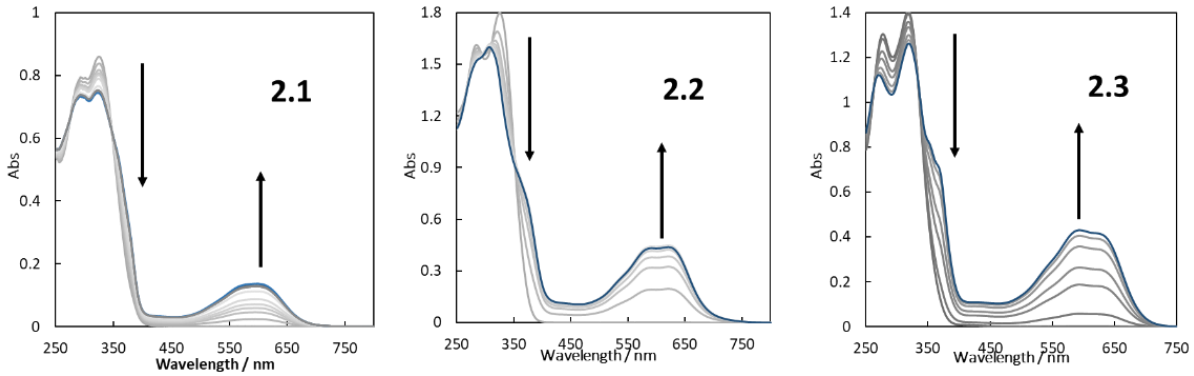

Figure 2.3. UV-Vis absorption spectra upon illumination with UV light. Each spectra was taken after 10s illumination. Spectra in blue shows PSS state.

Compound **2.1*o*** gave the smallest quantum yield for photocyclization reaction ($\varphi_{o\text{-}c}$ = 12 %). Compound **2.2*o*** was reported to have a helical conformation that stabilizes the photoreactive geometry so that $\varphi_{o\text{-}c}$ as high as 60 %[31] was achieved while the original compound **2.3*o*** was reported to possess a non-photoreactive geometry as a preferential conformation to give a relatively small $\varphi_{o\text{-}c}$ of 40 %.[27] The steric effect of the bulky phenyl substituents on the reactive carbon atoms may further hamper the adaptation of photoreactive conformation for **2.1*o***. DFT compound calculations showed a non-photoreactive conformer more stable by 1.7 kJ/mol may be present. Assuming a Boltzmann distribution, this energy difference could result to 67 % of the population of the adopting this non-reactive conformation. In addition, the thorough down-field shift of ^{1}H NMR signals in the aromatic region from **2.1*o*** to **2.1*c*** suggested that strong π-π interactions operate between side-aryl units in **2.1*o*** (Figure 2.4), which could be an energy barrier for the ring-cyclization reaction even in the photoreactive conformer. Unlike the values of $\varphi_{o\text{-}c}$, negligible deviation was observed in the photocycloreversion reaction quantum yields ($\varphi_{c\text{-}o}$), indicating the small effect of substituents on this photochemical process.

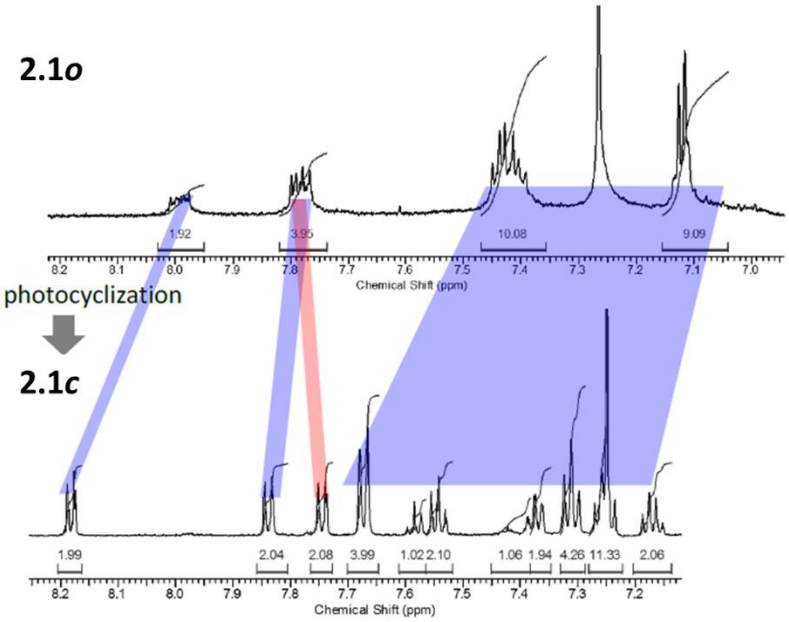

Figure 2.4. Comparison between ^{1}H NMR spectra of the aromatic regions of **2.1*o*** and **2.1*c*** in $CDCl_3$ showing the resolution of more aromatic peaks in ***c*** forms.

Oxidation potentials were measured by cyclic voltammetry experiments. The neutral open forms consistently had higher oxidation potentials than those of the closed forms. It is also noteworthy that the closed forms had similar oxidation potentials for **2.1*c***–**2.3*c*** due to the identical π-conjugated system which is responsible for the oxidation of closed forms.

The kinetics of non-photochemical cycloreversion reaction was evaluated for the neutral ***c*** forms (Table 2.2). Toluene was used as a solvent in these measurements in order to avoid changes in concentration caused by evaporation upon heating. A systematic decrease in non-photochemical ***c*-*o*** conversion activation energy upon the addition of aromatic rings on the

reactive carbon atoms was observed, in agreement with previous reports for diarylethenes.[18,19] Consistently, additional aromatic rings rendered the formation of transition state which was less endothermic and less entropic (Table 2.2). It should be noted that the acceleration in thermal cycloreversion reaction was only by one order of magnitude from **2.3*c*** to **2.1*c*** at 20 °C and even **2.1*c*** gave the moderate thermal stability similar to other typical terarylenes.[27]

Table 2.2. Non-photochemical cycloreversion reaction kinetics for **2.1*c*-2.3*c***.[a]

	E_a/ kJ mol^{-1}	$\Delta H^{\ddagger}$/ kJmol^{-1}	$\Delta S^{\ddagger}$/ J(mol-K)$^{-1}$	$t_{1/2}$ / day[c]
2.1*c*	104	101	-11.5	1.4×10^2
2.2*c*	107	104	-25.0	1.2×10^2
2.3*c*[b]	112	109	-27.9	1.2×10^3

[a] Measured in toluene; [b] Data from ref. 27; [c] at 20 °C.

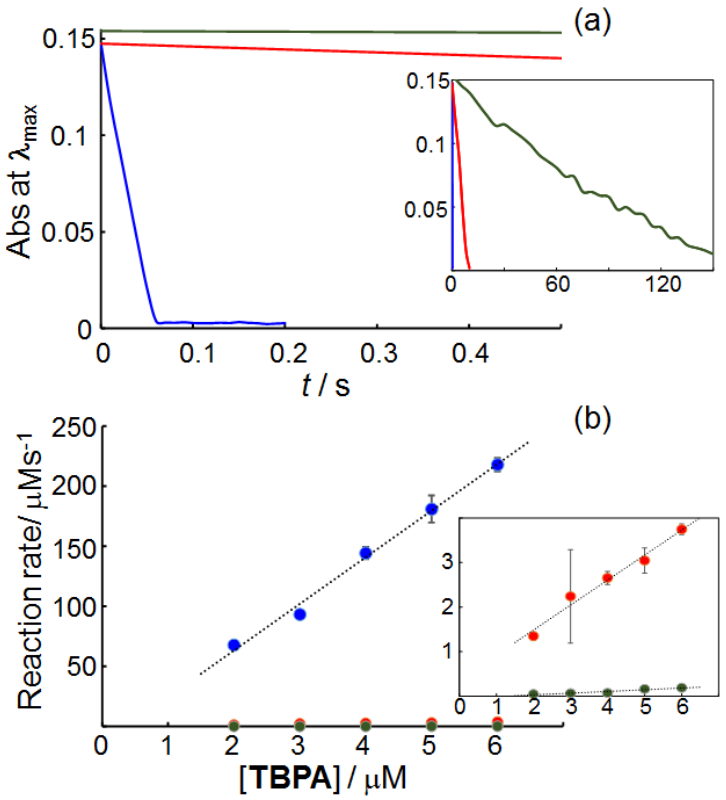

Figure 2.5. (a) Decay profiles of peak absorbance in the visible range by oxidative cycloreversion reaction of **2.1**(blue), **2.2**(red) and **2.3**(green) on the addition of TBPA with 20mol% equivalent to ***c*** form. Inset: decay profile at longer time span. (b) Plots of zero-order reaction rate constants for **2.1**(blue), **2.2**(red) and **2.3**(green) as a function of initial TBPA concentration. Inset: enlarged plots with a y-axis below 4 μMs^{-1}. [***c*** forms] = 20 μM.

2.3.3 Oxidative cycloreversion kinetics. Tris-(4-bromophenyl)ammonium hexachloroantimonate (TBPA) was used as a one-electron oxidant.[16] The addition of 20 mol% equivalent of TBPA to the pre-irradiated colored solutions resulted in complete bleaching, indicating the aforementioned chain reaction mechanism. Figure 2.5a shows the decay of absorbance at the visible band corresponding to ***c*** forms upon addition of 20 mol% equivalent TBPA. Each compound showed a linear decay profile indicating that the bleaching reaction with a catalytic amount of TBPA proceeded with zero-order chain reaction kinetics. The bleaching rates for **2.1*c*** and **2.2*c*** are apparently higher than **2.3*c***. It took more than 150 s for complete bleaching of **2.3*c***, while it finished within 10 s for **2.2*c*** and less than 0.1 *s* for **2.1*c*** (Figure 2.5a). The relative reaction rate was evaluated by comparing slopes in Figure 2.5b. Compared with the rate constant for **2.3**, that of **2.2** was 20-times faster while that of **2.1** was surprisingly boosted by three orders of magnitude.

Considering each step in the chain reaction mechanism shown on Scheme 2.3 as elementary steps, the decay of ***c*** during the chain reaction process (after the initial oxidation by the catalytic amount of TBPA) as monitored on Figure 2.5 may be modelled by the following equation:

$$\frac{d\boldsymbol{c}}{dt} = -k_4[\boldsymbol{o}^{\bullet+}][\boldsymbol{c}] \qquad Eq.\,2.1$$

The decay of $\boldsymbol{c}^{\bullet+}$ and $\boldsymbol{o}^{\bullet+}$ are modelled by the following:

$$\frac{dc^{\bullet+}}{dt} = -k_2[\boldsymbol{c}^{\bullet+}] + k_4[\boldsymbol{o}^{\bullet+}][\boldsymbol{c}] \qquad Eq\ 2.2$$

$$\frac{do^{\bullet+}}{dt} = k_2[\boldsymbol{c}^{\bullet+}] - k_4[\boldsymbol{o}^{\bullet+}][\boldsymbol{c}] - k_3[\boldsymbol{o}^{\bullet+}] \quad Eq\ 2.3$$

We attempt to show the origin of the apparent zero-order behaviour (Figure 2.5a). Since it shows that Eq. 2.1 $^{dc}/_{dt}$ is a constant; [c] should decrease quasi-linearly, and quasi-reciprocal to $[\boldsymbol{o}^{\bullet+}]$. Here, we introduce assumption 1: $k_3 << 1$ so that Eq. 2.3 becomes:

$$\frac{do^{\bullet+}}{dt} = k_2[\boldsymbol{c}^{\bullet+}] - k_4[\boldsymbol{o}^{\bullet+}][\boldsymbol{c}] \quad Eq\ 2.4$$

This assumption also means slow quenching of radicals and that the total concentration of the charged species remains constant. That is,

$$[\boldsymbol{c}^{\bullet+}] + [\boldsymbol{o}^{\bullet+}] = [\mathrm{TBPA}]_0 \quad Eq\ 2.5$$

Since $\frac{do^{\bullet+}}{dt} > 0$ and $k_4[\boldsymbol{o}^{\bullet+}][\boldsymbol{c}] > 0$, the following inequality follows: $\frac{do^{\bullet+}}{dt} < k_2[\boldsymbol{c}^{\bullet+}]$

We manipulate Eq. 2.4 and Eq 2.1 to show that:

$$\frac{dc}{dt} = \frac{do^{\bullet+}}{dt} - k_2[\boldsymbol{c}^{\bullet+}] \quad Eq\ 2.6$$

Since $k_4[o^{\bullet+}][c] > 0$, Eq 2.4 implies that $\frac{do^{\bullet+}}{dt} < k_2[c^{\bullet+}]$. At the beginning of reaction, $[c^{\bullet+}] = [\mathrm{TBPA}]_0$ and $[o^{\bullet+}] = 0$. The latter gradually increases from the isomerization of $\boldsymbol{c}^{\bullet+}$. The initial gradient

are thus given as $\frac{do^{\bullet+}}{dt} = k_2[\mathrm{TBPA}]_0$; $\frac{dc^{\bullet+}}{dt} = -k_2[\mathrm{TBPA}]_0$. Therefore, $\frac{do^{\bullet+}}{dt}$ is initially equal to $k_2[\mathrm{TBPA}]0$ and decreases gradually with the increase of $k_4[\boldsymbol{o}^{\bullet+}][\boldsymbol{c}]$. We here consider a situation in which the electron transfer between $\boldsymbol{o}^{\cdot+}$ and $\boldsymbol{c}$ is fast at the middle stage of reaction. With enough high concentration of $\boldsymbol{c}$ and large value of k_4 ($k_4 > 10^4$ $M^{-1}s^{-1}$)[16], $\boldsymbol{o}^{\cdot+}$ must be consumed as soon as it is produced. In such a situation, $\frac{do^{\bullet+}}{dt}$ should quickly become much less than $k_2[\boldsymbol{c}^{\bullet+}]$ before $[\boldsymbol{o}^{\bullet+}]$ reaches to the similar extent of $[\boldsymbol{c}^{\bullet+}]$. In this occasion, Eq 2.5 can be roughly approximated as

$$[\boldsymbol{c}^{\bullet+}] \fallingdotseq [\mathrm{TBPA}]_0$$

And Eq 2.6 becomes

$$\frac{d\boldsymbol{c}}{dt} \fallingdotseq -k_2[\mathrm{TBPA}]$$

This clearly shows that the decay of $\boldsymbol{c}$ is 0-order with respect to $\boldsymbol{c}$ but dependent on the amount of oxidizing agent introduced. In this 0-order reaction, a constant amount of $\boldsymbol{c}$ is converted to the colorless $\boldsymbol{o}$ at any moment so that the absorbance decreases by a constant rate. (Figure 2.5a) This also illustrates that in Scheme 2.3, the electron transfer from $\boldsymbol{c}$ form to $\boldsymbol{o}^{\cdot+}$ form propagates the chain reaction even after the consumption of the initial oxidant species, the active species ($\boldsymbol{o}^{\cdot+}$) is consumed as soon as it was formed. The rate constant of diffusion-controlled electron transfer from neutral $\boldsymbol{c}$ to $\boldsymbol{o}^{\cdot+}$ form (k_4) is much larger than that of the spontaneous formation of $\boldsymbol{o}^{\cdot+}$ form (k_2). Eq. 2.6 also shows that the rate is dependent only on the concentration of $\boldsymbol{c}^{\cdot+}$ form which is approximated by the concentration of TBPA. To illustrate this, chain reaction experiments were performed with varying amounts of TBPA. A linear increase in the overall rate constant was observed as the amount of TBPA added was increased (Figure 2.5b). In addition, we showed that the overall reaction rate is dependent on the electron transfer reaction between $\boldsymbol{c}^{\cdot+}$ and $\boldsymbol{o}$, which is the slow rate-determining step.

Since the radical species ($\boldsymbol{o}^{\cdot+}$ and $\boldsymbol{c}^{\cdot+}$) are significant in the chain reaction, their fate during the oxidative cycloreversion was monitored by mixing an equivalent amount (100 mol%) of TBPA to the $\boldsymbol{c}$ form in a stopped-flow analysis experiment.[16] The reaction rate constants k_2 and k_3 were estimated based on the sequential reaction model, in which the $\boldsymbol{o}^{\cdot+}$ form is produced from the $\boldsymbol{c}^{\cdot+}$ form with the rate constant k_2 and transformed to the neutral $\boldsymbol{o}$ form with k_3 (Scheme 2.5). [16] Scheme 2.5 is just a simplification of Scheme 2.3 with the electron transfer (k_4) omitted since a complete conversion of $\boldsymbol{c}$ to $\boldsymbol{c}^{\cdot+}$ was assumed, essentially making the contribution of $k_4[\boldsymbol{o}^{\bullet+}][\boldsymbol{c}]$ zero.

$$\boldsymbol{c} \xrightarrow{k_1} \boldsymbol{c}^{\cdot+} \xrightarrow{k_2} \boldsymbol{o}^{\cdot+} \xrightarrow{k_3} \boldsymbol{o}$$

Scheme 2.5. Sequential reaction model for the stopped-flow experiments.

When 1:1 solutions of TBPA and **2.1*c*** were mixed, new bands at 430 nm and 730 nm appeared indicating the appearance of new species (Figure 2.6a,b). The time scales of the evolution of these two bands were radically different with the former decaying within milliseconds and the latter in the scale of minutes. The band at 430 nm disappeared extremely quickly within 0.005 s accompanying an emergence of a bend at 730 nm, (Figure 2.6a) which subsequently decreased in an exponential manner in the timescale of minutes (Figure 2.6b). Therefore, the former could be assigned to **2.1*c***$^{\cdot+}$ while the **2.1*o***$^{\cdot+}$ form is responsible for the latter absorption band. Figure 2.6a shows an apparent isosbestic point at 580 nm during the first 0.003 s of the reaction, indicating the two-component $\boldsymbol{c}^{\cdot+}$-$\boldsymbol{o}^{\cdot+}$ isomerization reaction, which completed far faster than the subsequent $\boldsymbol{o}^{\cdot+}$-$\boldsymbol{o}$ reaction.

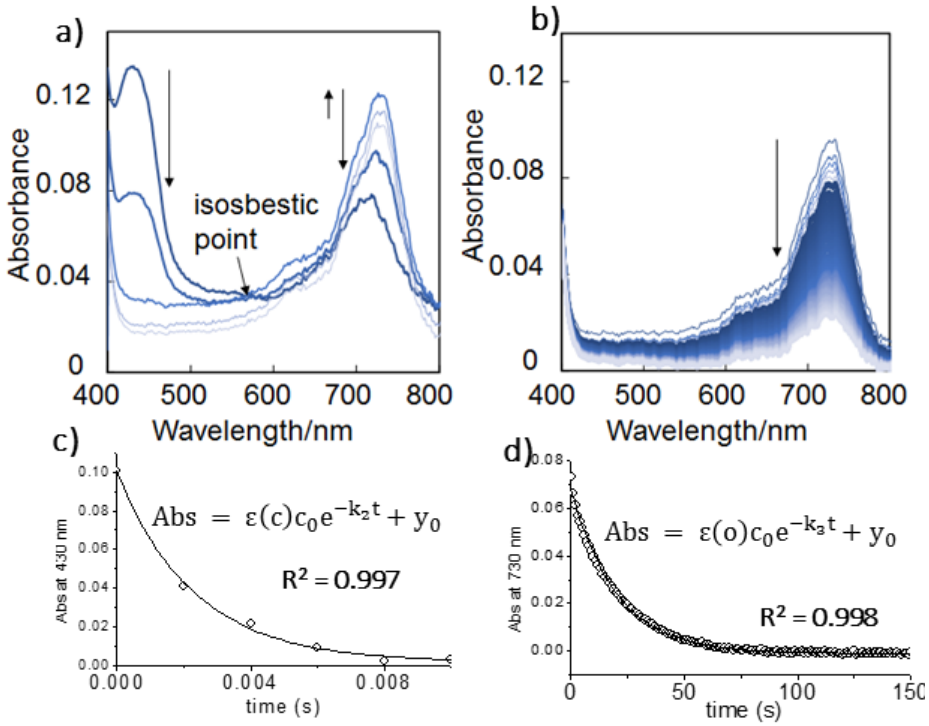

Figure 2.6. Stopped-flow absorption spectral change after a **2.1*c*** solution was mixed with a solution of equimolar amount of TBPA in dichloromethane. Time intervals are 0.001 s for 0.005 s for (a) and 1 s for 90 s for (b). c) and d) are curve fitting of respective evolutions of the peaks at a) and b). Circles are the experimental data while line is the curve fit.

Due to the different timescales of decay of the $\boldsymbol{c}^{\bullet+}$ and $\boldsymbol{o}^{\bullet+}$ forms, it is convenient to model their first-order decays by two independent exponential equations since the former does not affect the evolution of the latter anymore during its decay to the neutral form. In these equations, the complete conversion of the ***c*** to $\boldsymbol{c}^{\bullet+}$ is accomplished so that the contribution of k_1 is ignored. This is evidenced by the lack of a band at 600 nm in the first spectrum taken at 0.001 s after mixing.

$$\frac{dc^{\bullet+}}{dt} = -k_2[\boldsymbol{c}^{\bullet+}] \qquad Eq\ 2.7$$

$$\frac{do^{\bullet+}}{dt} = -k_3[\boldsymbol{o}^{\bullet+}] \qquad Eq\ 2.8$$

Integration of Eq 2.7 and 2.8 gives:

$$[c^{\bullet+}]_t = [c^{\bullet+}]_0 e^{-k_2 t} \qquad Eq\ 2.9$$

$$[o^{\bullet+}]_t = [o^{\bullet+}]_0 e^{-k_3 t} \qquad Eq\ 2.10$$

2.1c$^{\bullet+}$ and **2.1*o***$^{\bullet+}$ do not have overlapping absorption bands so that Beer-Lambert Law may be applied separately:

$$Abs\ \lambda_{max,c^{\bullet+}} = \varepsilon_{c^{+\bullet}}[c^{\bullet+}]_0 e^{-k_2 t} \qquad Eq\ 2.11$$

$$Abs\ \lambda_{max,o^{\bullet+}} = \varepsilon_{o^{+\bullet}}[o^{\bullet+}]_0 e^{-k_3 t} \qquad Eq\ 2.12$$

These equations were fitted to the evolution of time evolution of the peaks at 430 nm and 730 nm to extract the rate constants k_2 and k_3 in Scheme 2.3). (A baseline constant y_0 was added to the equations to improve the fit on Figure 2.6 c,d.) From k_2, the time constant τ for the thermal cycloreversion in the radical state (***c***$^{\bullet+}$ - ***o***$^{\bullet+}$ conversion) could be estimated for **2.1** at 0.002 s. (Table 2.3)

Meanwhile, **2.3*c*** gave a similar result to the previous one,[16] showing small modifications in kinetics due to solvent change. It gave an absorption band right after addition of TBPA at 680 nm corresponding to **2.3*c***$^{\bullet+}$, which turned to **2.3*o***$^{\bullet+}$ with an absorption peak at 510 nm (Figure 2.7b). The cycloreversion **2.3*c***$^{\bullet+}$-**2.3*o***$^{\bullet+}$ was found to have a time constant of 2.6 s in dichloromethane while previous measurements in acetonitrile was found to be 3.3 s.[16] Meanwhile, the time constant of decay of **2.3*o***$^{\bullet+}$ to its open form was 10 s slower in dichloromethane than in acetonitrile. The former seems to be within experimental error but the latter could not be ignored. Solvation of the less polar solvent around ***o***$^{\bullet+}$ form seemed to lead to greater stability than solvation by the more polar acetonitrile, which could have induced further charge polarization. For **2.2*c***, the exponential drop in the 580 nm peak led us to assign it to **2*c***$^{\bullet+}$ while the peak at 670 nm showing a slow decrease followed by the exponential decay was attributed to **2*o***$^{\bullet+}$ (Figure 2.7a).

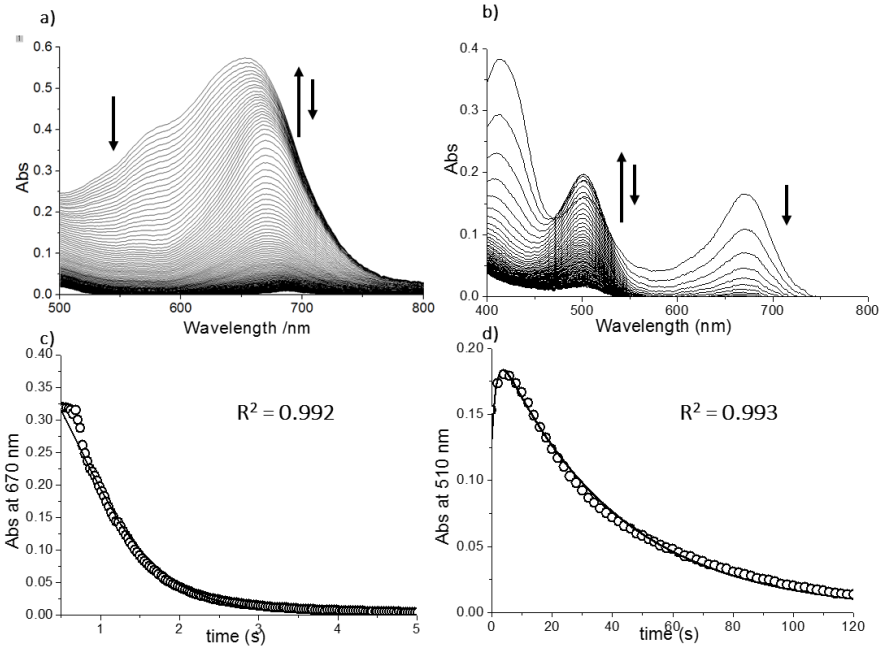

Figure 2.7. Stopped-flow absorption spectral change after (a) **2.2*c*** and (b) **2.3*c*** solution were mixed with a solution of equimolar amount of TBPA in dichloromethane. For (a), spectra were taken for 5 s every 30 ms while for b), spectra were taken for 120 s every 2 s. (c) and (d) are the respective fitting of the data to Eq 2.10 and 11. Circles are the experimental data while line is the curve fit.

In contrast to **2.1**, the evolution of radical species for the latter two compounds happen at the same time scale so the instantaneous concentration of the ***c***$^{\bullet+}$ forms affect the evolution of the ***o***$^{\bullet+}$ forms. Equation 2.7 must therefore be modified to take this into account:

$$\frac{do^{\bullet+}}{dt} = k_2[\boldsymbol{c}^{\bullet+}] - k_3[\boldsymbol{o}^{\bullet+}] \qquad Eq\ 2.13$$

The term $k_2[c^{+\bullet}]$, instantaneous concentration of $c^{\cdot+}$, is independent of the generated $o^{\cdot+}$ so the integrated form in Equation 2.3 can be substituted to eq 2.13:

$$\frac{do^{\bullet+}}{dt} = k_2[c^{\bullet+}]_0 e^{-k_2 t} - k_3[o^{\bullet+}] \quad Eq\ 2.14$$

This is a simple first order differential equation whose solution is trivial:

$$[o^{\bullet+}]_t = [c^{\bullet+}]_0 \frac{k_2}{k_3 - k_2}(e^{-k_2 t} - e^{-k_3 t}) \quad Eq. 2.15$$

Since $c^{\bullet+}$ and $o^{\bullet+}$ forms of **2.2** and **2.3** have overlapping peaks, the model for the absorbance at $\lambda_{max,o^{+\bullet}}$ must take into account the absorbance of both $c^{+\bullet}$ and $o^{+\bullet}$ forms at such wavelength

$$Abs_{\lambda_{max,o^{+\bullet}}} = \varepsilon_{c^{+\bullet} at \lambda_{max,o^{+\bullet}}}[c^{+\bullet}]_0 e^{-k_2 t} + \varepsilon_{o^{+\bullet}}[c^{+\bullet}]_0 \frac{k_2}{k_3 - k_2}(e^{-k_2 t} - e^{-k_3 t}) \quad Eq\ 2.16$$

This was the equation fit to the experimental evolution of the time observation for the absorbance at $\lambda_{max,o^{\bullet+}}$. The non-photochemical reaction rate constant k_2($c^{\cdot+}$-$o^{\cdot+}$) increased by 3-orders of magnitude from **2.3** to **2.1** (Table 2.3), which is in good agreement with the relative increase of zero-order reaction rate constants (Figure 2.5). The acceleration in the non-photochemical cycloreversion reaction by the introduction of phenyl groups was far more prominent in the oxidized form ($c^{\cdot+}$) in comparison with that in the neutral form (c), which clearly suggests that the phenyl groups on the reactive carbon atoms predominantly contribute to the stabilization of $o^{\cdot+}$ form.

Table 2.3 Kinetics of radical cation species formed during cycloreversion reaction.[a]

	τ_2($c^{\cdot+}$-$o^{\cdot+}$)/s (k_2^{-1})	τ_3($o^{\cdot+}$-o)/s (k_3^{-1})
2.1*c*	0.0023 ± 0.0001	20.5 ± 0.1
2.2*c*	0.56 ± 0.01	0.5 ± 0.1
2.3*c*	2.6 ± 0.4	40.0 ± 0.6

[a] [a]Measured in dichloromethane.

It must be noted that the peak assignments on the radical cations of **2.1** and **2.2** were consistent with those predicted by TD-DFT. (Table 2.4) The extended delocalization of spin in the radical cation $o^{\cdot+}$ is responsible for the significant red-shifted absorption for **2.1***o*$^{\cdot+}$ and **2.2***o*$^{\cdot+}$ compared to **2.3***o*$^{\cdot+}$. The relative position of absorption peaks for $c^{\cdot+}$ form and $o^{\cdot+}$ form was reversed in the measurements of **2.1***c* and **2.2***c*. Those of **2.3** are consistent with literature.[10]

Table 2.4. Comparison between calculated and observed λ_{max} of radical forms in nm. (Gaussian 09[32]B3LYP 6-31G+, vacuum)

	λ_{max}($c^{\cdot+}$) obs	λ_{max}($c^{\cdot+}$) calc	λ_{max}($o^{\cdot+}$) obs	λ_{max}($o^{\cdot+}$) calc
2.1	430	460	730	750
2.2	580	570	670	660

2.3.4 Increase in efficiency. We attempted to determine the minimum equivalent of oxidant (TBPA) necessary to trigger and complete the cycloreversion reaction in order to record the highest efficiency possible for the oxidative cycloreversion chain reaction. We express this value in terms of chain reaction length, the number of transformed molecules per initial oxidant molecule. In a sense, this is a measure of the sensitivity of the ***c*** forms to the switching stimuli which is the oxidant TBPA. A higher chain reaction length corresponds well to a high sensitivity to switching.

The solutions containing ***c*** forms were mixed with decreasing equivalents (ranging 5 to 0.1 mol%) of TBPA and the decay of absorbance peaks at λ_{max} in the visible region were recorded. The amount of ***c*** form converted to ***o*** form (as measured in change in absorbance) was divided by the amount of TBPA consumed to yield the reaction chain length. Compound **2.3*c*** exhibited the lowest reaction chain length of 12, which is in the same order of magnitude with the net current efficiency of 900% estimated in the previous electrolysis experiment.[16] Since the **2.3*c*$^{\cdot+}$**-**2.3*o*$^{\cdot+}$** isomerization is an equilibrium reaction favoring **2.3c$^{\cdot+}$**, a small amount of active species (**2.3*o*$^{\cdot+}$**) cannot drive the reaction forward for further oxidation of neutral ***c*** forms. Substantial concentration of thus active species must thus be kept during the reaction. Compound **2.2*c*** has a slightly higher reaction chain length of 16 mainly due to the thermodynamically favored formation of **2.2*o*$^{\cdot+}$** from **2*c*$^{\cdot+}$**, which supports irreversible and quantitative non-photochemical isomerization. **2.1*c*** was found to have the highest reaction chain length of 1000, which means that the overall reaction yield was 100 000 % relative to the oxidant. Mixing 0.1 mol% equivalent oxidant with **2.1*c*** resulted in the complete bleaching. The surprisingly short lifetime of **2.1*c*$^{\cdot+}$** contributed to the efficient formation of active species **2.1*o*$^{\cdot+}$**, since the ***c*$^{\cdot+}$** forms could be deactivated by circumjacent residual reductants.

2.3.5 DFT calculations. To gain further insight about cycloreversion in the radical state, energy differences (ΔE) between ***o*** and ***c*** forms were estimated by DFT calculations for both the neutral and radical cationic states using Gaussian 09 suite of programs.[33] For the geometry optimization, the B3LYP functional with the 6-31G+(d) basis set was employed in the gas phase. Photochromic reactive conformations with C_2-symmetry about the 6π-system were employed as initial input structures for the open forms. The introduction of aromatic groups on the reactive carbon atoms apparently increased the relative energy of ***c*** forms in comparison those of ***o*** forms (Figure 2.8). The more bulky substituents may distort the fused planar polycycle in the closed-ring isomer ***c*** forms.

Matsuda and co-workers proposed a hypothesis that the direction of oxidative isomerization reaction can be deduced from the relative potential energies of ***c*$^{\cdot+}$** and ***o*$^{\cdot+}$** form.[20] The ***o*$^{\cdot+}$** forms are more stable than the ***c*$^{\cdot+}$** forms (ΔE > 0) for **2.1** and **2.2**, suggesting that these molecules could undergo spontaneous cycloreversion reaction upon oxidation (Figure 2.8). The values of ΔE increased in order of **2.3**, **2.2** and **2.1** for the radical cationic state. This order accords well with that estimated for the neutral state. Since three thiazole rings participating in the 6π-electrocyclization reaction are common constitutents of all molecules, the difference in ΔE values are attributed to the effect of substituents at the R_1 and R_2 positions. The bulky units introduced at the ends of the 6π-system destabilized the closed-ring form with increased structural distortion.

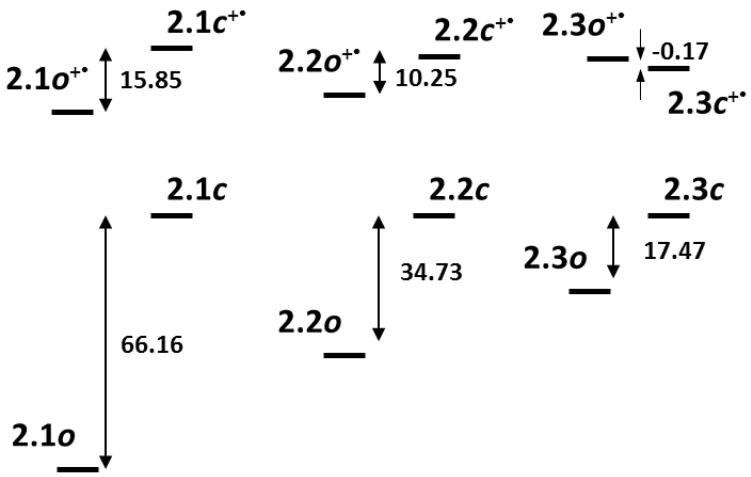

Figure 2.8 Estimated energy differences [ΔE = E(close) – E(open)] between open and closed forms of dithiazolylthiazoles in the neutral and radical cationic states. The energy unit is kcal/mol. All calculations are in vacuum.

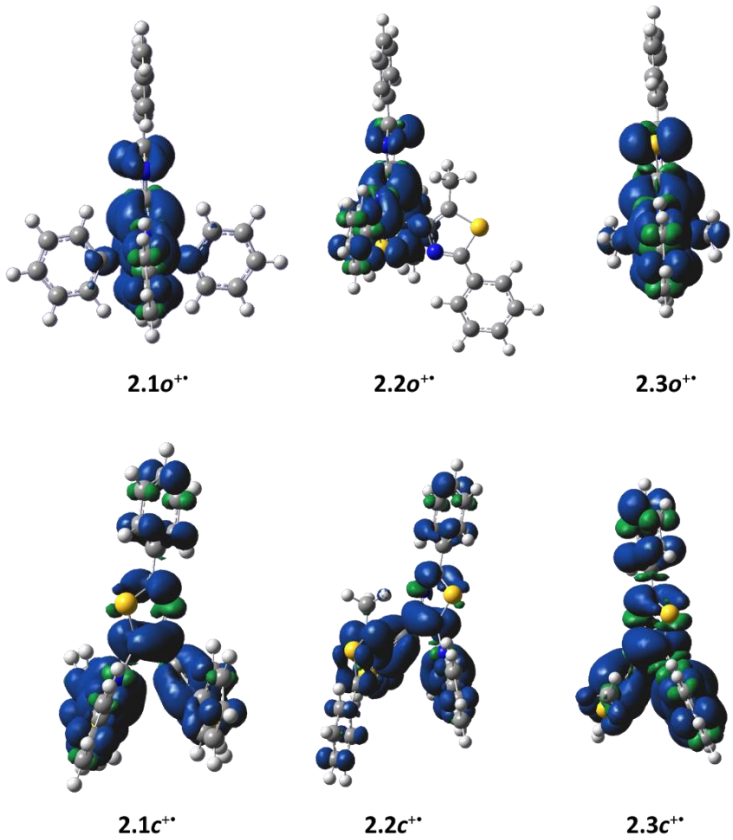

Figure 2.9. Side views of optimized structures of radical cationic forms with spin density distribution.

Moreover, the extended π-system should also specifically stabilize the $o^{\cdot+}$ forms for **1** and **2** by distributing the spin (Figure 2.9). The spin density was calculated to be distributed in a similar region for all $c^{\cdot+}$- forms. The substituents seem to have negligible effect on the delocalization of spin in the $c^{\cdot+}$ forms probably because they orthogonally stick to the planar fused cycle without conjugation. Meanwhile, spin delocalization clearly extended to the aromatic substituents on the reactive carbon atoms for **2.1***o*$^{\cdot+}$ and **2.2***o*$^{\cdot+}$ forms. This delocalization

most likely stabilizes these radical cation states. Charge distribution may also contribute to the systematic change in ΔE values.

2.4 Conclusion

In this chapter, we discussed the development of terarylenes sensitive to switching stimuli. A fundamental understanding of the conical intersection of the ground state and the photoexcited state was first presented in order to maximize photocyclization quantum yield. The same conical intersection was responsible for low cycloreversion quantum yields, so that an alternate route for cycloreversion was sought by a different stimulus.

This was through an oxidative chain-reaction process involving the radical cationic states of the $c^{\cdot+}$ and $o^{\cdot+}$ forms. This is especially promising because electron transfer could also be observed by scanning tunneling microscopy (STM) on metallic/semi-conducting surfaces. We showed that by introducing aromatic rings on the reactive carbons, we could control the speed of the rate-determining step of this chain reaction, thus improving the overall chain reaction process. Incidentally, we found out that oxidant equivalents down to 0.1 % could induce full conversion back to the ***o*** form. The bulk of the aromatic rings, however, prevented majority of the population to adopt the reactive conformation for photocyclization so that this process is effectively compromised ($\phi_{o\text{-}c}$ = 12 %).

In summary, we have a selection of terarylenes switchable by a minimum amount of stimulus. Due to the nature of the conical intersection, it seems difficult to design molecules exclusively switchable by light in both directions so that the two different stimuli were developed for the two directions, i.e., light for cyclization and redox agent for cycloreversion. Both these switching have so far been observed in solution or in the solid state. In the next chapter, we modify these molecules further so they could be studied as single molecules by the use of low-temperature ultra-high vacuum STM.

2.5 References

[1] *Molecular Switches* (Ed. B. L. Feringa), Wiley-VCH, Weinheim, 2001.

[2] *Photon-Working Switchers* (Eds. Y. Yokoyama,K. Nakatani), Springer, 2017.

[3] *New Frontiers in Photochromism* (Eds. M. Irie, Y. Yokoyama, T. Seki), Springer, Tokyo, 2013.

[4] M. Irie, T. Fukaminato, K. Matsuda, S. Kobatake, Photochromism of diarylethene molecules and crystals: memories, switches, and actuators, *Chem. Rev.* 2014, *114*, 12174-12277.

[5] M. Takeshita, C. N. Choi, M. Irie, Synthesis and photochromic properties of thiophenophan-1-enes containing a polyether bridge, *Chem. Commun.* 1997, 2265-2266.

[6] K. Matsuda, Y. Shinkai, T. Yamaguchi, K. Nomiyama, M. Isayama, Very high cyclization quantum yields of diarylethene having two n-methylpyridinium ions, M. Irie, *Chem. Lett.* 2003, *32*, 1178-1179.

[7] M. Takeshita, M. Nagai, T. Yamato, A photochromic thiophenophan-1-ene, *Chem. Commun.* 2003, 1496-1497.

[8] T. Yamaguchi, M. Irie, Photochromism of bis(2-alkyl-1-benzothiophen-3-yl)perfluorocyclopentene derivatives, *J. Photoch. Photobio. A* 2006, *178*, 162-169.

[9] S. Fukumoto, T. Nakashima, T. Kawai, Photon-quantitative reaction of a dithiazolylarylene in solution, *Angew. Chem. Int. Ed.* 2011, *50*, 1565-1568.

[10] R. Li, T. Nakashima, O. Galangau, S. Iijima, R. Kanazawa, T. Kawai, Photon-quantitative 6π-electrocyclization of a diarylbenzo[b]thiophene in olar medium, *Chem. Asian J.* 2015, *10*, 1725-1730.

[11] T. Nakashima, K. Tsuchie, R. Kanazawa, R. Li, S. Iijima, O. Galangau, H. Nakagawa, K. Mutoh, Y. Kobayashi, J. Abe, T. Kawai, Self-contained photoacid generator triggered by photocyclization of triangle terarylene backbone, *J. Am. Chem. Soc.* 2015, *137*, 7023-7026.

[12] O. Galangau, S. Delbaere, N. Ratel-Ramond, G. Rapenne, R. Li, J.P.D.C. Calupitan, T. Nakashima, T. Kawai, Dual photochemical bond cleavage for a diarylethene-based phototrigger containing both methanolic and acetic sources, *J. Org. Chem.* 2016*, 81*, 11282-11290.

[13] M. Murakami, H. Miyasaka, T. Okada, S. Kobatake, M. Irie, Dynamics and mechanisms of the multiphoton gated photochromic reaction of diarylethene derivatives, *J. Am. Chem. Soc.* 2004, *126*, 14764−14772.

[14] Y. Tsuboi, R. Shimizu, T. Shoji, N. Kitamura, Near-infrared continuous-wave light driving a two-photon photochromic reaction with the assistance of localized surface plasmon, *J. Am. Chem. Soc.* 2009, *131*, 12623−12627.

[15] S. Kobatake, I. Yamashita, Synthesis of photochromic diarylethene polymers for a write-by-light/erase-by-heat recording system, *Tetrahedron* 2008, *64*, 7611−7618.

[16] T. Nakashima, Y. Kajiki, S. Fukumoto, M. Taguchi, S. Nagao, S. Hirota, T. Kawai, *J. Am. Chem. Soc.* 2012, Efficient oxidative cycloreversion reaction of photochromic dithiazolythiazole *134*, 19877-19883.

[17] T. Koshido, T. Kawai, K. Yoshino, Optical and electrochemical properties of cis-1, 2-dicyano-1, 2-bis (2, 4, 5-trimethyl-3-thienyl) ethane, *J. Phys. Chem.* 1995, *99*, 6110-6114.

[18] A. Peters, N. R. Branda, Electrochromism in photochromic dithienylcyclopentenes, *J. Am. Chem. Soc.* 2003, *125*, 3404-3405.

[19] B. Gorodetsky, N. R. Branda, Didirectional ring - opening and ring - closing of cationic 1, 2 - dithienylcyclopentene molecular switches triggered with light or electricity, *Adv. Funct. Mater.* 2007, *17*, 786-796.

[20] Y. Moriyama, K. Matsuda, N. Tanifuji, S. Irie, M. Irie, Electrochemical cyclization/cycloreversion reactions of diarylethenes, *Org. Lett.* 2005, *7*, 3315-3318.

[21] G. Guirado, C. Coudret, J. P. Launay, Electrochemical remote control for dithienylethene-ferrocene switches, *J. Phys. Chem. C* 2007, *111*, 2770-2776.

[22] S. Lee, Y. You, K. Ohkubo, S. Fukuzumi, W. Nam, Mechanism and fluorescence application of electrochromism in photochromic dithienylcyclopentene, *Org. Lett.* 2012, *14*, 2238-2241.

[23] S. Lee, Y. You, K. Ohkubo, S. Fukuzumi, W. Nam, Photoelectrocatalysis to improve cycloreversion quantum yields of photochromic dithienylethene compounds, *Angew. Chem. Int. Ed.* 2012, *51*, 13154-13158.

[24] S. Lee, Y. You, K. Ohkubo, S. Fukuzumi, Highly efficient cycloreversion of photochromic dithienylethene compounds using visible light-driven photoredox catalysis, W. Nam, *Chem. Sci.* 2014, *5*, 1463-1474.

[25] M. A. Kishida, T. Kusamoto, H. Nishihara, Photoelectric signal conversion by combination of electron-transfer chain catalytic isomerization and photoisomerization on benzodimethyldihydropyrenes, *J. Am. Chem. Soc.* 2014, *136*, 4809-4812.

[26] Q. Ai, S. Pang, K. H. Ahn, Photoswitchable “turn-on” fluorescence diarylethenes: substituent effects on photochemical properties and electrochromism, *Chem. Eur. J.* 2016, *22*, 656-662.

[27] T. Nakashima, K. Atsumi, S. Kawai, T. Nakagawa, Y. Hasegawa, T. Kawai, Photochromism of thiazole-containing triangle terarylenes, *Eur. J. Org. Chem.* 2007, *19,* 3212-3218

[28] A. Staykov, J. Areephong, W. R. Browne, B. L. Feringa, K. Yoshizawa, Electrochemical and photochemical cyclization and cycloreversion of diarylethenes and diarylethene-capped sexithiophene wires, *ACS Nano* 2011, *5*, 1165-1178.

[29] K. Morimitsu, K. Shibata, S. Kobatake, M. Irie, Dithienylethenes with a novel photochromic performance, *J. Org. Chem.* 2002, *67*, 4574-4578.

[30] S. Nakamura, M. Irie, Thermally irreversible photochromic systems. A theoretical study, *J. Org. Chem.* 1988, *53*, 6136-6138.

[31] G. Gavrel, P. Yu, A. Leaustic, R. Guillot, R. Metivier, K. Nakatani, 4, 4′ -Bithiazole-based tetraarylenes: new photochromes with unique photoreactive patterns, *Chem. Commun.* 2012, *48*, 10111-10113.

[32] T. Nakashima, K. Yamamoto, Y. Kimura, T. Kawai, Chiral photoresponsive tetrathiazoles that provide snapshots of folding states, *Chem. Eur. J.* 2013, *19*, 16972-16980.

[33] M. J. Frisch, *et al*, *Gaussian 09 Revision A.02*, Gaussian Inc. Wallingford CT, 2009. (See section 7.4 for complete citation.)

Chapter 3

Synthesis and photochromism of terarylenes designed for STM

Practical and logistical constraints of scanning tunneling microscopy (STM) such as machine availability limit the range of molecules that can be studied by STM. A significant effort is therefore necessary to choose appropriate molecules with desired properties and designing them for STM studies.

We selected compounds **3.1** and **3.2** in Figure 3.1 for their high sensitivity to switching stimuli. (Note that **2.3** is the same as **3.2**; the label is changed in favor of ease of reference from this chapter on.) As elucidated in Chapter 2, the open form **3.1*o*** preserves a reactive conformation to display photon-quantitative photocyclization[1] while the closed form **3.2*c*** may be converted to the open form in an autocatalytic oxidative cycloreversion reaction with electron efficiencies reaching up to 2 000 %[2]. Although we showed that oxidant-based yields can be improved to 100 000 % in derivatives having aromatic rings on reactive carbons, we opted not to take advantage of this because such derivatives simultaneously have low photocyclization quantum yields.[3] Further, in this chapter, we designed these molecules to harbor functional groups which could be valuable for STM investigations. Results presented in this chapter were published in the article:

> *Synthesis and photochromism of chloro- and* tert*-butyl-functionalized terarylene derivatives for surface deposition,* by J.P.D.C. Calupitan, O. Galangau, O. Guillermet, R. Coratger, T. Nakashima, G. Rapenne, and T. Kawai, in *Eur. J Org. Chem.* **2017***, 17,* 2451-2461.

3.1 Molecular design and syntheses

Tert-butyl groups (**3.3*o*** and **3.4*o***) and chloro-substituents (**3.5*o*** and **3.6*o***) were incorporated on both sides of these molecules. These substituents are routinely used for molecules studied under STM because of the following substituents: they show bright contrast in STM images, minimize aggregation on the surface, and slightly decouple the electronic properties of the molecule from the surface; their steric bulky groups elevate aromatic cores from the surface thereby preventing physisorption or chemisorption that would otherwise cause a loss of molecular properties.[4-9] On the other hand, the chlorine group has been selected because halogen substituted molecules have been shown to direct their surface assembly by surface-molecule dipole interactions on insulating substrates composed of crystalline NaCl or KCl bilayer previously grown over a metallic substrate.[10] In addition, halogens are especially useful for forming stable assemblies of molecules on semi-conducting surfaces by a combination of molecule-molecule and surface-molecule interactions.[11-12]

To prepare the *tert*-butyl and chloro derivatives, two thiazole precursors were utilized. Scheme 3.1 shows the synthetic route to access the 5-methyl-2-phenylthiazolyl groups for molecules **3.3*o*** to **3.6*o***. 4-bromo-2-(3,5-di-*tert*-butylphenyl)-5-methylthiazole (**3.8**) was synthesized from the commercially available 2,5-di-*tert*-butyl-1-bromobenzene. It was first coupled with 4,5-dibromothiazole to produce 4-bromo-2-(3,5-di-*tert*-butylphenyl)-5-methylthiazole (**3.7**) followed by

S_N2 reaction of its deprotonated adduct (by LDA) with methyl iodide. Meanwhile, a similar synthetic route for 4-bromo-5-methyl-2-phenylthiazole from thiobenzamide[13-14] was used to produce the chloro derivative 4-bromo-2-(*p*-chlorophenyl)-5-methylthiazole (**3.11**) from *p*-chlorothiobenzamide. (See section 7.1 for details.)

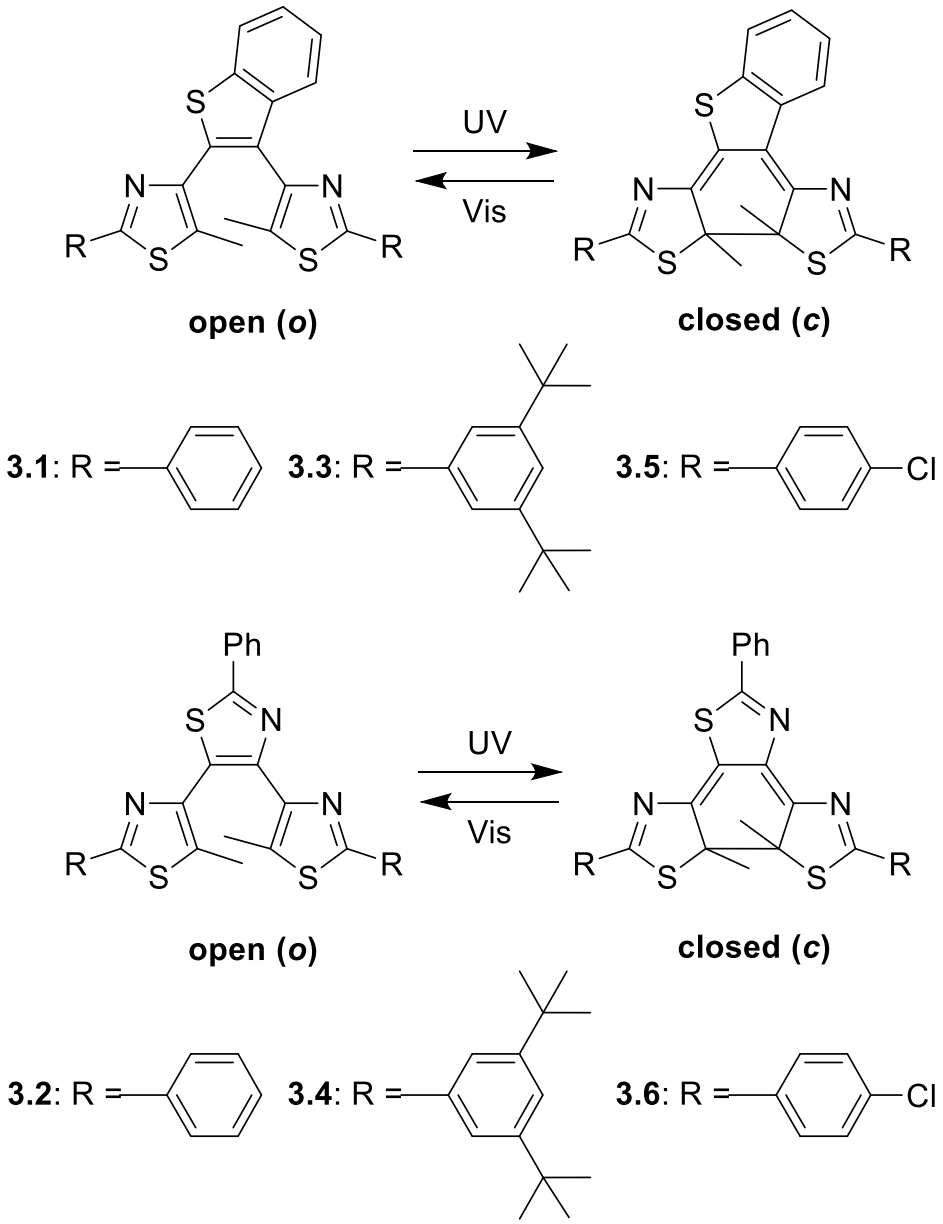

Figure 3.1. Molecules chosen for this study. The mother molecules **3.1*o*** and **3.2*o*** were known for their highly sensitive switching properties. Each one were further functionalized with *tert*-butyl (**3.3*o*** and **3.4*o***) and chloro (**3.5*o*** and **3.6*o***) groups to aid in STM studies.

3.1*o*[1] and **3.2*o***[15] were previously synthesized by a double Suzuki coupling of the side moieties to the central rings 2,3-dibromobenzothiophene and 4,5-dibromo-2-phenylthiazole respectively. However, the carbon atoms involved in these double coupling reactions have markedly different

reactivities. For example, for **3.2*o***, the same one-pot conditions were used to attach the 5-methyl-2-phenylthiazol-4-yl moiety to the reactive carbons at the 5-position and the non-reactive 4-position of the thiazole ring. We therefore chose a different route for the synthesis that respects the different reactivities of the carbon atoms in these positions, taking inspiration from previous works.[16-17]

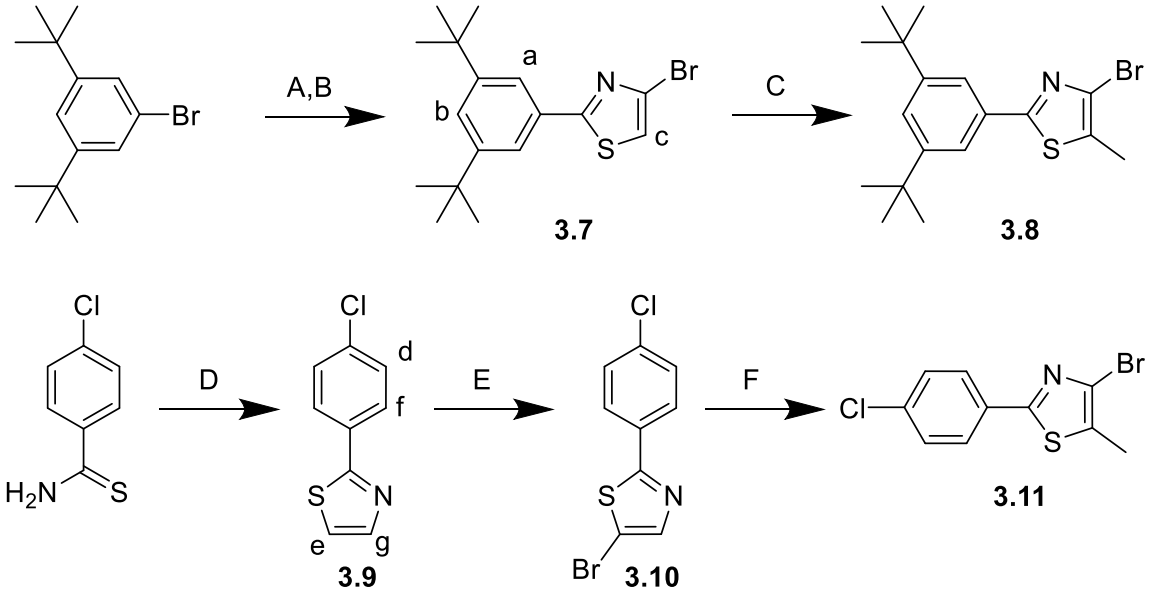

Scheme 3.1. Synthetic route to access 2-phenyl-5-methylthiazol-5-yl side groups of the new compounds bearing *tert*-butyl (**2.8**) and chloro groups (**3.11**) groups. A) n-BuLi, $B(OMe)_3$, THF; B) 2,4-dibromothiazole, $Pd(OAc)_2$, Xantphos, K_3PO_4, THF, 60 °C; C) LDA, THF, CH_3I -78 °C to RT; D) 2-bromo-1,1-diethoxyethane, EtOH, 70 °C; E) NBS, THF, 60 °C; F) LDA, CH_3I, THF.

We opted for consecutive coupling to these different positions. For **3.1*o*** (Scheme 3.2), 4-bromo-5-methyl-2-phenylthiazole[14] was first connected to the 3-position of the benzothiophene substituent by Suzuki coupling with the commercially available benzo[b]thien-3-ylboronic acid to yield 4-(benzothiophen-3-yl)-2-phenyl-5-methylthiazole (**3.12**). Only then was the second 5-methyl-2-phenylthiazol-4-yl derivative attached to the electron-poor carbon in the 2-position by C-H direct arylation using $Pd(OAc)_2$, Cs_2CO_3, pivalic acid, di-*tert*-butyl(methyl)phosphonium tetrafluoroborate in mesitylene to produce **3.1*o***. It should be noted that this gave a small increase in the synthetic yield from the reported 57%[1] to an overall yield of 62% from the two consecutive coupling reactions (87 % and 71 % for each step).

Meanwhile, the carbon in the 4-position of thiazoles is known to be the least reactive so this was prioritized for the first attachment. The boronic acid derivative of 5-bromo-4-methyl-2-phenylthiazole was first generated *in situ* before adding 4-bromo-2-phenylthiazole and other reagents for Suzuki coupling were added to produce 2-phenyl-5-methyl-4-(2-phenylthiazol-4-yl)-thiazole (**3.13**). The electron-poor carbon in the 5-position of the thiazole ring is then free for C-H direct arylation to yield **3.2*o***. In this case, with yields of 96% and 26% for the two consecutive steps, the overall yield for the two coupling reactions has been improved from 6% in the previously reported synthesis [15] to 25%.

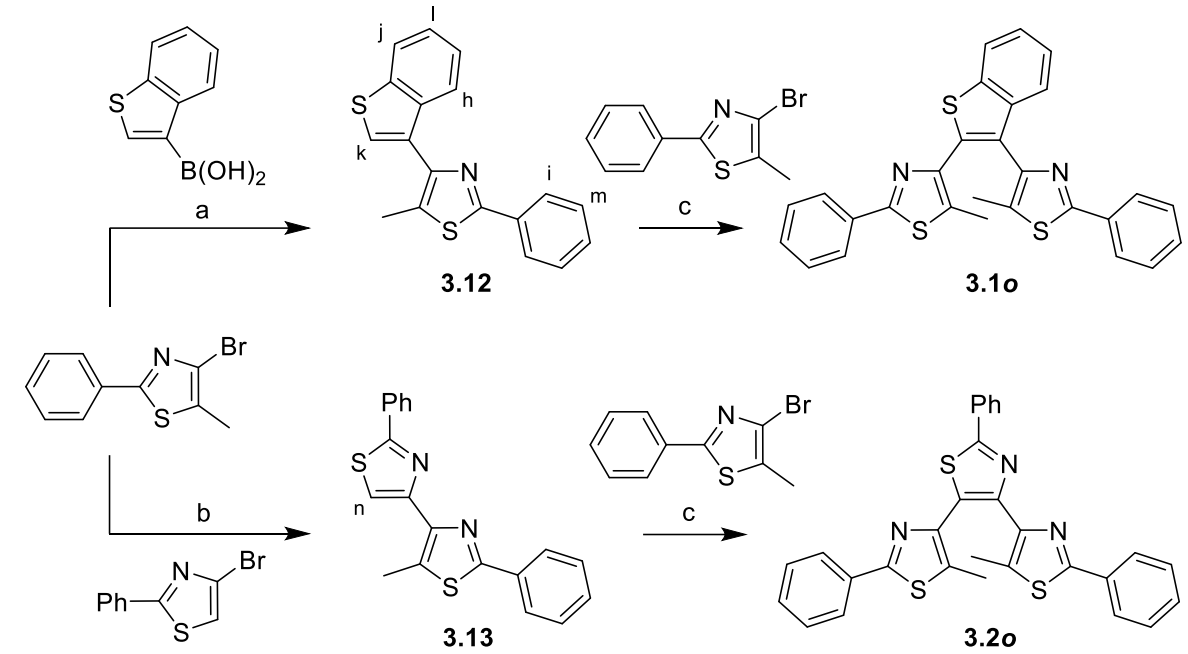

Scheme 3.2. Synthesis of model compounds **3.1*o*** and **3.2*o*** by a new synthetic pathway. a) benzo[b]thien-3-ylboronic acid $Pd(PPH_3)_4$, K_3PO_4, DME, H_2O; b) 1. n-BuLi, $B(OMe)_3$, THF 2. 4-bromo-2-phenylthiazole, $Pd(PPh_3)_4$, K_3PO_4, DME, H_2O; c) 4-bromo-5-methyl-2-phenylthiazole, $Pd(OAc)_2$, Cs_2CO_3, pivalic acid, di-*tert*-butyl(methyl)phosphonium tetrafluoroborate, mesitylene.

The same consecutive coupling reactions were utilized to synthesize respective *tert*-butyl derivatives **3.3*o*** and **3.4*o*** from **3.8** (Scheme 3.3) and chloro-derivatives **3.5*o*** and **3.6*o*** from **3.11** (Scheme 3.4). Detailed synthetic procedures may be found in Section 7.1.

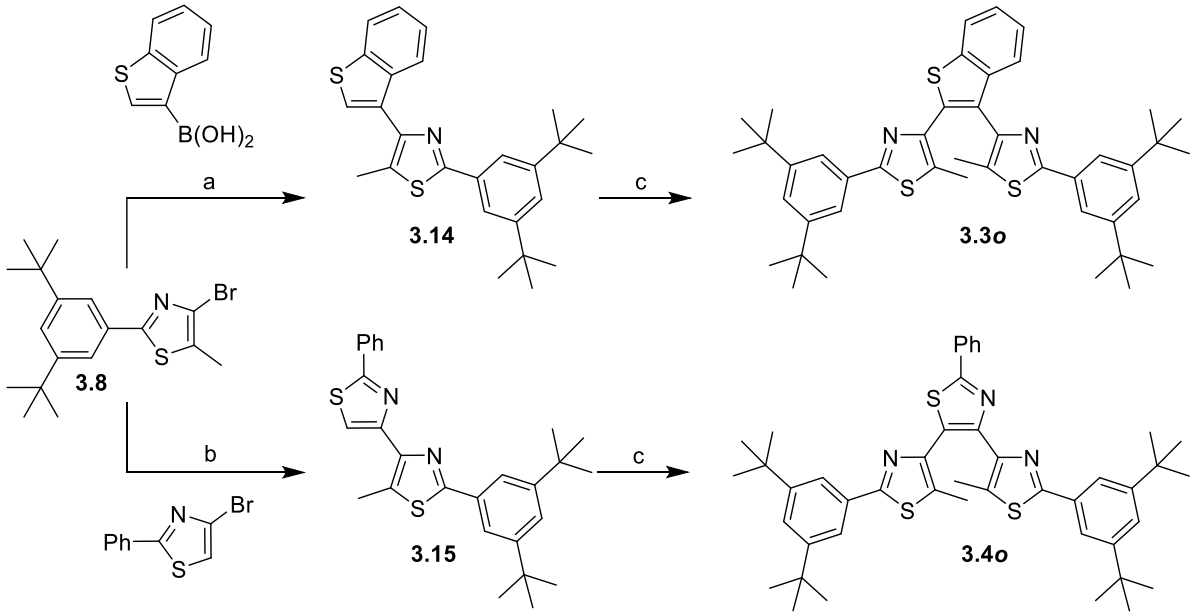

Scheme 3.3. Synthesis of the *tert*-butyl-functionalized terarylenes **3.3*o*** and **3.4*o***. a) benzo[b]thien-3-ylboronic acid $Pd(PPH_3)_4$, K_3PO_4, DME, H_2O; b) 1. n-BuLi, $B(OMe)_3$, THF; 2. 4-bromo-2-phenylthiazole, $Pd(PPh_3)_4$, K_3PO_4, DME, H_2O; c) **3.8**, $Pd(OAc)_2$, Cs_2CO_3, pivalic acid, di-*tert*-butyl(methyl)phosphonium tetrafluoroborate, mesitylene.

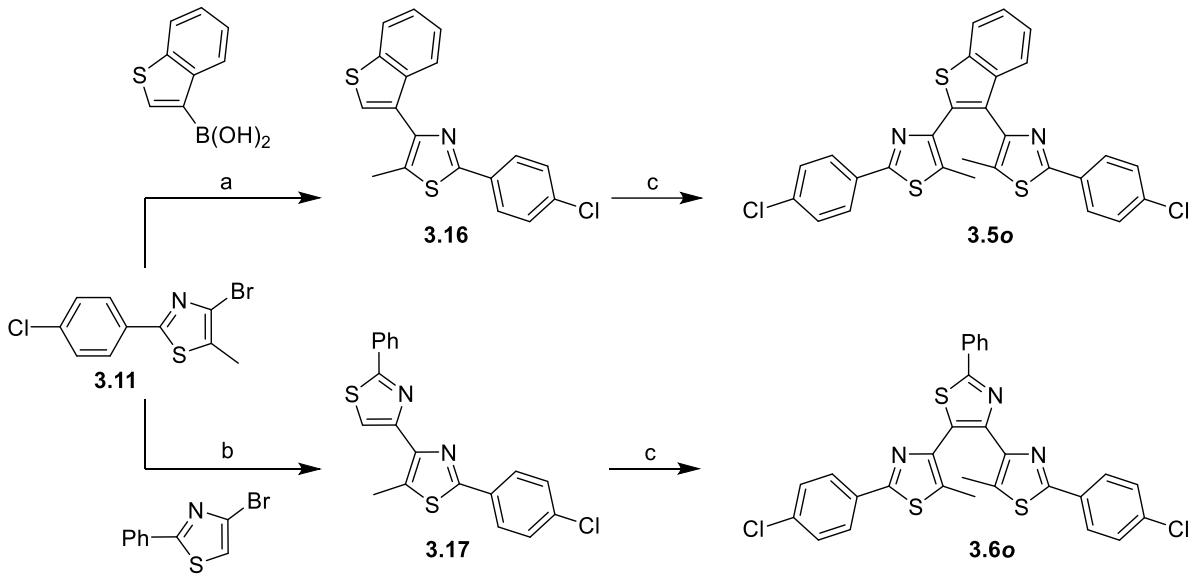

Scheme 3.4. Synthesis of chloro-functionalized terarylenes **3.5o** and **3.6o**. a) benzo[b]thien-3-ylboronic acid $Pd(PPh_3)_4$, K_3PO_4, DME, H_2O; b) 1. n-BuLi, $B(OMe)_3$, THF; 2. 4-bromo-2-phenylthiazole, $Pd(PPH_3)_4$, K_3PO_4, DME, H_2O; c) **3.11**, $Pd(OAc)_2$, Cs_2CO_3, pivalic acid, di-tert-butyl(methyl)phosphonium tetrafluoroborate, mesitylene.

3.2 Photochemical properties of compounds

Photochemical properties of respective derivatives of **3.1*o*** and **3.2*o*** are not significantly different from each other (Table 3.1). Maximum wavelengths (**λ**) recorded in dichloromethane for **3.1*o*,** **3.3*o***, and **3.5*o*** are very similar with bands at 308 nm, 310 nm, and 313 nm respectively. (Figure 3.2) Those of **3.2*o***, **3.4*o***, and **3.6*o*** are at 327 nm, 318 nm, and 322 nm respectively; they also displayed a second peak at lower wavelengths. No solvatochromism was observed as these peaks were very similar to those reported for **3.1*o***[1] and **3.2*o***[8] in hexane.

Table 3.1. Photochemical properties of compounds

	$\lambda_{max,o}(\varepsilon)$[a]	$\lambda_{max,c}(\varepsilon)$[b]	$\phi_{o\text{-}c}$[c]	$\phi_{c\text{-}o}$[d]	$\lambda_{max,o,\,calc}$[e]	$\lambda_{max,c,\,calc}$[f]
3.1	308(3.51)	600(1.04)	0.95	0.02	297	640
3.2	327(3.21)[g]	591(1.32)[f]	0.5	0.03[f]	294	632
3.3	310(3.43)	595(1.06)	0.94	0.03	310	635
3.4	318(3.21)	594(1.31)	0.5	0.04	295	632
3.5	313(3.40)	607(1.12)	0.95	0.02	303	654
3.6	322(3.36)	600(1.27)	0.5	0.03	303	643

All experimental measurements were done in dichloromethane. [a] λ_{max} of open forms in nm, ε in 10^4 $M^{-1}cm^{-1}$ [b] λ_{max} of closed forms in the visible region in nm, ε in 10^4 $M^{-1}cm^{-1}$ [c] photocyclization quantum yield of ***o*** forms [d] cycloreversion quantum yield of ***c*** forms; theoretical (TD-DFT) λ_{max} for the [e]***o*** form in UV region and the [f]***c*** in the visible region; [g] data from reference 3. All data were reported according to significant digits afforded by standard deviation from regression analyses (for the ε values) or multiple measurements.

Upon irradiating of solutions of all the compounds in dichloromethane with UV light (256 nm), bands increased in the 550-650 nm region of the visible spectrum accompanied by a decrease and red-shifting of peaks in the UV region (Figure 3.2). These are due to the simultaneous loss of aromaticity of the thiazole rings and the formation of a planar π-conjugated structure at the center of the molecule. Similar peaks centered around 600 nm were observed for the closed forms, with a fine structure appearing for those of **3.4*c*** and **3.6*c*** similar to that reported for **3.2*c***. All these compounds displayed clear isosbestic points at about 350 nm, supporting the well-defined two-component reaction in Figure 3.1. No marked spontaneous bleaching was observed in the colored solution at room temperature similar with unfunctionalized diarylethene derivatives. Molar absorption coefficients of both open and closed forms of respective derivatives of **3.1** and **3.2** are similar within 4% relative standard deviation. The bulky electron-donating *tert*-butyl groups and electronegative chlorine atoms do not seem to affect the electronic structure of the molecules.

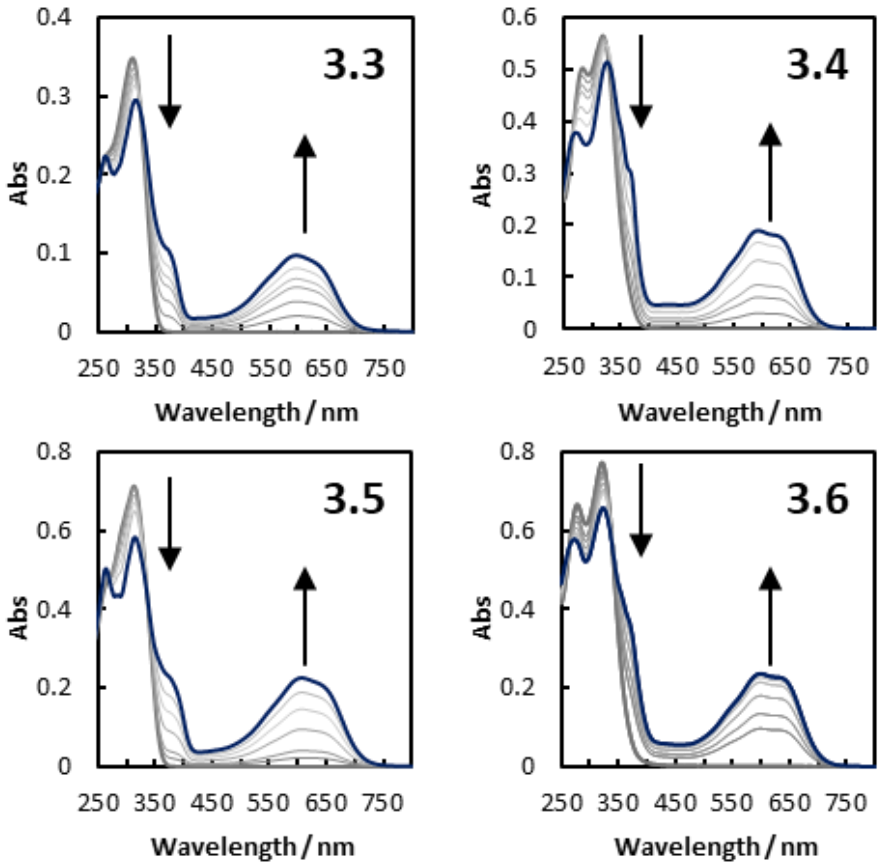

Figure 3.2. Changes in spectra of terarylenes upon illumination of UV-light (254 nm) in dichloromethane solvent. Spectra in blue shows photostationary state.

It can be noted that the photocyclization quantum yield of **3.1*o*** and its derivatives slightly decreased to around 95 % from 98 % reported in reference 1. It is suspected that solvent polarity caused a small disruption to the intramolecular CH-π interactions as previously mentioned. The ^{1}H-NMR signal responsible for H-bonding (labeled h in Scheme 3.2) is well resolved in nonpolar solvents such as toluene but mixes with other aromatic proton signals in dichloromethane (Figure 3.3a). This may be

due to solvent effects on the spectra. Meanwhile, ^{1}H-NMR signals of two methyl groups are indistinguishable in nonpolar solvents but are split in polar solvents. X-ray crystal structure and DFT calculations of **3.1*o*** show that: (1) the aromatic rings are skewed from each other's planes so that there is no communication among them by π-conjugation and; (2) the closeness of the methyl groups to the aromatic thiazole planes associates with CH-π interactions.[1] Due to these reasons, the methyl protons are chemically equivalent in the ^{1}H NMR spectra of anti-parallel conformation. The observed resolution of methyl peaks in dichloromethane therefore suggests a disruption of the structure that dissymetrizes methyl protons. These observations are similar to when intramolecular forces are disrupted by heating or when measuring the spectra in H-bonding-disruptive solvents such as methanol.[1] Given that it is also known that weak CH-π interactions are easily affected by solvent polarity, the small change in photocyclization quantum yield must be due to disruption of these interactions.

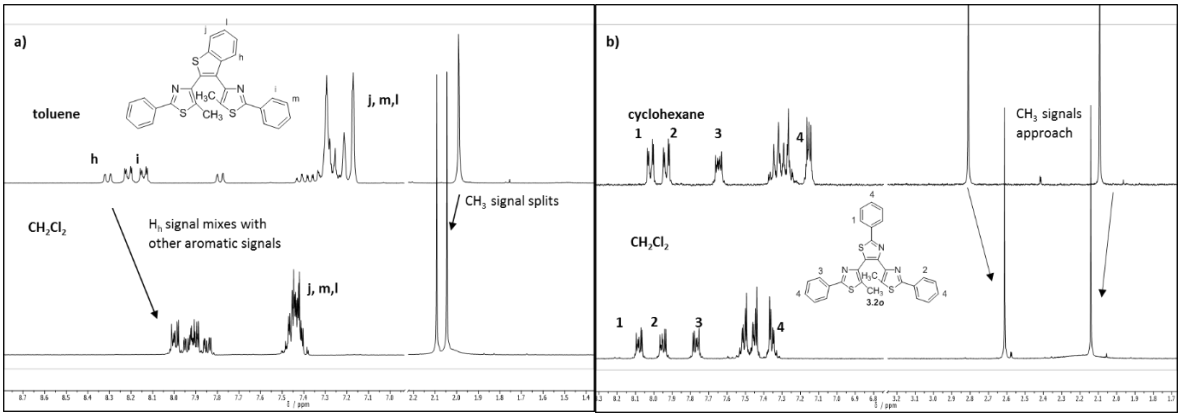

Figure 3.3. ^{1}H NMR spectra of (a) **3.1*o*** and (b) **3.2*o*** in nonpolar vs polar solvents.

On the other hand, photocyclization quantum yields of **3.2*o*** and its derivatives slightly increased to 50 %. A similar comparison of NMR spectra in cyclohexane and in dichloromethane showed no difference in the aromatic peaks. On the other hand, methyl peaks are closer to each other (Figure 3.3b). Consequent to the analysis above, the slightly stronger CH_3-aryl interactions may have contributed to a slight shift of the equilibrium between the reactive anti-parallel conformation and the non-reactive parallel conformation to the reactive one.

3.3 DFT calculations and prediction of multiple forms

Due to the mentioned loss of aromaticity in the ***c*** forms, they are generally less stable than the ***o*** forms. This was confirmed by performing geometry optimizations of these two forms by using the Gaussian 09 suite of programs.[18] We used the functional B3LYP with basis set 6-31G(d,p). Geometry optimizations in the gas phase of the reactive conformations of the open forms and of the closed forms were first performed with zero-point correction. IR spectra calculations showed no negative vibrations, ensuring that calculated energies corresponded to absolute minima. The relative stabilities between the two forms of these compounds are similar across the derivatives of compounds **3.1*o*-*c*** and **3.2*o*-*c*** (Figure 3.4). The ***c*** forms of compounds **3.1**, **3.3**, and **3.5** are destabilized by ~600 meV relative to that of their respective ***o*** forms. Meanwhile, the relative stabilities of the ***c*** and ***o*** forms of **3.2**, **3.4**, and **3.6** differ by ~700 meV.

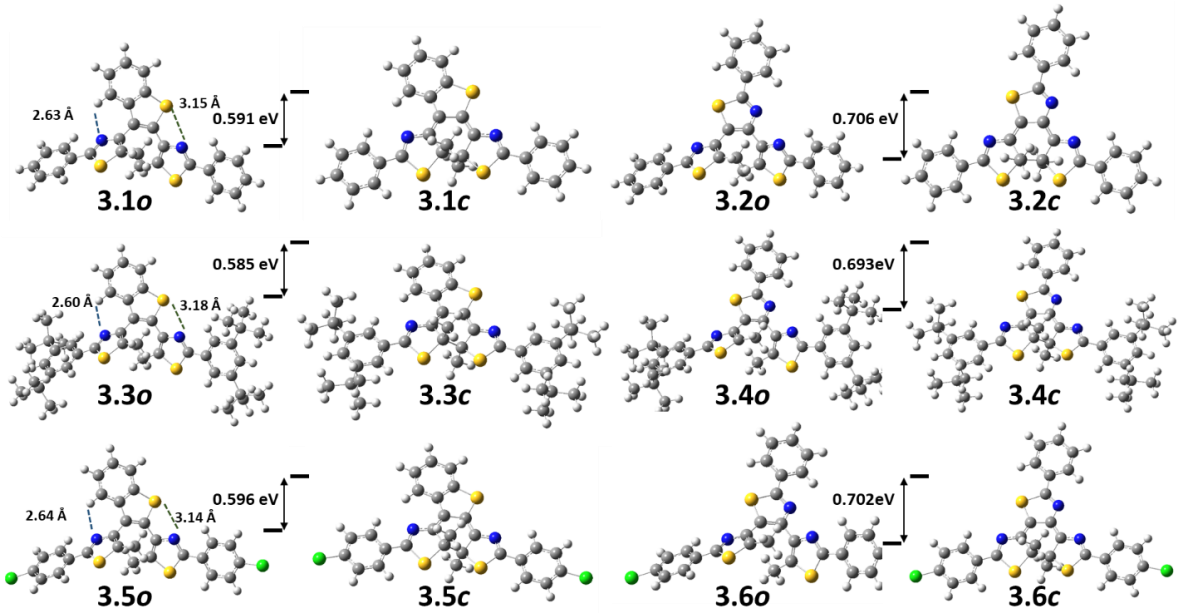

Figure 3.4. Relative stabilities of the ***o*** and ***c*** forms from the geometry optimizations of the structure. The functional B3LYP with basis set 6-31G(d,p) in vacuum using the Gaussian 09 program was used.

After the geometry optimizations, we did TD-DFT to predict the absorption spectra of all compounds. These predict the observed λ_{max} values quite well (Table 3.1). It is noteworthy that TD-DFT calculates similar absorption spectra for corresponding molecules whether or not the auxiliary *tert*-butyl or chloro groups were attached (Figure 3.5).

To gain insight about the observed photochemistry observed and predict the behavior of molecules under vacuum, a closer look at the geometry of the compounds is needed. Similar results as published for **3.1*o***[1] were obtained for its derivatives. For **3.5*o***, the distance between the sulfur atom of the benzothiophene moiety and the nitrogen of the side-thiazolyl group was 3.14 Å while the interatomic distance between H_h (Scheme 3.2) and the other side-thiazolyl N was 2.64 Å. Interestingly, the S-N and N-H distances for **3.3*o*** were slightly different at 3.18 Å and 2.60 Å respectively (Figure 3.4, **3.3*o***). This could be due to a slight twisting of the C-C bonds between the thiazolyl and phenyl moieties to avoid steric hindrance. All measurements were smaller than the sum of the van der Waals radii of the respective atoms involved (3.35 Å for S-N and 2.75 Å for N-H). All these measurements indicate that the strong intramolecular interactions involved in keeping **3.1*o*** in its reactive conformation are maintained for its derivatives **3.3*o*** and **3.5*o***. This rationalizes the similarly high photocyclization quantum yields observed for these three compounds. Similarly, the geometries of reactive conformations of **3.4*o*** and **3.6*o*** are relatively the same to that of **3.2*o*** (Figure 3.4). These calculations showed that the peripheral groups, including the bulky *tert*-butyl groups, have little effect on the geometry, energy, and thus the photochemistry and switching properties of the molecules.

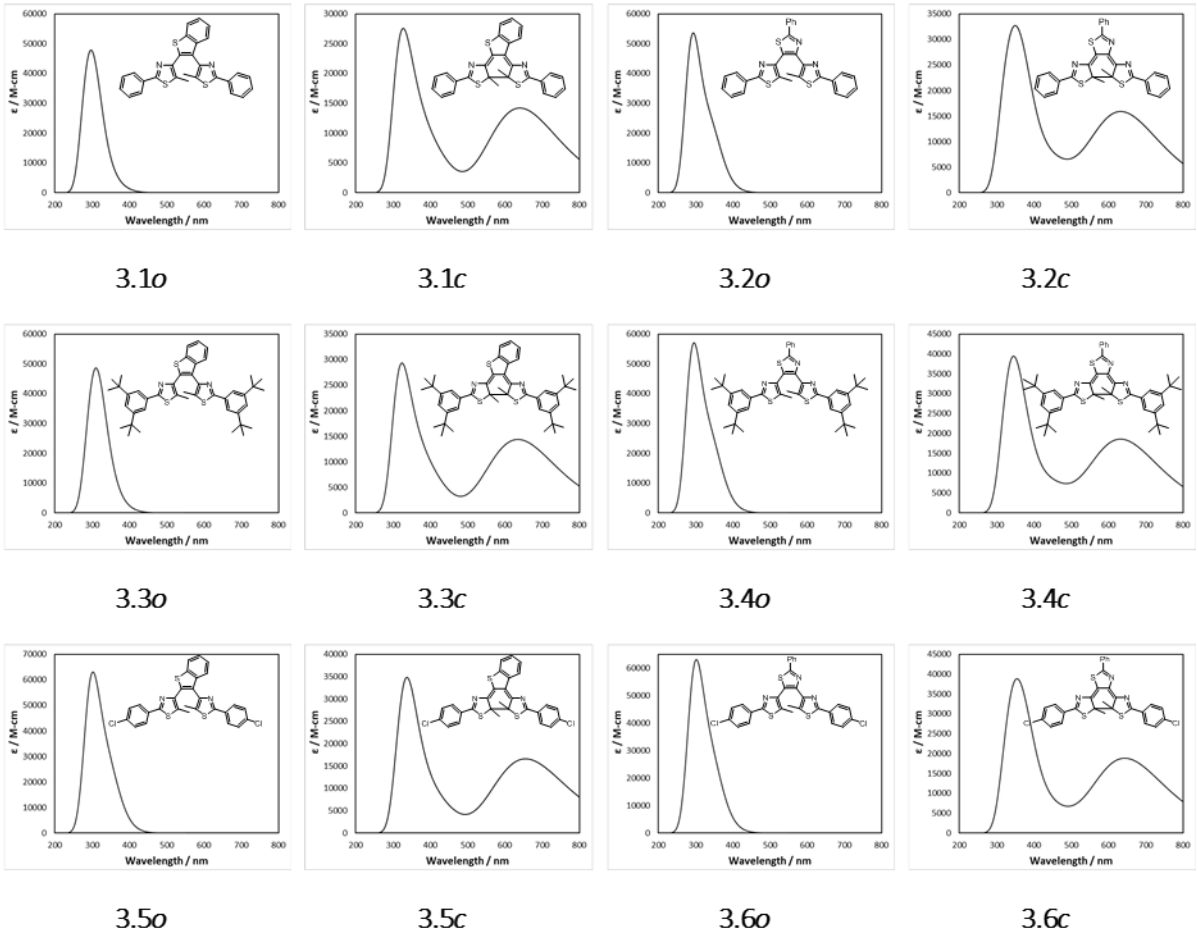

Figure 3.5. Predicted UV-Vis absorption spectra of the ***o*** and ***c*** forms of the compounds by the software Gaussian 09. TD-DFT calculations set to solve up to N = 10 states in vacuum were used to predict the spectra of the molecules optimized in Figure 3.3.

To probe further how molecules would behave under UHV, DFT calculations were employed for the molecules with *tert*-butyl groups in the periphery, **3.3*o*** and **3.4*o*.** We investigated the equilibrium between the parallel and anti-parallel conformations in vacuum by rotating the dihedral angles involved and calculating the energies of DFT-optimized structures (Figure 3.6a). For **3.3*o***, the dihedral angle between the benzothiophene and one of the 2-phenylthiazolyl moieties was rotated. Torsional energy scans yielded three minima: the first one corresponds to the anti-parallel conformation which has both the S-N and N-H interactions (**3.3*o***-C_0); the second one preserved only the N-H (**3.3*o***-C_1) and; the last one only the S-N interaction (**3.3*o***-C_2 Figure 3.6) Then, the structures of these minima were further geometry-optimized by the same method as above. The lack of S-N interactions in **3.3*o***-C_1 caused a destabilization of 7.8 kJ/mol (81 meV) while the lack of the stronger N-H interactions in **3.3*o***-C_2 caused a destabilization of up to 9.3 kJ/mol (96 meV). Using the calculated energy differences of the conformations and following the Boltzmann equation, we predict that 93.7 % of the population of molecule stays in the reactive C_0 conformation at room temperature in vacuum. This goes down to 77.8 % at elevated temperatures (250°C) necessary for sublimating the molecule during vacuum-deposition of samples for STM measurements (Table 3.2). It is therefore expected, due to surface deposition that exposes the molecule to higher temperatures, that STM images of **3.3*o*** may reveal more than one conformation of the molecule.

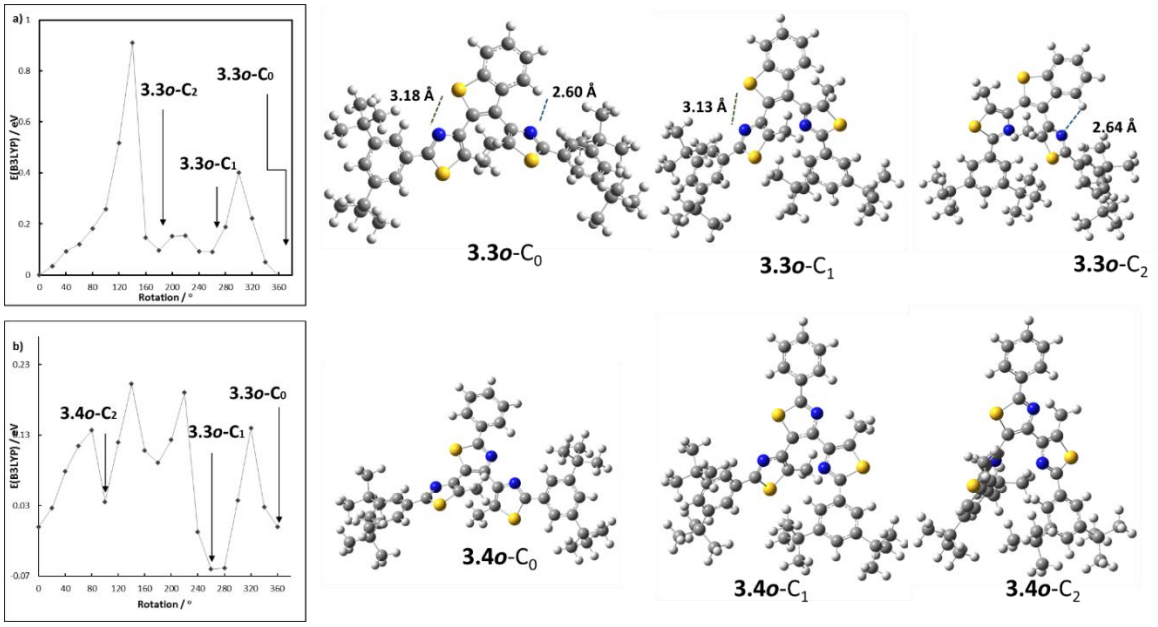

Figure 3.6. Rotational scan of relevant torsion angles and optimized structures of the minima found for a) **3.3*o*** and b) **3.4*o***.

Table 3.2 Boltzmann distribution of conformers of **3.3*o*** and **3.4*o*** in the gaseous state at different temperatures.

Temp / K	Population in %					
	3.3*o*-C_0	**3.3*o***-C_1	**3.3*o***-C_2	**3.4*o***-C_0	**3.4*o***-C_1	**3.4*o***-C_2
298.15	94	4	2	6	89	5
523.15	78	13	9	16	71	14

For **3.4*o***, the geometry-optimized energy of the reactive conformation (**3.4*o***-C_0) was found to lie between those of two non-reactive conformations (**3.4*o***-C_1, C_2 Figure 3.6). Thus, the ratio of species found in the reactive *vs* non-reactive conformation are switched relative to those of **3.3*o***. Majority of the molecules (89 %) are in the non-reactive conformation at room temperature in vacuum. This is an extension of the behavior in solution in which most of the molecules adopt this non-reactive conformation as evidenced by low photocyclization quantum yields. This goes down to 70.7 % once temperature is increased. This predicts that the majority of the molecules would be in the non-reactive conformation once deposited on a solid surface.

3.4 Preliminary STM results

To probe the impact of *tert*-butyl groups on STM images, we performed initial STM experiments under low-temperature ultra-high vacuum conditions on compounds **3.1*o*** and **3.3*o***. We have chosen **3.1*o*** and its *tert*-butyl derivative **3.3*o*** for the first experiments because DFT predictions and photocyclization quantum yields indicate that majority of the molecules would remain in the reactive conformation.

Samples were first deposited onto a W filament by immersion in a dichloromethane solution of the compound. After drying, the filament was heated to about 523 K for sublimation molecules.

Successful deposition of **3.1*o*** was observed on a Ag(111) substrate which was cooled down to 4.5 K. As shown in Figure 2.7, the molecule appeared as a unique and almost large circular bright spots and no discernible structure was found. This symmetric shape did not reveal the fine structure of the molecule.

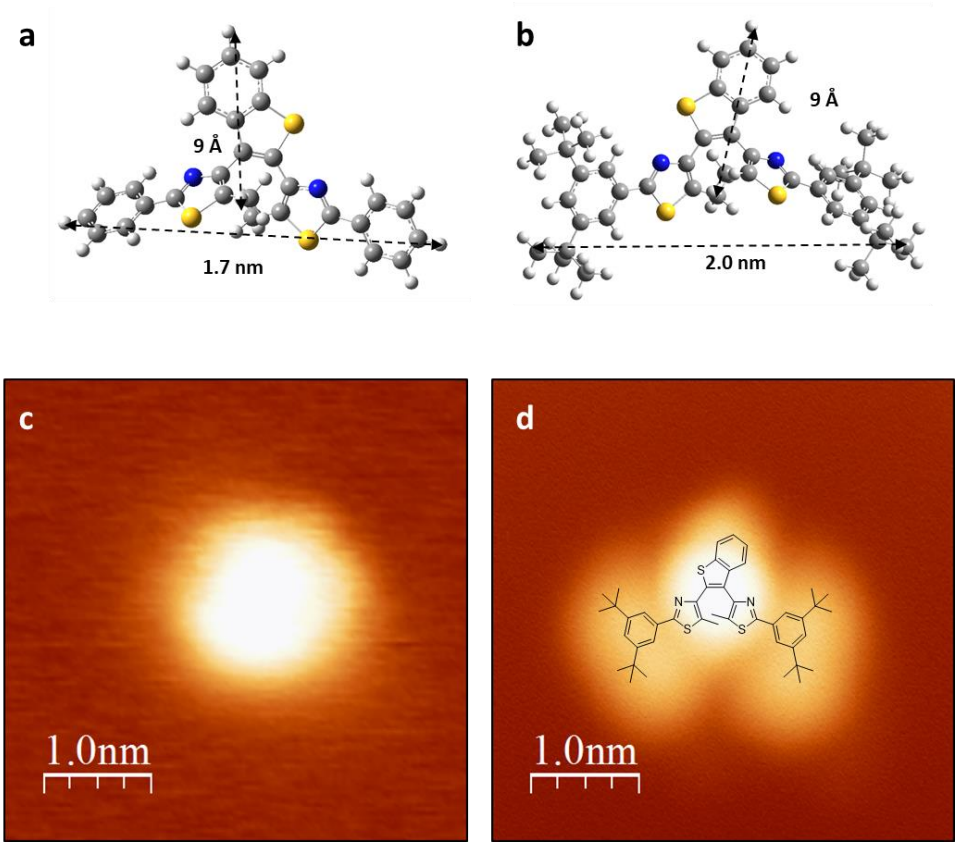

Figure 3.7. DFT-optimized structure of (a) **3.1*o*** and (b) **3.3*o*** with measured interatomic distances. The arrows start and end with the specific atoms in which measurements were done. (c) Deposition of **3.1*o*** on Ag(111) produced bright spots with no apparent fine structure. (d) Deposition of **3.3*o*** on Ag(111) revealed a much more resolved structure which show prominent circular lobes characteristic of *tert*-butyl groups.

The bright contrast could be partly due to a strong physisorption of the molecule on the surface as well as a continuous electronic density throughout the molecule due to π-conjugation. In the optimized structure of **3.1*o*** (Figure 3.7a), the distance between the hydrogens in the 4-position of the phenyl groups is 1.7 nm, which is considerably larger than the observed size of 1.2nm (Figure 3.7c) as measured by line scans. This claim about the electronic structure of the molecule and the anomalous size of the spot could have been explained by how the STM tip approaches the molecule on the surface, i.e., its surface configuration upon adsorption. However, the lack of geometric information on the STM image renders this impossible.

Sublimation of **3.3*o*** on the other hand showed a bright spot and four lobes skewed around it (Figure 3.7d). The distance between these spots are approximately 2.2 nm. The width of the central bright spot is 9 Å. These measurements correspond well with DFT calculations on **3.3*o*** that place the distance between respective *tert*-butyl groups at 2.0 nm and between the benzo-group of the

benzothiophene moiety and the methyl groups at 9 Å (Figure 3.7b). Based on DFT predictions, we propose that the peripheral lobes correspond to *tert*-butyl groups, consistent with previous STM observations of molecules with *tert*-butyl groups.[8-9] The central bright spot could correspond to the central aromatic structure of the molecule. Aside from π-conjugation due to the aromatic rings, the sulfur atoms which are known to interact well with silver contribute to the bright contrast. Moreover, at least two other conformations of the molecule were observed on the same surface. This is consistent with DFT calculations that predict different conformations on the surface. (A more detailed discussion of the images and their conformations on the surface will be discussed in Chapter 5.)

3.5 Conclusions

In this chapter, we selected highly sensitive terarylenes for STM studies. **3.1*o*** was selected for its photon quantitative cyclization while **3.2*o*** was chosen because its ***c*** form undergoes highly efficient oxidative cycloreversion reaction. We further modified them with *tert*-butyl (**3.3*o*** and **3.4*o***) and chlorine groups (**3.5*o*** and **3.6*o***) as the former was shown to display bright spots in STM studies and the latter could aid in the formation of assemblies through dipole interactions. Since we had placed these groups in the periphery of the molecules, they preserved the photochemical, switching, and thus the electronic properties of the compounds.

Although oxidative cycloreversion experiments were not done on the derivatives of **3.2*o*** (**3.4*o*** and **3.6*o***), we believe that due to the similarities in the photochemical properties of the three molecules such compounds should likewise undergo efficient oxidative cycloreversion. Also, even if this oxidative chain reaction process could be improved further by attachment of phenyl groups as we have shown in the first chapter, we decided not to since such bulky attachments on the reactive carbons could lower photocyclization quantum yields.

Moreover, we showed in this chapter that this family of compounds have majority of its population (in solution and ingaseous state) in the non-reactive conformation. We therefore chose **3.1*o*** and **3.3*o*** for initial STM experiments because majority of their population is expected to be in the reactive conformation. We showed that the introduction of *tert*-butyl groups did aid in the identification of the molecule on the surface. From these two molecules alone, many new interesting phenomena could be observed. The next couple of chapters will focus on the STM studies of these two molecules.

3.6 References

[1] S. Fukumoto, T. Nakashima, T. Kawai, Photon-quantitative reaction of a dithiazolylarylene in solution, *Angew. Chem. Int. Ed.* 2011, *50*, 1565-1568.

[2] T. Nakashima, Y. Kajiki, S. Fukumoto, M. Taguchi, S. Nagao, S. Hirota, T. Kawai, Efficient oxidative cycloreversion reaction of photochromic dithiazolythiazole, *J. Am. Chem. Soc.* 2012, *134*, 19877-19883.

[3] J.P. Calupitan, T. Nakashima, Y. Hashimoto, T. Kawai., Fast and efficient oxidative cycloreversion reaction of a π - extended photochromic terarylene, *Chem. Eur. J.* 2016, *22*, 10002-10008.

[4] J. K. Gimzewski, C. Joachim, R. R. Schlittler, V. Langlais, H. Tang, I. Johannsen, Rotation of a single molecule within a supramolecular bearing, *Science* 1998, *281*, 531-533.

[5] M. Schunack, L. Petersen, A. Kuhnle, E. Laegsgaard, I. Stensgaard, I. Johannsen, F. Besenbacher, Anchoring of organic molecules to a metal surface: HtBDC on Cu (110), *Phys. Rev. Lett.* 2001, *86*, 456-459.

[6] F. Chiaravalloti, L. Gross, K. H. Rieder, S. Stojkovic, A. Gourdon, C. Joachim, F. Moresco, A rack-and-pinion device at the molecular scale, *Nat. Mater*. 2007, *6*, 30-33.

[7] H.P. Jacquot de Rouville, R. Garbage, R.E. Cook, A.R. Pujol, A.M. Sirven, G. Rapenne, Synthesis of polycyclic aromatic hydrocarbon - based nanovehicles equipped with triptycene wheels, *Chem. Eur. J.* 2012, *18*, 3023-3031.

[8] M. Alemani, M. V. Peters, S. Hecht, K. H. Rieder, F. Moresco, L. Grill, Electric field-induced isomerization of azobenzene by STM, *J. Am. Chem. Soc.* 2006, *128*, 14446-14447.

[9] M. Alemani, S. Selvanathan, F. Ample, M. V. Peters, K. H. Rieder, F. Moresco, C. Joachim, S. Hecht, L. Grill, Adsorption and switching properties of azobenzene derivatives on different noble metal surfaces: Au (111), Cu (111), and Au (100), *J. Phys. Chem. C* 2008, *112*, 10509-10514.

[10] T. K. Shimizu, J. Jung, H. Imada, Y. Kim, Supramolecular assembly through interactions between molecular dipoles and alkali metal ions, *Angew. Chem. Int. Ed.* 2014, *53*, 13729-13733.

[11] B. Baris, V. Luzet, E. Duverger, P. Sonnet, F. Palmino, F. Cherioux, Robust and open tailored supramolecular networks controlled by the template effect of a silicon surface, *Angew. Chem. Int. Ed.* 2011, *50*, 4094-4098.

[12] Y. Makoudi, B. Baris, J. Jeannoutot, F. Palmino, B. Grandidier, F. Cherioux, Tailored molecular design for supramolecular network engineering on a silicon surface, *Chem. Phys. Phys. Chem.* 2013, *14*, 900-904.

[13] M. Begtrup, L. B. L. Hansen, New methods for the introduction of substituents into thiazoles, *Acta Chem. Scand.* 1992, *46*, 372-383.

[14] G. Gavrel, P. Yu, A. Leaustic, R. Guillot, R. Metivier, K. Nakatani, 4, 4′ -Bithiazole-based tetraarylenes: new photochromes with unique photoreactive patterns, *Chem. Commun.* 2012, *48*, 10111-10113.

[15] T. Nakashima, K. Atsumi, S. Kawai, T. Nakagawa, Y. Hasegawa, T. Kawai, Photochromism of thiazole - containing triangle terarylenes, *Eur. J. Org. Chem.* 2007, *19,* 3212-3218.

[16] T. Nakashima, K. Imamura, K. Yamamoto, Y. Kimura, S. Katao, Y. Hashimoto, T. Kawai, Synthesis, structure, and properties of α, β - linked oligothiazoles with controlled sequence, *Chem. Eur. J.* 2014, *20*, 13722-13729.

[17] O. Galangau, T. Nakashima, F. Maurel, T. Kawai, Substituent effects on the photochromic properties of benzothiophene-based derivatives, *Chem. Eur. J.* 2015, *21*, 8471-8482.

[18] M. J. Frisch, *et al*, *Gaussian 09 Revision A.02*, Gaussian Inc. Wallingford CT, 2009. (See section 7.4 for complete citation.)

Chapter 4
STM tip induced assembly of terarylenes

STM can address molecules either in supramolecular two-dimensional (2D) assemblies or at the single molecular level. Equipped with an array of candidate molecules for STM studies, we start with STM studies of highly sensitive terarylenes in 2D assemblies which could be useful for applications such as photovoltaic devices and molecular circuits. In this chapter, we present a new bottom-up approach to form such assemblies on surfaces by a technique that utilizes an electric field induced between the STM tip and the surface. These results were published in the article:

> *Scanning Tunneling Microscope Tip-Induced Formation of a Supramolecular Network of Terarylene Molecules on Cu(111),* by J.P.D.C. Calupitan, O. Galangau, O. Guillermet, R. Coratger, T. Nakashima, G. Rapenne, and T. Kawai, in *J Phys. Chem. C* 2017*, 121,* 25384-25389*.*

4.1 Electric field as stimulus for assembly formation

Bottom-up approaches relying on supramolecular interactions are foundations for new molecular-scale machines, switches, and other nanoscale energy transfer devices.[1] For photovoltaic or molecular circuit applications, it is necessary to address candidate molecules or supramolecular structures on a solid surface so that enormous research attention is focused on supramolecular interactions and functions in 2D assemblies.[2-3] These studies deal with one less dimension than that of solution-based supramolecular chemistry. That is, whereas for a (supra)molecule in three-dimensional space, there are three degrees of freedom for translational motion and two or three for rotation (depending on the shape of the molecule), these are each reduced by one in two-dimensions due to the hindrance induced by the solid surface. In this sense, the solid substrate affords an orientation to the system under study.[2] However, the presence of such surface also necessitates other considerations such as new symmetry elements and surface-molecule interactions.[2-3]

In addition, developments in real-space imaging of periodic 2D networks via the scanning tunneling microscope (STM) coupled with other techniques allowed deeper understanding of molecule-molecule and molecule-substrate interactions.[1-3] Due to these, new techniques to induce the formation of surface supramolecular assemblies have recently been developed. These include: (1) chemical modification to control molecule-molecule and molecule-surface interactions;[2-3] (2) codeposition of metal ions that could reorient molecules through dipole interactions;[4] and (3) surface annealing that gives molecules enough energy to reconfigure and form assemblies.[5-6]

Aside from being a powerful tool to precisely address molecules and their interactions, the STM may also induce an electric field between the tip and the scanned surface. This has been shown to play a major role in the rotation of molecular networks[7-9] and chemical reactions.[10] Meanwhile, in solution chemistry, it is well-known that due to the polarizability of polar molecules in a nonpolar solvent, they realign their dipole moment along field lines upon application of an external electric field. From the works of Debye and Guggenheim,[11-12] experimental methods based on this phenomenon are available

in order to calculate the dipole moment of a molecule.[13-14] The electric field applied by the tip of a scanning tunneling microscope (STM) therefore can be a potential trigger to induce the ordering of molecules on a surface. External electric field-induced molecular reorientation in a molecular junction was first predicted in 2002.[15] Thereafter, subsequent studies focused on consequent conductance modulation to demonstrate single molecular switching capabilities.[16-17] To the best of our knowledge, this electric field has not been applied yet on large numbers of molecules which could realign in one direction, allowing for intermolecular forces to take over and form a stable supramolecular network. A couple of recent works come close to this but the ordering of assemblies was induced by hot tunneling electrons. In one, the hot electrons coming from the STM tip to the surface were shown to induce surface phase changes of an assembly of a dipolar perylene derivative[18] while in another, transition from disordered to an ordered assembly was induced by injecting hot electrons onto the surface.[19]

This chapter focuses on the formation of on-surface molecular networks of compound **3.1*o*** shown on Figure 4.1. Diarylethene assemblies in the solid-liquid interface[20-26] and self-assembled monolayers of terarylenes[27-28] have been reported at the solid-liquid interface. Meanwhile, under ultra-high vacuum conditions, diarylethenes were assembled only through dipole-dipole interactions[29-30] and ion-dipole interactions.[4] For terarylenes, this is the first of such report on surface assemblies under ultra-high vacuum conditions.

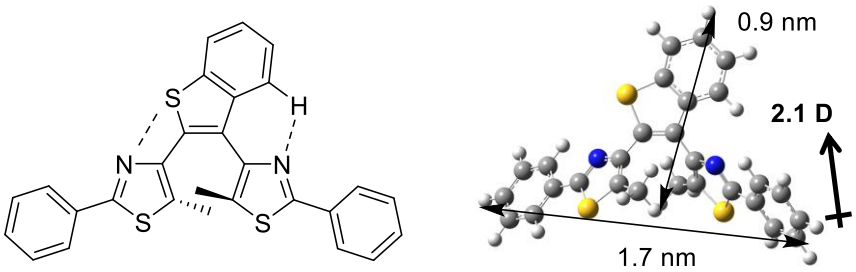

3.1*o*

Figure 4.1. Skeletal and ball-and-stick model of the molecule **3.1*o*** (2,3-dithiazolylbenzothiophene) The structure and the dipole moment was calculated by Gaussian 09. The functional B3LYP with basis set 6-31G(d,p) was employed.

4.2 Choice of molecule

3.1*o* has been selected because of its promising switching sensitivity to light stimulus in solution and solid states.[31] Figure 4.1 shows the molecular structure and the gas-phase DFT-optimized geometry. Due to several intramolecular forces that lock it in its reactive conformation, **3.1*o*** displayed photon quantitative reaction with photocyclization quantum yield close to unity in solution.[31]

Furthermore, the combination of two thiazoles and one benzothiophene subunit (Figure 4.1) is most likely at the origin of an important intrinsic dipole moment (2.1 D) which could be manipulated with an external electric field. We show in this chapter that the application of an external electric field through a bias pulse from an STM-tip could induce the spontaneous formation of assemblies of molecules without any solvent under ultra-high vacuum conditions.

3.1*o* was synthesized as previously reported.[33] STM experiments were performed in an Omicron low-temperature scanning tunneling microscope (LT-STM) working at a base pressure of 1.5 x 10^{-11} mbar on single-crystalline Cu(111). A dichloromethane solution of the terarylene was first

deposited on a W wire 0.15 mm in diameter and then subjected to high-temperature degassing under UHV. The molecules present on the filament were sublimated at about 200 °C while the Cu substrate was kept at 77 K. These sublimation conditions usually minimize the decomposition of molecules. STM-tips were 250 µm diameter tungsten wires prepared by electrochemical etching. Tip quality was confirmed by observing the characteristic surface state of Cu(111) at 400 meV below the Fermi level through tunneling spectroscopy. All bias voltages reported refer to the surface relative to the tip. All images were taken at 77 K under constant current mode and processed by WSxM.[34]

4.3 Controlled formation of assemblies

Deposition of molecules (up to 20 % monolayer coverage) resulted in STM images with fuzzy objects moving below the tip particularly close to the step edges (Figure 4.2a). The streaking patterns show movement of molecules during scans. Although a couple of columns of seemingly ordered structure could be found (Figure 4.2a white arrow), line scans of the island of these fuzzy objects show generally no long-range order (Figure 4c-e). Deposition was repeated under similar conditions several times and no long-range order was found.

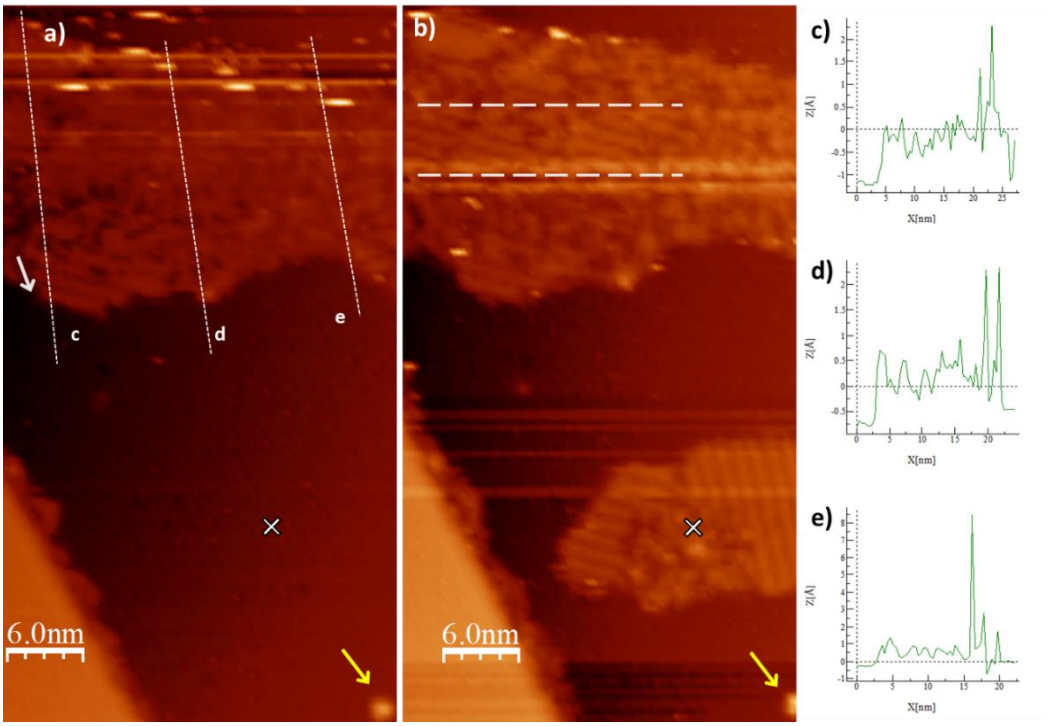

Figure 4.2. a) Islands of fuzzy objects moving on the surface or close to the tip. The yellow arrow points onto an adatom as a landmark. White arrow points to partially formed rows with no long-range order. Dotted lines labelled *c*, *d*, and *e* are line scans shown on c-e. b) After application of a bias pulse on the point indicated by a white cross, a new ordered island appeared at the bottom of the image. Some order was also induced in the island above (gray lines), but the induced electric field seemed not enough to overcome already high entropy in such a disordered island. Imaging conditions: -1.0 V at 1pA.

Then, the STM tip was retracted 1 nm from the surface and a controlled bias pulse of 3.0 V for 100 ms was applied and the tip potential was settled back to 0 V. Because of this tip to surface distance during the pulse, no appreciable net current was derived. Subsequent approach of the tip to the surface and imaging at -1.0 V and 1pA shows the formation of islands with well-defined rows of molecules

(Figure 4.2b). The adatom (Figure 4.2a-b, yellow arrows) served as a landmark to ensure that the same region was imaged. Between the dashed white lines on Figure 4.2b, some molecules rearranged to form two ordered rows of molecules. The applied bias pulse seemed to be insufficient to overcome the already highly entropic island of molecules. The surrounding disordered molecules seemed to prevent the formation of long-range order. However, the induced electric field was enough to allow some molecules to move at the lower part of the image and form a more ordered island.

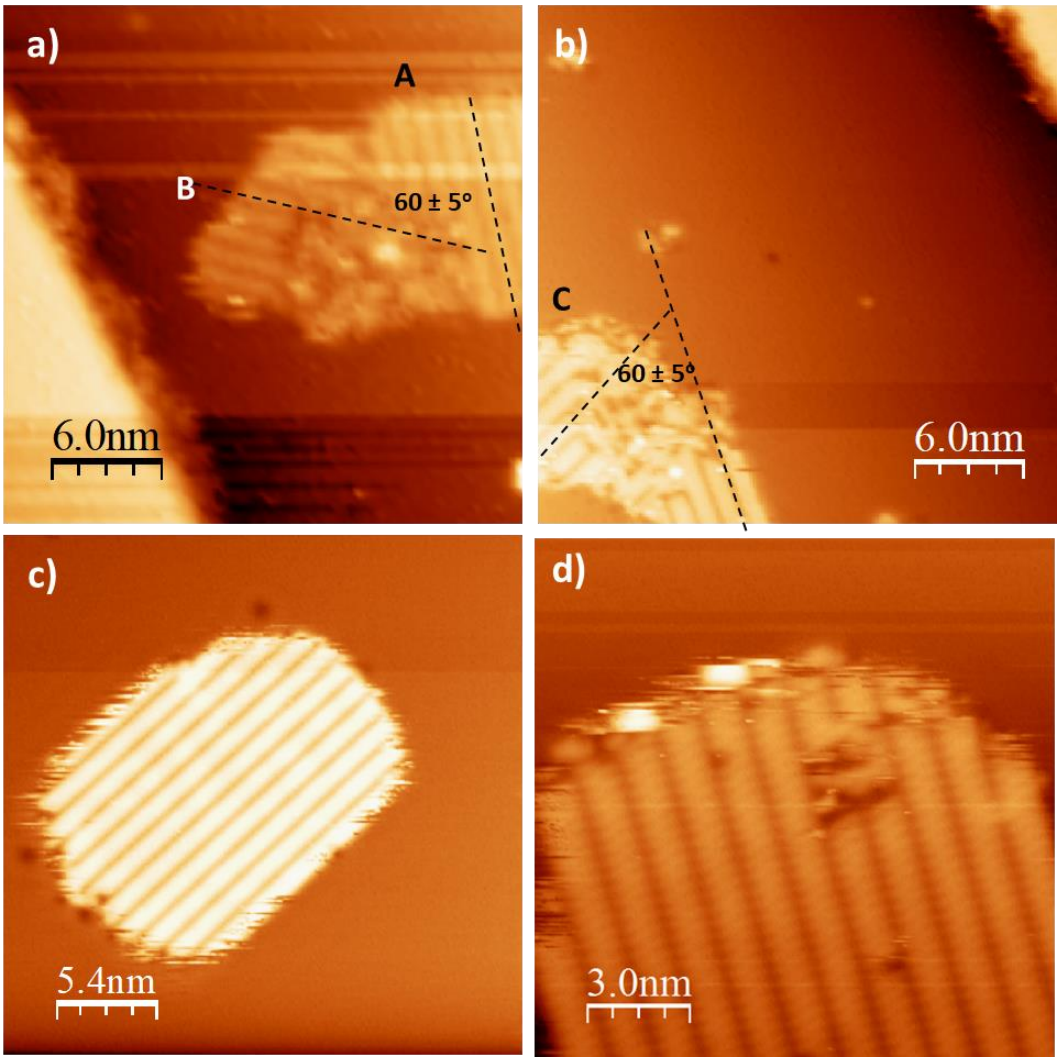

Figure 4.3. a) Extract of island from Figure 4.2b showing two apparent orientations of the ordered regions rotated 60° from each other. b) Experiment repeated on another region showing the other 60° rotation, indicating the influence of the three-fold symmetry of the Cu(111) surface on orienting the assemblies. c-d) Islands of **3.1*o*** assembling in one direction only, showing that long-range order is possible if there is only one direction of formation. Imaging conditions for were -1.0 V, 1pA for c and -1.6 V, 1pA for a,b,d.

The new island has two regions A and B (Figure 4.3a). Both regions are composed of well-defined rows of molecules. As shown by the guidelines on Figure 4.3a, rows of B are oriented 60° counterclockwise relative to those of A. This angle value suggests that the threefold symmetry of the Cu(111) surface plays a role in orienting the assemblies of molecules. This was confirmed by finding an

orientation in the opposite rotational direction relative to region A. Repeating the experiment in other regions yielded exactly this expected outcome. The rows of region C in Figure 4.3b are rotated 60° in the clockwise direction relative to those of A. Only these three orientations were found in all assemblies observed. We found almost equal probabilities of forming orientations A, B, and C.

The disorder between two regions in Figures 4.3 a and b seems to be the direct effect of competition between nucleating sites attempting to expand to a larger domain with longer-range order. When perfectly-ordered islands were formed so that only one orientation of rows was observed, no such disorder was observed over the whole island (Figure 4.3 c,d).

The duration of the bias pulse suggests that the self-assembly formation was very fast relative to the time scale of STM scans. The large tip-surface distance shows that only the applied electric field and not the STM current causes the formation of assemblies. Bias pulses of lower voltages could not induce network formation whereas, at 3 V, the assembly could be induced 90 % of the time. The tunneling current during scanning does not to affect the stable assemblies as there are no spontaneous changes in the assembly during scanning of the islands (Figure 4.3a-c). This is unlike the observation by Niederhausen *et al*., in which a dipolar perylene derivative (with a large dipole moment of 12 D) undergoes phase changes while scanning[18] nor that of Li *et al*. in which tunneling electrons applied over a timescale of minutes induce the formation of assemblies.[19]

The dipole moment (2.1 D) of **3.1*o*** is large enough to be influenced by the 3 V electric field. To compare this to another work, electric-field induced rotational switching of a molecule with a higher dipole moment (8 D) required a bias pulse of only 0.93 V.[7] This is unsurprising as a lower dipole moment would require higher voltages to be influenced by an electric field.

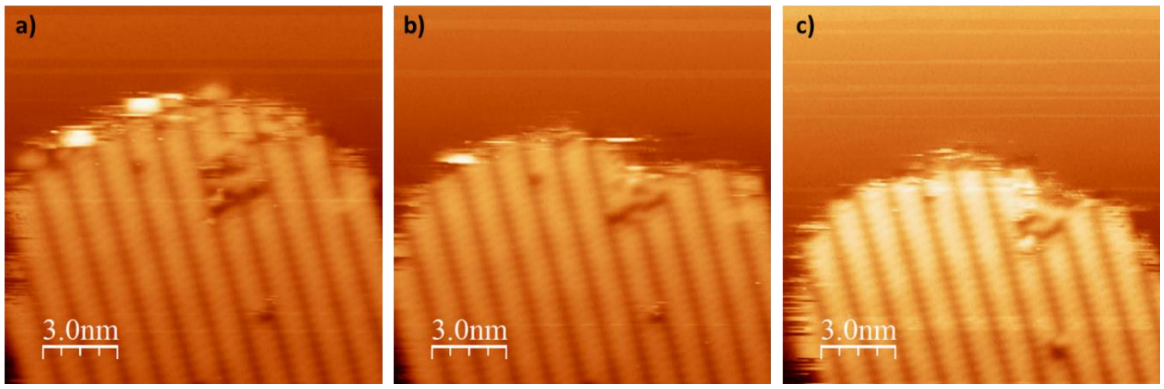

Figure 4.4. Evolution of the assemblies during consecutive scans. The assemblies are stable for several hours even without scanning. Imaging conditions: -1.6 V, 1pA, T = 77 K.

The stability of the network suggests that the intermolecular forces among molecules are strong enough to hold the assemblies at this temperature. However, streaking patterns at the peripheries indicate that molecules in these regions are more mobile than those in the interior of the island (Figure 4.4a). As expected, subsequent scans showed the disappearance of some molecules at the edge of the islands due to less neighbors that contribute to the stability (Figure 4.4a-c). It must be noted, however, that consecutive scans are not necessary for the stability of the islands as the tunneling

current do not have an effect on the assemblies. The assemblies could be reformed upon reapplication of a bias pulse. Interestingly, application of a negative bias pulse did not result in any distortion of the networks.

This method for inducing the formation of assembly is also different from that reported by Rabe, Müllen, and co-workers, in which an assembly was induced by application of an external electric field parallel to the surface during liquid deposition and subsequent drying.[35] This uses the same well-known phenomena as electric-field alignment in a nonpolar solvent.[11-14] In our system, the assemblies were formed without any solvent under ultra-high vacuum conditions.

This is a clear sign that, between the assembly and the surface, there is only weak interaction and no covalent bond nor charge transfer is happening upon deposition. Further, we discount the possibility of degradation of molecules because we did not observe any fragments of molecules before and after the bias pulse. Such fragmentation would have caused heterogeneity in the network and prevented the formation of regular assemblies which is not the case. Also, it has been shown that, after a few hours, the network slowly becomes disordered with some molecules diffusing on the surface. Then, application of a new pulse regenerates the self-assembled monolayer. This reproducibility would have been impossible to achieve if the molecule had been previously destroyed by the pulse.

The molecular network has the following packing dimensions: a = 1.42 ± 0.04 and b = 0.35 ± 0.01 nm with an oblique lattice (Figure 4.3d). These correspond well, respectively, with the distance between the terminal hydrogens in Figure 4.1 and typical π-π stacking interaction distances. The ***a*** vector is aligned to the $[\bar{1}10]$ direction on the Cu(111) surface. A typical pulse produces islands with an average size of 300 ± 80 nm^2 stable for several hours.

In the solid-liquid interface, typical distances between neighbouring diarylethenes stabilized by van der Waals forces between long alkyl groups are in the 1.0 – 1.5 nm range.[21-27] Since the observed intermolecular distance in this supramolecular network (distance **b** in Figure 4.5) is far lower (0.35 nm instead of 1.0 – 1.5 nm) and the molecules do not harbor these long alkyl groups but only aromatic rings, we postulated π-stacking interactions as the main intermolecular interactions stabilizing the assemblies. This was confirmed by a molecular mechanics calculation (Materials Studio 7.0) of π-stacking conformation between two molecules predicting a stacking distance of 0.34 nm (Figure 4.6). Due to the S-N and N-H interactions that contribute to the rigid structure of the molecule[31], the planes of the side 5-methyl-2-phenyl-thiazol-4-yl moieties are almost parallel to each other so they could stack neatly to neighbouring molecules. Dihedral angles between the benzothiophene and the two left and right thiazolyl moieties have been calculated to be 45° and 55° respectively. The coplanarity of the benzothiophene moiety also contributes to these π-stacking interactions.

For the domain shown on Figure 4.5d, the sulfur atoms of the thiazole rings seem to align with copper atoms on the $[10\bar{1}]$ atoms of the FCC surface. On an FCC unit cell, two copper atoms lying along the corners of one plane are 0.51 nm apart. Meanwhile, the distance between sulfur atoms on thiazole rings are found to be 0.58 nm according to the crystal structure and DFT calculations. This packing explains the three possible domains observed in Figure 4.3 as there are three equivalent directions onto which the sulfur atoms may align. In addition, the ***a*** direction traverses six copper atoms along the $[\bar{1}10]$ direction. Considering an atomic radius of 0.128 nm, the 6 copper atoms have an approximate length of 1.54 nm which corresponds well with the size of ***a*** indicating a clear influence of the surface on assembly formation.

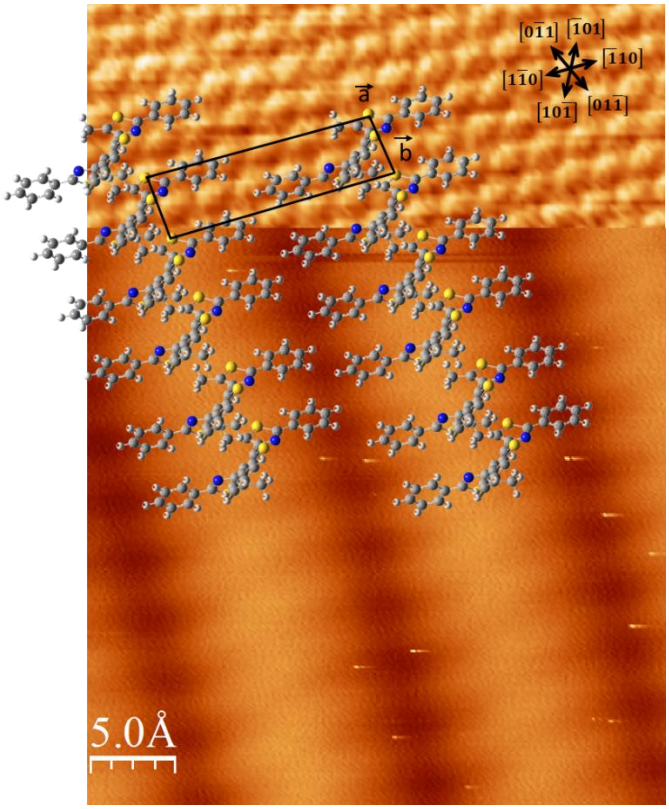

Figure 4.5. Orientation of the molecules as overlayed over the assemblies. Imaging conditions: -1.6 V, 1pA, T = 77 K.

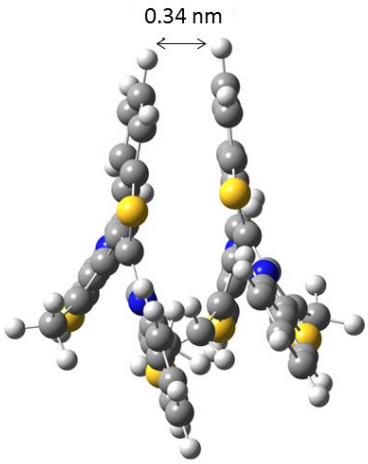

Figure 4.6. Molecular mechanics(Materials Studio 7.0) calculation of π-π interaction stacking distance.

Meanwhile, the average height of the islands was found to be around 0.91 ± 0.04 nm, which is in accordance with the distance between the topmost hydrogen of the benzothiophene moiety and methyl hydrogens in Figure 4.1. With these, the terarylenes seem to stand on the surface through its side phenylthiazole moieties with the benzothiophene moieties sticking out of the surface (Figure 4.5). As expected, the topographically higher and electron-richer heteroaromatic rings contribute more to the contrast of the central part of the molecules than the side phenyl rings.

4.4 Mechanism

Finally, we propose a mechanism by which the molecules assemble under the influence of the STM tip. During deposition, the molecule is first sublimated at about 200°C before it lands on the substrate kept at 77 K. DFT calculations have been performed by doing torsion angle scan on the relevant dihedral angle, and we found out that, other than the conformation C_0 shown on Figure 4.1 where both N-H and S-N interactions are present, the molecule has two other stable conformations C_{N-H} and C_{S-N} where only one interaction is conserved, the N-H or the S-N interaction respectively (Figure 4.7). The former is slightly stronger than the latter. By using the Boltzmann equation, we found out that these other conformations increase in population at the high temperatures of sublimation similar to that reported for molecule **3.3*o*** discussed in chapter 3. (Table 4.1)

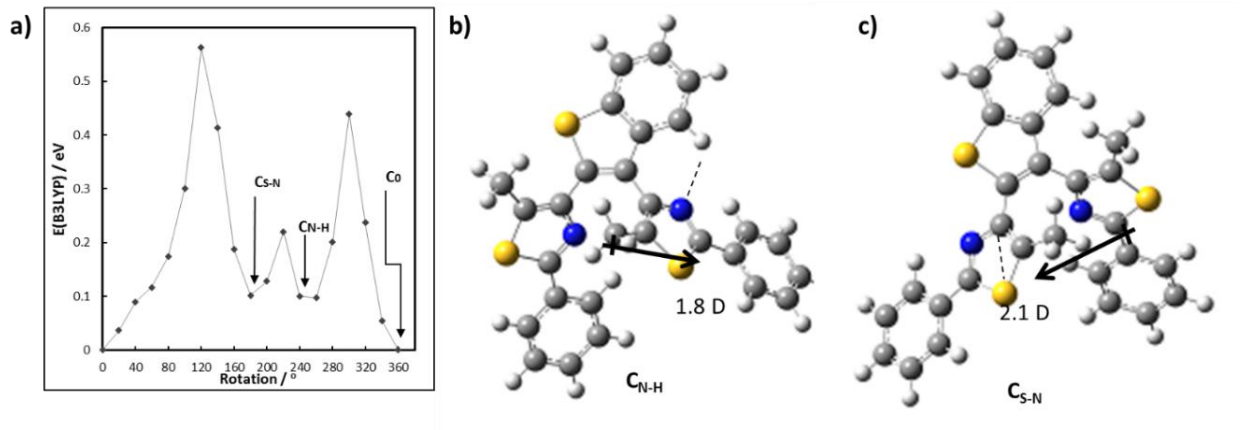

Figure 4.7. a) Rotational scan of of **3.1*o*** showing two other stable conformations C_{N-H} and C_{S-N} kept by N-H and S-N interactions respectively.

So that upon sublimation and subsequent deposition on the surface, a disordered state could be observed. In addition to this, each respective conformation would have different surface-induced conformations depending on their orientation once they land on the surface. Further, molecules seem to have enough energy to allow random motion and slight diffusion. This is evidenced by streaking patterns in some images before the application of a bias pulse (Figure 4.2a). At 77 K, the molecules seem to have enough degrees of freedom to orient to the electric field lines. Further, once stabilized on the surface, the molecules are hindered from rotation not only geometrically (by the surface and the network) but also energetically, as the rotation barriers are 1 to 2 orders of magnitude greater than the thermal energy at this temperature. (Table 4.2) The disordered state upon deposition is proven by the scan lines on Figure 4.2c-e.

Table 4.1 Conformer distribution of **3.1*o*** in the gas phase at room vs sublimation temperature.

	Population in %		
Temp / K	C_0	C_{N-H}	C_{S-N}
298.15	94	4	2
523.15	78	13	9

Table 4.2 Estimated energy barriers for rotation

Rotation	Barrier / eV
C_0 to C_{N-H}	0.439
C_0 to C_{S-N}	0.562
C_{N-H} to C_{S-N}	0.131
C_{N-H} to C_0	0.350
C_{S-N} to C_{N-H}	0.090
C_{S-N} to C_0	0.432
thermal energy (kT) at 77K:	0.002

In our system, bias voltage refers to the potential with respect to the tip, which means that the electric field points to the tip when a positive bias voltage is applied (Figure 4.8). Meanwhile, the dipole moment of the molecule is mainly due to the aromatic thiazole rings with the benzothiophene ring having almost no net charge. Then, the negative end of the dipole moment is located around the center of the triangular molecule coplanar with the nitrogen atoms of the thiazole rings. The diffusive mobility of the molecules on top of the surface is hindered by the electric field; the dipole moments orient themselves parallel to the electrical field and point upward. In this way, the electric field lines and dipole moments realign in the same direction. Induced dipole moment under the applied field seems also to associate cooperatively with the static dipole moment in this field induced orientation. The extended π-conjugation system of the triangular terarylene structure may contribute to the enhanced induced polarizability.

When an electric field is induced by the tip far from the surface, a large number of molecules could be influenced and therefore aligned in one direction according to the direction of their dipole moment. A large number of molecules seems to be necessary so that intermolecular forces (π-π stacking) and surface-molecule interactions could be strong enough to takeover resulting to assemblies being extended and stabilized. The electric field is therefore instrumental in inducing a change in the system from a disordered state to an ordered one stabilized by intermolecular forces of attraction, similar to electric field-induced crystallization for the realignment of polymer fibers,[36] tuning of molecular packing in thin films,[37] and purification from a liquid suspension.[38]

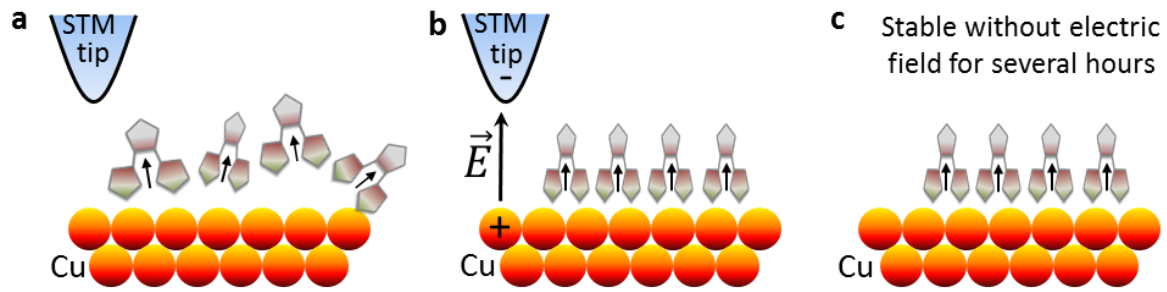

Figure 4.8 Description of the process: a) Molecules deposited on the surface are disordered. b) When a positive bias voltage pulse is applied, the STM tip is negatively charged while the Cu(111) substrate is positively charged and the molecules align their dipole following the lines of the electric field. c) The supramolecular assembly is maintained after the pulse. The calculated dipole moment of the molecule has a magnitude of 2.1 D.

4.5 Conclusion

In this chapter, we focused on STM of an assembly of terarylenes. By taking advantage of the electric field induced by the bias voltage between the STM-tip and the surface under ultra-high-vacuum conditions, we succeeded to induce the formation of an ordered supramolecular self-assembled network from a disordered system. To the best of our knowledge, this is the first report utilizing the well-known electric-field-induced realignment of molecules to form assemblies in ultra-high vacuum conditions without solvent. This expands the repertoire of bottom-up approaches that could be exploited to form supramolecular assemblies of functional molecules. For future works, the formation of assemblies could be instrumental in observing electron-transfer chain reactions, so-called "domino reactions", of diarylethenes/terarylenes on surfaces as developed in Chapter 3.[3]

As mentioned in the main text, the effect of bias pulse at higher voltages was not fully explored for fear of other events (switching, degradation, etc.) happening. In order to develop this technique further, a more careful investigation of these effects is thus recommended for further studies. The force applied on the molecules may be varied by keeping the bias pulse voltage constant while changing the tip-surface distance in order to specifically change the electric field force on the molecules. Also, the type of surface may be modified. Aside from exploring other metallic surfaces Ag(111), Au(111), the effect of surface reconstruction may be explored by using as Ag(110) or Cu(110). Also, surfaces having a certain polarity such as semi-conducting surfaces may be used.

4.6 References

[1] V. Balzani, A. Credi, M. Venturi, The bottom-up approach to molecular-level devices and machines, *Chem. Eur. J*, 2002, *8*, 5524-5532.

[2] K.S. Mali, N. Pearce, S. De Feyter, N.R. Champness, Frontiers of supramolecular chemistry at solid surfaces, *Chem. Soc. Rev.,* 2017, *46*, 2520-2542.

[3] X. Bouju, C. Mattioli, G. Franc, A. Pujol, A. Gourdon, Bicomponent supramolecular architectures at the vacuum–solid interface, *Chem. Rev.,* 2014, *117*, 1407-1444.

[4] T.K. Shimizu, J. Jung, H. Imada, Y. Kim, Supramolecular assembly through interactions between molecular dipoles and alkali metal ions, *Angew. Chem. Int. Ed.* 2014, *53*, 13729-13733.

[5] L. Grill, M. Dyer, L. Lafferentz, M. Persson, M. Peters, S. Hecht, Nano-architectures by covalent assembly of molecular building blocks, *Nat. Nanotech.*, 2007, *2*, 687-691.

[6] C. Li, L. Liu, T. Zhang, C. Yuan, L. Peng, S. Hou, Y. Wang, Kinetically controlled hierarchical self-assemblies of all-trans-retinoic acid on Au(111), *Chem. Commun.*, 2017, *53*, 2252-2255.

[7] Y. Zhang, H. Kersell, R. Stefak, J. Echeverria, V. Iancu, U.G.E. Perera, Y. Li, A. Deshpande, K.-F. Braun, C. Joachim, G. Rapenne, S.-W. Hla, Simultaneous and coordinated rotational switching of all molecular rotors in a network, *Nat. Nanotechnol*., 2016, *11*, 706-712.

[8] N.A. Wasio, D.P. Slough, Z.C. Smith, C.J. Ivrimey, S.W. Thomas, III; Y.-S. Lin, E.C.H. Sykes, Correlated rotational switching in two-dimensional self-assembled molecular rotor arrays, *Nat. Commun*., 2017, *8*, 16057.

[9] P. Matvija, F. Rozbořil, P. Sobotik, I. Ošťádal, B. Pieczyrak, L. Jurczyszyn, P. Kocán, Electric-field-controlled phase transition in a 2D molecular layer, *Sci. Rep.*, 2017, *7*, 7357.

[10] A. C. Aragonès, N.L. Haworth, N. Darwish, S. Ciampi, N.J. Bloomfield, G.G. Wallace, I. Diez-Perez, M.L. Coote, Electrostatic catalysis of a Diels-Alder reaction, *Nature,* 2016, *531*, 88-91.

[11] P. Debye, *Polar Molecules*; W.H. Freeman and Co., San Francisco, 1963.

[12] E.A. Guggenheim, The computation of electric dipole moments, *Trans. Faraday Soc.,* 1951, *47*, 573-576.

[13] G.M. Janini, A.H. Katrib, Determination of the dipole moment of polar compounds in nonpolar solvents, *J. Chem. Ed.*, 1983, *60*, 1087-1088.

[14] H.B. Thompson, The determination of dipole moments in solution, *J. Chem. Ed.*, 1966, *43*, 66-73.

[15] A. Troisi, M.A. Ratner, Molecular rectification through electric field induced conformational changes, *J. Am. Chem. Soc.*, 2002, *124*, 14528-14529.

[16] E.G. Emberly, G. Kirczenow, The smallest molecular switch, *Phys. Rev. Lett.,* 2003, *91*, 188301.

[17] D. Xiang, X. Wang, C. Jia, T. Lee, X. Guo, Molecular-scale electronics: from concept to function, *Chem. Rev.*, 2016, *116*, 4318-4440.

[18] J. Niederhausen, H.R. Kersell, C. Christodoulou, G. Heimel, H. Wonneberger, K. Müllen, J.P. Rabe, S.-W. Hla, N. Koch, Monolayer phases of a dipolar perylene derivative on Au(111) and surface potential build-up in multilayers, *Langmuir*, 2016, *32*, 3587-3600.

[19]Q. Li, C. Han, M. Fuentes-Cabrera, H. Terrones, B. Sumpter, W. Lu, J. Bernholc, J. Yi, Z. Gai, A.P. Baddorf, P. Maksymovych, M. Pan, Electronic control over attachment and self-assembly of alkyne groups on gold, *ACS Nano*, 2012, *6*, 9267-9275.

[20]D. Frath, T. Sakano, Y. Imaizumi, S. Yokoyama, T. Hirose, K. Matsuda, Diarylethene self-assembled monolayers: cocrystallization and mixing-induced cooperativity highlighted by scanning tunnelling microscopy at the liquid/solid interface, *Chem. Eur. J.,* 2015, *21*, 11350-11358.

[21]S. Yokoyama, T. Hirose, K. Matsuda, Effects of alkyl chain length and hydrogen bonds on the cooperative self-assembly of 2-thienyl-type diarylethenes at a liquid/highly oriented pyrolytic graphite interface, *Chem. Eur. J.,* 2015, *21*, 13569-13576.

[22]S. Yokoyama, T. Hirose, K. Matsuda, Phototriggered formation and disappearance of surface-confined self-assembly composed of photochromic 2-thienyl-type diarylethene: a cooperative model at the liquid/solid interface, *Chem. Commun.*, 2014, *50*, 5964-5966.

[23]T. Sakano, Y. Imaizumi, T. Hirose, K. Matsuda, Formation of two-dimensionally ordered diarylethene annulated isomer at the liquid/hopg interface upon in situ uv irradiation, *Chem. Lett.*, 2013, *42*, 1537-1539.

[24]S. Bonacchi, M. El Garah, A. Ciesielski, M. Herder, S. Conti, M. Cecchini, S. Hecht, P. Samori, Surface-induced selection during in situ photoswitching at the solid/liquid interface, *Angew. Chem. Int. Ed.,* 2015, *54,* 4865-4869.

[25]N. Maeda, T. Hirose, S. Yokoyama, K. Matsuda, Rational design of highly photoresponsive surface-confined self-assembly of diarylethenes: reversible three-state photoswitching at the liquid/solid interface, *J. Phys. Chem. C*, 2016, *120*, 9317-9325.

[26]N. Maeda, T. Hirose, K. Matsuda, Discrimination between conglomerates and pseudoracemates using surface coverage plots in 2-D self-assemblies at the liquid/graphite interface, *Angew. Chem. Int. Ed.*, 2017, *56*, 2371-2375.

[27]S.V. Snegir, A. Marchenko, P. Yu, F. Maurel, O. Kapitanchuk, S. Mazerat, M. Lepeltier, A. Léaustic, E. Lacaze, STM observation of open- and closed-ring forms of functionalized diarylethene molecules self-assembled on a Au(111) surface, *J. Phys. Chem. Lett.* 2011, *2*, 2433-2436.

[28]S.V. Snegir, P. Yu, F. Maurel, O. Kapitanchuk, A. Marchenko, E. Lacaze, Switching at the nanoscale : light- and STM-tip-induced switch of a thiolated diarylethene self-assembly on Au(111), *Langmuir*, 2014, *30*, 13556-13563.

[29]J. Wirth; N. Hatter, R. Drost, T.R. Umbach, S. Barja, M. Zastrow, K. Rück-Braun, J.I. Pascual, P. Saalfrank, K.J. Franke, Diarylethene molecules on a Ag(111) surface: stability and electron-induced switching, *J. Phys. Chem. C*, 2015, *119*, 4874-4883.

[30]G. Reecht, C. Lotze, D. Sysoiev, T. Huhn, K. Franke, Visualizing the role of molecular orbitals in charge transport through individual diarylethene isomers, *ACS Nano*, 2016, *10*, 10555-10562.

[31]S. Fukumoto, T. Nakashima, T. Kawai, Photon-quantitative reaction of a dithiazolylarylene in solution, *Angew. Chem. Int. Ed.* 2011, *50*, 1565-1568.

[32] M. J. Frisch, *et al*, *Gaussian 09 Revision A.02*, Gaussian Inc. Wallingford CT, 2009. (

[33]J.P.D.C. Calupitan, O. Galangau, O. Guillermet, R. Coratger, T. Nakashima, G. Rapenne, T. Kawai, Synthesis and photochromism of chloro- and tert¬-butyl functionalized terarylene derivatives for surface deposition, *Eur. J. Org. Chem.* 2017, *17*, 2451-2461.

[34]R. Horcas, J.M. Fernandez, J. Gomez-Rodriguez, J. Colchero, J. Gomez-Herrero, A. M. Baro, Synthesis and photochromism of chloro- and tert¬-butyl functionalized terarylene derivatives for surface deposition, *Rev. Sci. Instrum.*, 2007, *78*, 013705.

[35]A. Cristadoro, M. Ai, H.J. Räder, J.P. Rabe, K. Müllen, Synthesis and photochromism of chloro- and tert¬-butyl functionalized terarylene derivatives for surface deposition, *J. Phys. Chem. C*, 2008, *112*, 5563-5566.

[36] Y, Xi, L. D. Pozzo, Electric field directed formation of aligned conjugated polymers, *Soft Matter*, 2017, *13*, 3894-3908.

[37] F. Molina-Lopez, H. Yan, X. Gu, Y. Kim, M.F. Toney, Z. Bao, Electric Field Tuning Molecular Packing and Electrical Properties of Solution-Shearing Coated Organic Semiconducting Thin Films, *Adv. Funct. Mater.* 2017, *27*, 1605503.

[38]W.W. Li, N. Radasci, H.J.M. Kramer, A.E.D. van der Heijden, Solid separation from a mixed suspension through electric-field-enhanced crystallization, J.H. ter Horst, *Angew. Chem.* 2016, *128*, 16322-16325.

Chapter 5

Single-molecule studies on terarylenes: STM and DFT

From 2D supramolecular networks, we go down to the single molecular level on surfaces in this chapter. For the first time, terarylenes are studied at the single molecular level on Ag(111) and mapping of occupied and unoccupied states were achieved on NaCl(001)/Ag(111).

Of the six compounds designed for STM in chapter 3 we prioritized **3.1*o*** and its *tert*-butyl derivative **3.3o** because majority of their species maintain the conformation reactive to cyclization even at high temperatures necessary for sublimation and subsequent deposition on the solid substrate. **3.2*o*** (Figure 3.1) was known to be more stable in its non-reactive parallel conformation due to C-H and π-π interactions.[1] Since it was shown that big peripheral *tert*-butyl groups do not have any effect to this stability of the non-reactive conformation in its derivative **3.4*o*,**[2] this must also be true for its chloro derivative **3.6*o***.

In this chapter, we focus on investigating **3.1*o*** and **3.3*o*** deposited on Ag(111). The structues and DFT-optimized geometries in the gaseous state of these compounds are shown on Figure 5.1. **3.1*o*** seems to undergo switching but the exact molecular level phenomenon seems elusive from mere analyses of images.

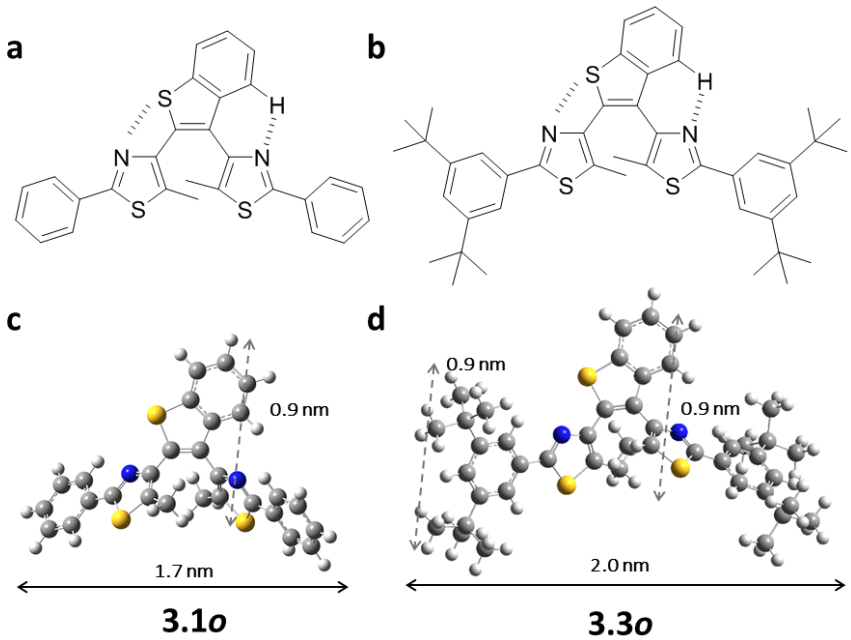

Figure 5.1. Structures of (a) **3.1*o*** and (b) **3.3*o*** showing the intramolecular forces that keep them in their reactive conformation and their DFT-optimized structures shown in (c) and (d) respectively.

We show that the STM contrast could be improved by the *tert*-butyl groups in **3.3*o*** but, in the case of our molecule, the switching properties seem to be lost. We explain both (1) the origin of improved contrasts and the (2) lost of switching properties by DFT calculations. Further, **3.3*o*** displays several conformations on a solid surface despite the strong forces that keep it in its reactive conformation.[2] With the aid of ESQC calculations, we assign these conformations to the different

images found on the surface. Lastly, we end the chapter with STM results of **3.3*o*** on NaCl(001)/Ag(111) surface that permitted the mapping of occupied and unoccupied states. This results were submitted and under revision for publication in the Journal of Physical Chemistry C as:

> *Adsorption of Terarylenes on Ag(111) and NaCl(001)/Ag(111): an STM and DFT Study,* by J.P.D.C. Calupitan, O. Guillermet, O. Galangau, M. Yengui, J. Echeverria, X. Bouju, J. Echeverria, R. Coratger, T. Nakashima, G. Rapenne, T. Kawai, *under revision.*

5.1 STM Imaging of 3.1

The open form **3.1*o*** was first deposited on a Ag(111) substrate. (See Chapter 7.3 for detailed experimental details.) Figure 5.2a shows bare atomically-flat Ag(111) surface while 5.2b shows the surface after deposition of the compound. Identical bright circular spots were observed for all compounds with no bias dependence (Figure 5.2c). Inset on Figure 5.2c shows a zoom in of the spots: the perfect symmetry of the spot did not reveal any feature that could be assigned to the triangular configuration of the aromatic rings in Figure 5.1a. The observed diameter of the circular spot was found to be 1.2 nm, which is far lower than the predicted end-to-end distance between any peripheral atom of **3.1*o*** in the gas phase.

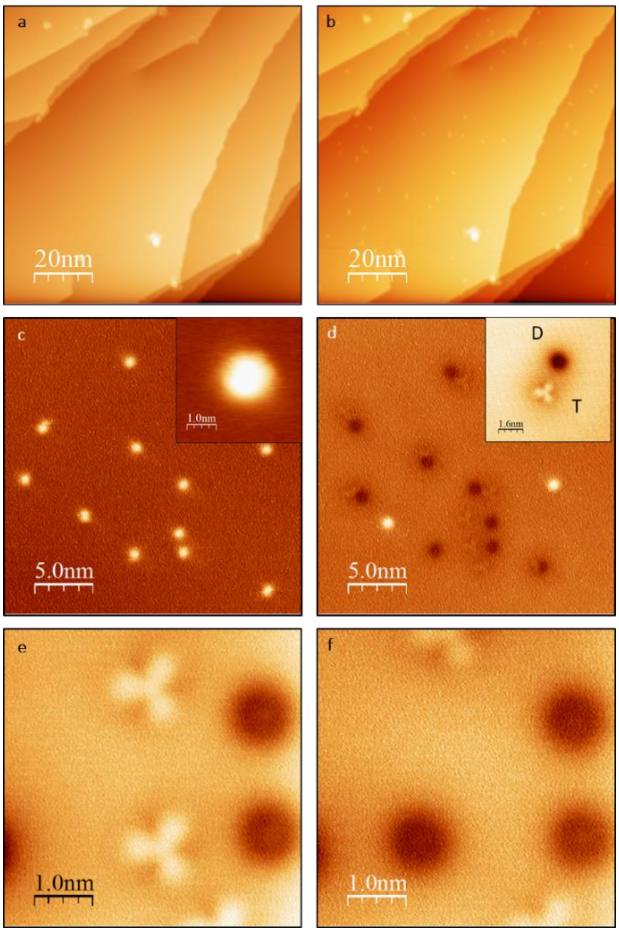

Figure 5.2. (a) Bare Ag(111) surface (b) after deposition of **3.1*o***. (c) shows a zoom in, in-set shows a zoom on a spot while (d) shows imaging after switching with a 2.8 V. (e) shows pairs of these D and T spots before and (f) after further switching. Imaging conditions: -1 V, 1pa.

When the surface was applied with a bias voltage of 2.8 V, the spots turned to pairs of dark (D) spots and triangular (T) spots (Figure 5.2d, inset shows a zoom on a D-T pair). The distance between the D and T spots vary from spot to spot, but the switching from bright spots to these two species was consistent in all molecules. Further, when T spots were applied with a subsequent 3.0 V, they could irreversibly turn to D spots (Figure 5.2e-f).

The formation of two separate species from one spot led us to believe that the initial bright spots in Figure 5.2b-c are dimeric forms of the molecules. Application of the first bias pulse causes two events: the separation of these two forms and the switching of one of the species. The subsequent pulse could then switch one of the molecules to the form similar to the previously switched form.

We attempted to solve this problem by depositing the closed form **3.1*c***, but deposition of the molecule did not produce isolated single molecules on surfaces but instead aggregates with no apparent order. Line scans of spots b and c as marked in Figure 5.3a (Figure 5.3b,c) show irregular sizes while zoom in on spots e and f in Figure 5.3d show different shapes. This could be explained by the DFT-optimized geometry of **3.1*c*** which shows a flat aromatic ring which could form aggregates by dispersion and π-π interactions (Figure 5.3g).

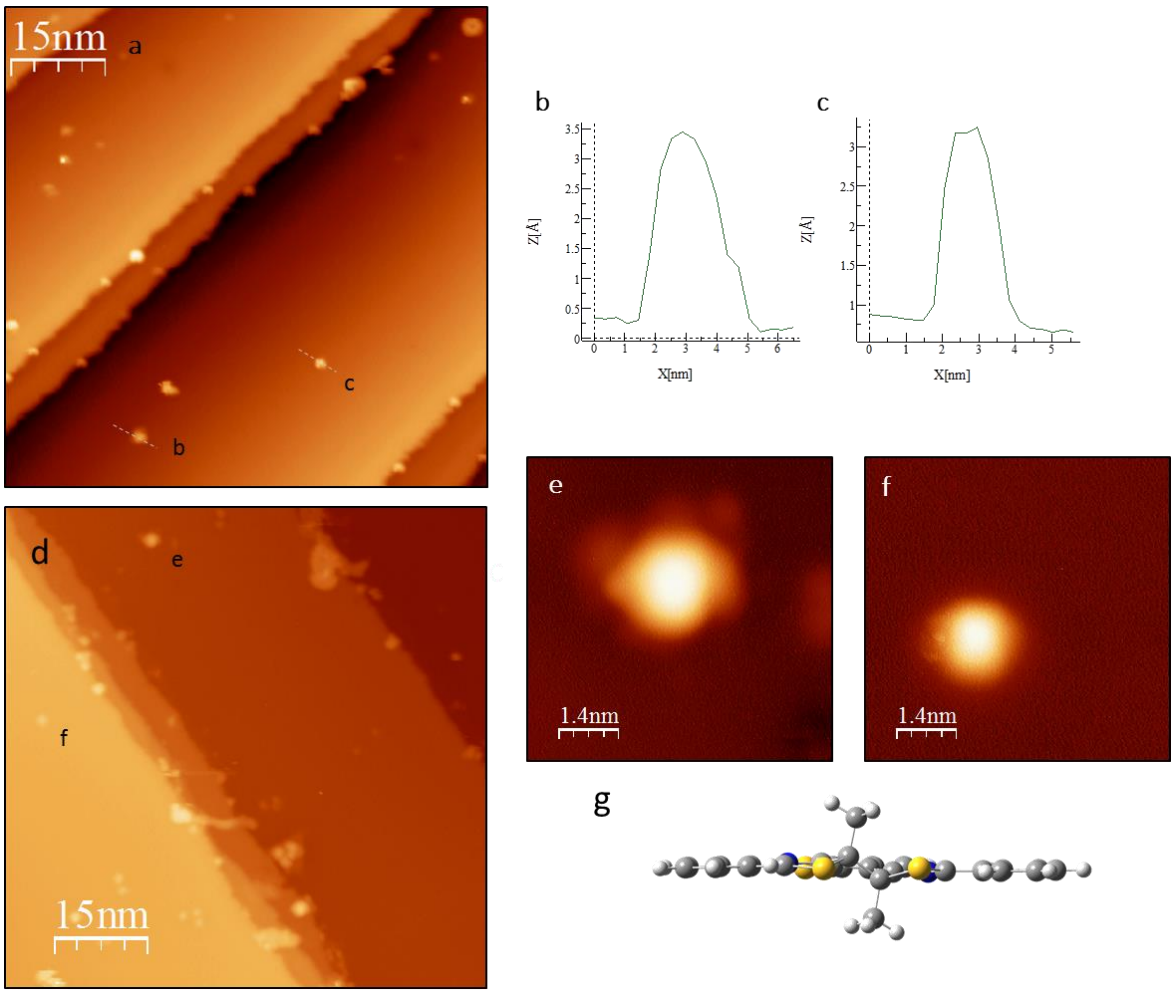

Figure 5.3. (a,d) shows Ag(111) deposited with **3.1*c***. (b-c) show line scans of spots as labelled in (a) while (e-f) show zoom in on the spots as labelled in (d). Imaging conditions: -1 V, 1pa. (g) shows the DFT-optimized structure of **3.1*c*** as seen from the plane of the photoswitching unit.

5.2 STM imaging of 3.3*o*

We therefore proceeded to image **3.3*o*** which has *tert*-butyl groups that could prevent aggregation.[2-5] Further, these *tert*-butyl groups were shown to preserve the excellent photoswitching capabilities of **3.1**. These peripheral groups do not have considerable effect on the electronic properties of the molecule. This is also confirmed as these groups do not contribute to the maps of the molecular orbitals HOMO-2 to LUMO+2 (Figure 5.4).

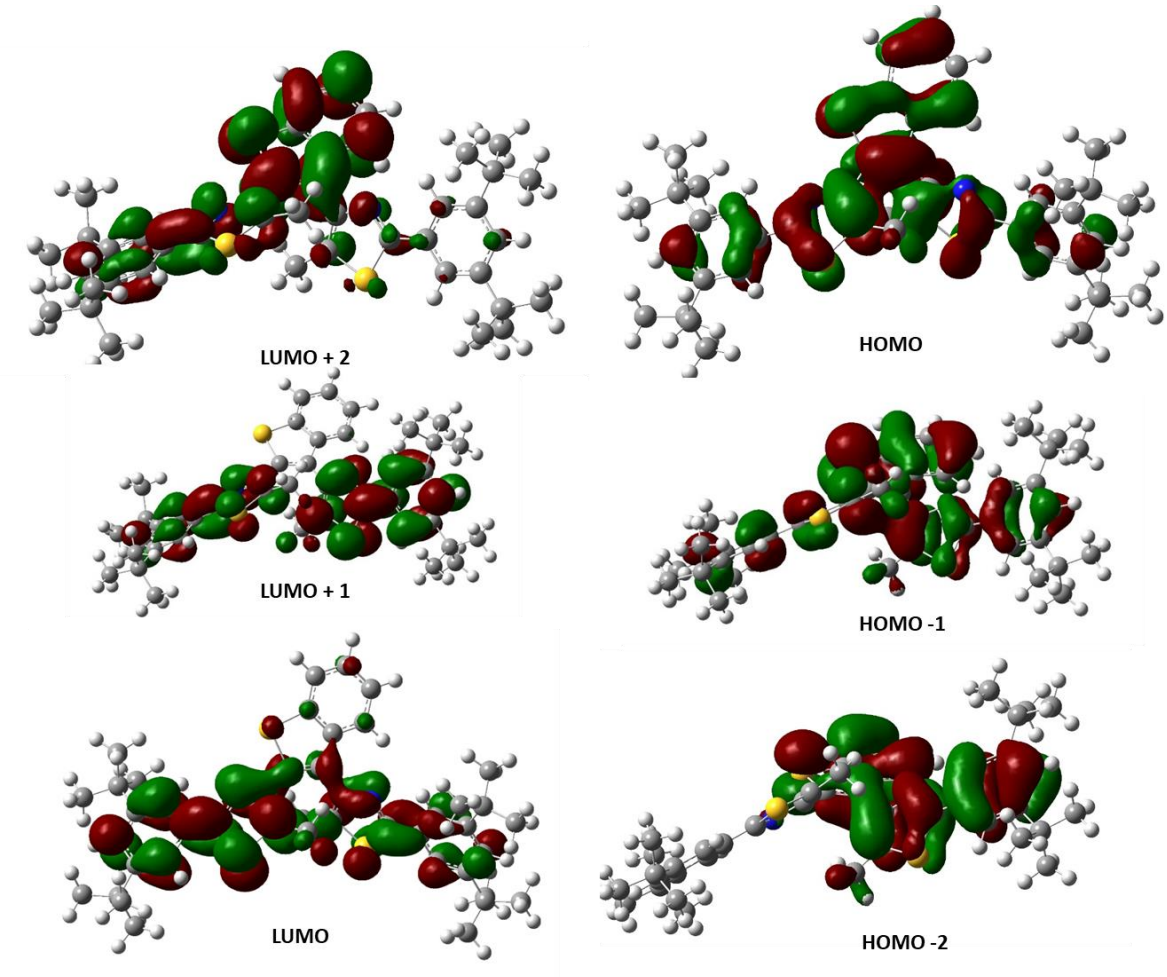

Figure 5.4. Maps of HOMO-2 to LUMO+2 of **3.3*o*** showing that the *tert*-butyl groups do not contribute to these orbitals.

Figure 5.5a shows **3.3*o*** single molecules adsorbed on Ag(111) with 20 % coverage of a bilayer of NaCol(001). The NaCl bilayer may be identified by the presence of the characteristic islands close to the Ag steps and by their 90° corners due to the square lattice of the NaCl(001) face (Figure 5.5a, dark arrows). Three shapes of **3.3*o*** single molecules could be identified as labelled on Figure 5.5a. These are labelled as Forms 1,2, and 3. This could be due to the presence of different surface absorption structures as predicted by an increase in the population of *cis* conformers upon heating by DFT calculations.

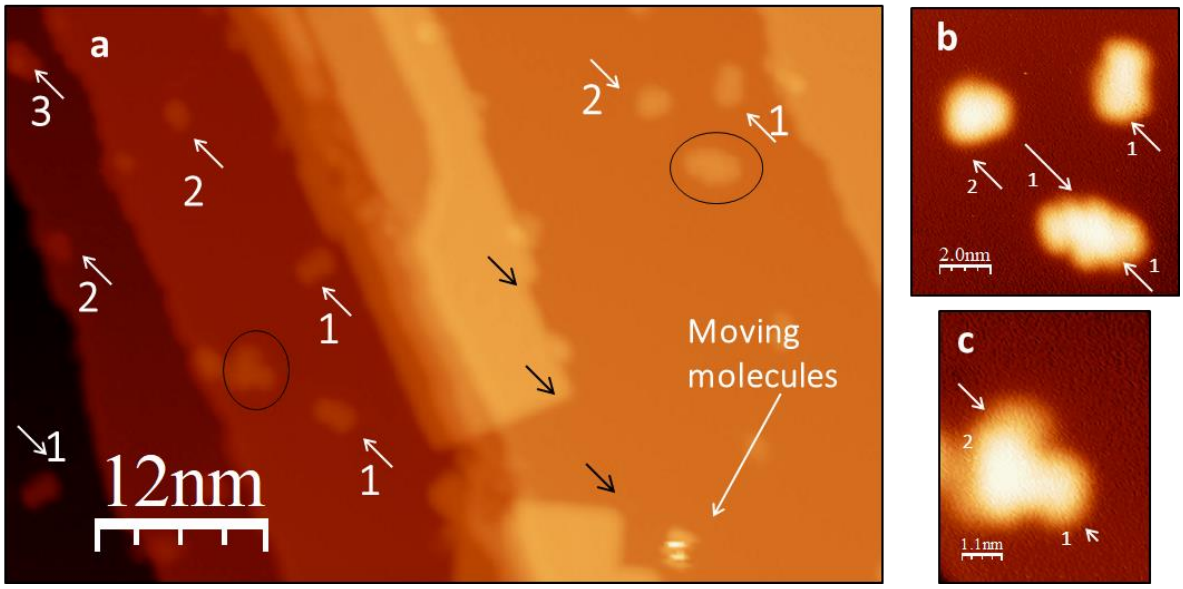

Figure 5.5. a) Sample of a large scale image (1.4 V, 1pA, T = 4.5 K) of Ag(111) with 2 monolayers of NaCl followed by subsequent deposition of **3.3*o***. Dark arrows point to 90° corners characteristic of NaCl(001) crystal structure; dark ovals on aggregates of molecules; white arrows point to different forms of the compound with their corresponding label. b-c) Zoom in on the species inside the dark arrows

In the ~200 molecules we observed, Forms 1, 2, and 3 displaued a distribution of 60%, 26%, and 14%. Some molecules looked like they started to aggregate (Figure 5.5a dark circles) but upon zooming in on them, they could still be discriminated into different forms (Figure 5.5b-c). It must be noted that majority of molecules observed (>95 %) are found on the metallic surface rather than on the NaCl. Due to the nonpolar nature of the *tert*-butyl groups, the interactions with NaCl are even weaker and thus less favored than those with the metallic surface.

We focus first on the results on Ag(111). Due to the bulky *tert*-butyl groups that interact with the surface mainly by weak van der Waals forces, no preferred direction or conformation on the surface could be observed for all forms. Another consequence is that some of our images show fuzzy objects that move on the surface (Figure 5.5a) and made imaging under some conditions difficult. For large-scale images, relatively high voltages (typically 1.4 V), corresponding to higher tip-surface distances, were necessary to minimize molecule displacement.

On the other hand, it was possible to obtain images at low voltages when smaller areas were scanned. Figure 5.6 shows a single isolated molecule and two other molecules (seemingly interacting with each other having the conformation of Form 1. Form 1 displays four lobes surrounding a bright central lobe. At bias voltages 1.2-2.2 V (Figure 5.6c-i), the four lobes are easier to discriminate. However, at other bias voltages, two lobes on the same side start to become indistinguishable (Figure 5.6a,b). At higher bias voltages starting at 1.8V, the bright central structure becomes more prominent than the surrounding lobes (Figure 5.6f-i).

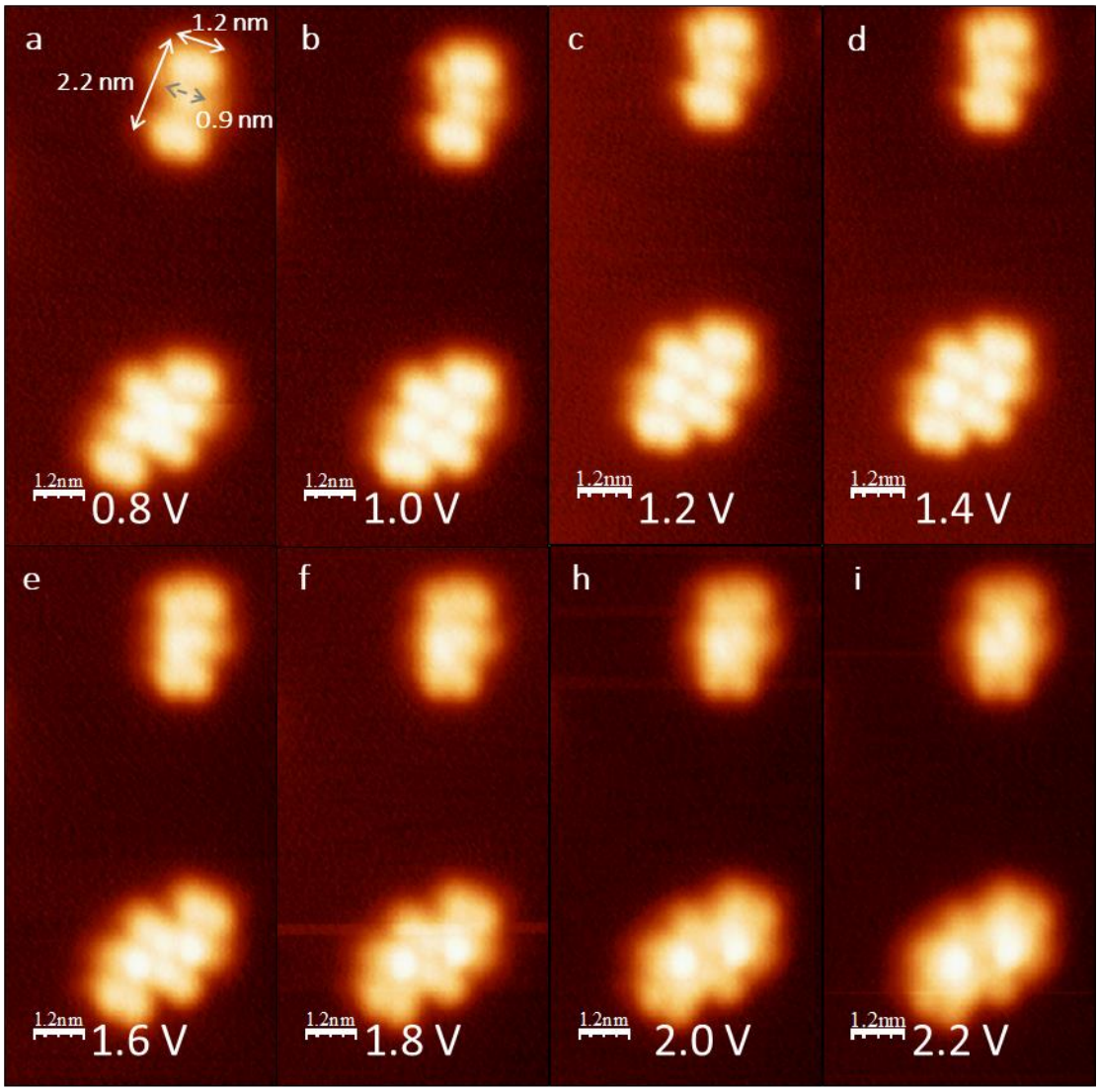

Figure 5.6. Zoom in on Form 1 and their bias-dependent images (1pA, T=4.5 K). Measurements are from linescans of the images.

The four small lobes in total are arranged in an almost rectangular manner similar to the arrangement of *tert*-butyl groups on Figure 5.1d. These arrangements and shapes are reminiscent of STM images of *trans*-azobenzene functionalized with 4 *tert*-butyl groups reported by L. Grill *et al*.[6-7] The length of the molecule, i.e. the distance between ends of two lobes on the same side, is 2.2 nm while the width between two side-lobes is 1.2 nm (see Figure 5.6a) These correspond well with the interatomic distances in Figure 5.1d. The bright central spot could be due to the central part of the molecule. It has a width of about 1 nm, similar to the 0.9 nm distance between the methyl and benzothiophene moieties of **3.3*o*** (Figure 5.1d). We therefore ascribe the four bright peripheral lobes to the bulky *tert*-butyl groups while the spot between them to the central aromatic rings.

Form 2 on the other hand seems to have the four lobes and the central part skewed out of the rectangular arrangement of Form 1 (Figure 5.7). One side roughly maintains a 2.2 nm length and another at 1.2 nm width previously seen. The other side appears to be lifted from the surface so that the central part is brighter (Figure 5.7a). These are reminiscent of *cis*-azobenzene studied by L. Grill et al.[6-7] We therefore postulate that this form is a stable rotational conformation of the molecule previously predicted.[2] (Figure 3.6) At higher voltages, the molecule seems to shift its contrast to a

different part, similar to the behavior of Form 1. Due to the dissymmetry of Form 2, it is notable that chirality is expected on the surface. This is presented in Figure 5.8a,b where the two enantiomers can be observed. In the gaseous state, **3.3*o*** is not chiral *per se* but the dissymmetry due to the benzothiophene moiety may render it chiral once adsorbed. Figure 5.8c illustrates this for one of the conformational isomers of **3.1*o*** (C_2 conformer, Figure 3.6). We will return to this issue of chirality in section 5.4.

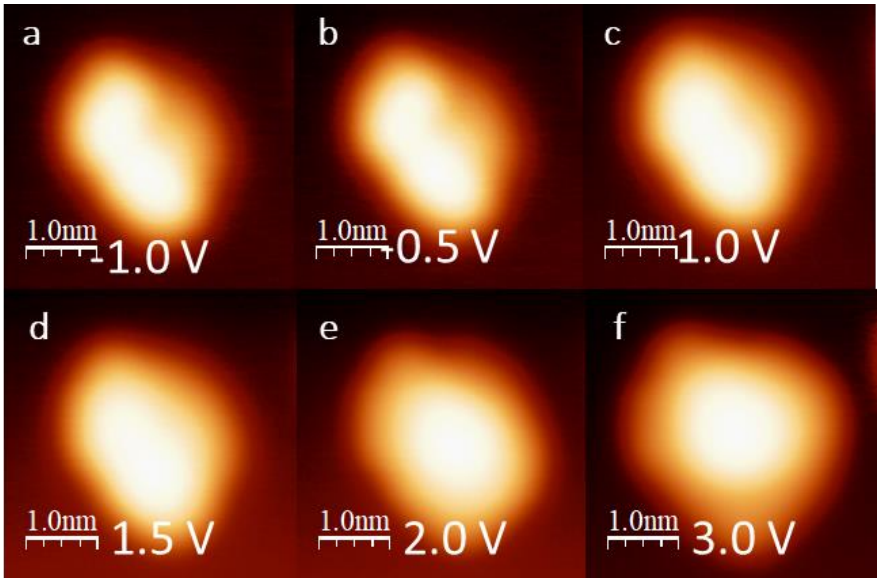

Figure 5.7. Zoom in on Form 2 and their bias-dependent images (1pA, T=4.5 K).

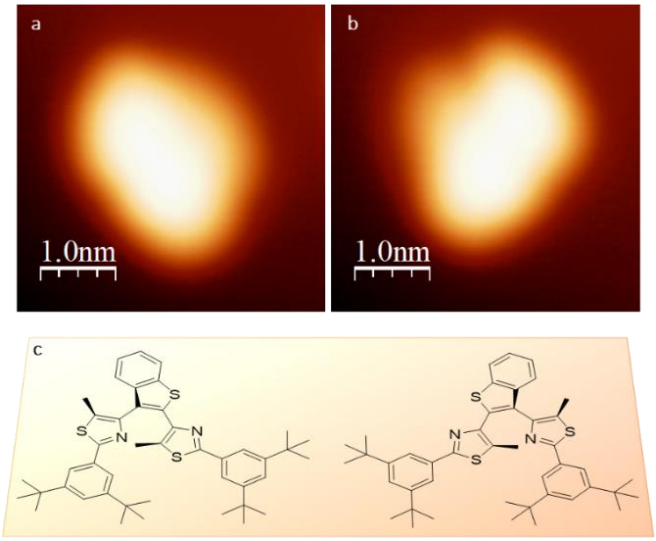

Figure 5.8. a-b) Enantiomeric forms of Form 2. Imaging conditions: 1.0 V, 1pA, T=4.5 K. c) Illustration of chirality of **3.3*o***-C_2 when in contact with a 2D surface.

STM images of Form 3 as a function of bias voltage are shown in 5.9. This has almost similar measurements as those of Forms 1 and 2 (Figure 5.9a). The main difference is that the lobes on each

of the two sides are slightly skewed from the rectangular arrangement and are less intense than the central spot even at the same imaging conditions. This form displays similar behavior as Forms 1 and 2 at different scanning voltages. Up to 1.5 V, no remarkable difference could be observed (Figure 5.9c) but at 2.0 V, the surrounding lobes decrease in contrast while the central spot gets brighter (Figure 5.9d-f).

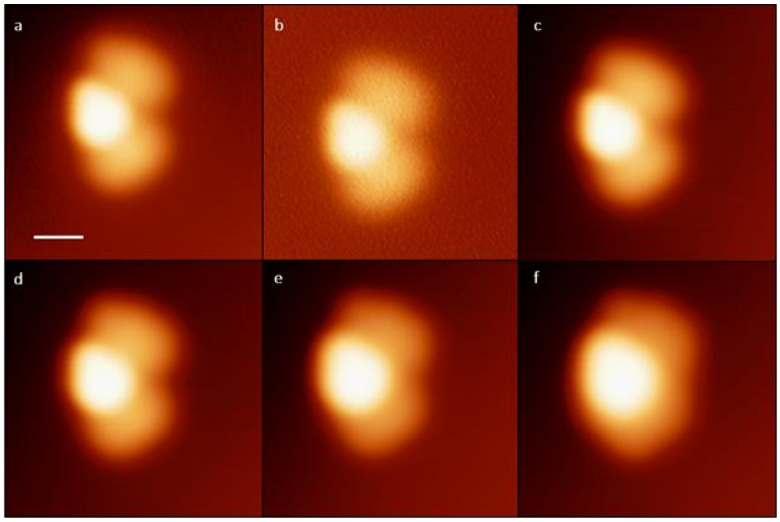

Figure 5.9. Zoom in on Form 3 and bias-dependent images at a) -0.2 V b) 0.3 V c) 1.0 V d) 1.5 V e) 2.0 V f) 2.5 V Images were taken at constant current (1pA, T=4.5 K). Scale bar = 1 nm.

For all forms, the presence of *tert*-butyl groups clearly helped identify **3.3*o*** molecules on the surface. This is a great improvement compared to **3.1*o*** giving only bright symmetric spots (Figure 5.2c). Further, the observed decrease in contrast of *tert*-butyl groups as the imaging potential increases means that unoccupied states are being probed. (In our system, the bias is applied to the sample so that a positive voltage generates a tunneling current from the tip to the surface.) This is consistent with the location of the unoccupied states near the center of the molecule and not on the *tert*-butyl groups, as shown in the maps of LUMO and LUMO+1 of **3.3*o*** (Figure 5.4).

We therefore performed scanning tunneling spectroscopy (STS) measurements. The original I(V) spectra are then numerically derived and are presented in Figure 5.10. They all display strong resonance peaks at -1.3 and 2.1 V which have resonance onset at -0.4 and 1.5 V respectively, resulting to an estimated gap of 1.9 V. All STS spectra measured on all forms showed the same peaks, indicating that they are almost chemically identical, differing only as surface conformational isomers.

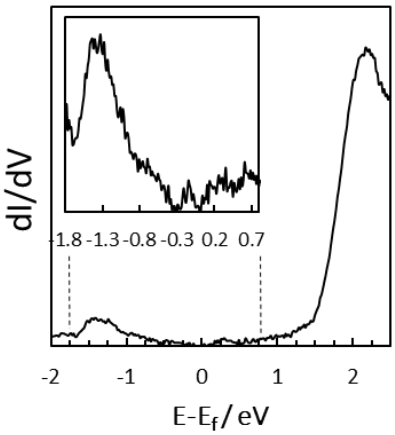

Figure 5.10. Typical STS spectrum of **3.3*o*** on Ag(111). All forms displayed similar peaks at -1.5 and 2.1 V relative to the Fermi level.

5.3 DFT calculations on the surface[8]

We postulate the existence of different conformers of **3.1*o*** on the surface because of the variety of forms observed. In order to understand these experimental STM images vis-à-vis such plurality of conformations, we performed a comprehensive computational study to obtain adsorption energies, adsorption geometry, and predicted STM images of different conformers. Table 5.1 summarizes the adsorption energies calculated for these forms while Figure 5.11 shows the calculated adsorption geometries. STM images were predicted by elastic scattering quantum chemistry (ESQC). In this technique, the molecule absorbed on the atom is considered an impurity in the otherwise periodic electronic structure of the metallic surface. In this technique, the effect of this defect on the change in the surface density of states is calculated.[8] Aside from the optimized conformation shown on Figure 5.1d which may correspond to a *trans* form with respect to the directions of the methyl groups, we also considered a conformation in which the methyl groups are pointing to the same direction, corresponding to a *cis* form. These may correspond to conformations C_1 and C_2 which were shown to be possible stable conformations in the gas phase. (See section 3.3, Figure 3.6) We also opened the possibility of another conformation in which the sulfur atoms of the thiazole rings anchor the molecule on the surface through Ag-S interactions.

Table 5.1. Adsorption energies of the different surface conformations of **3.1*o*** and **3.3*o*** on the Ag(111) surface calculated as $E_{ads} = E_{m\text{-}s} - E_m - E_s$, where $E_{m\text{-}s}$ is the total electronic energy of the molecule-surface system and E_m and E_s are the energies of the relaxed silver slab and of the relaxed gas-phase molecule (both in the same unit cell), respectively of different conformations. All results were rounded off to meV units.

	E_{ads} (eV)	
Conformer	**3.1*o***	**3.3*o***
open (*trans*$_1$)	-3.476	-4.572
open (*cis*)	-3.390	-4.321
closed (*trans*)	-3.070	-4.620
open (*cis*)	-3.705	-4.187
open (*trans*$_2$) [†]	NA	-5.836

[†] This conformation refers to **3.1*o*** in which benzothiophene is sticking out of the surface and a strong bond is found between a sulfur atom from a thiazole and a silver atom ont eh surface as in Figure 5.11d,e.

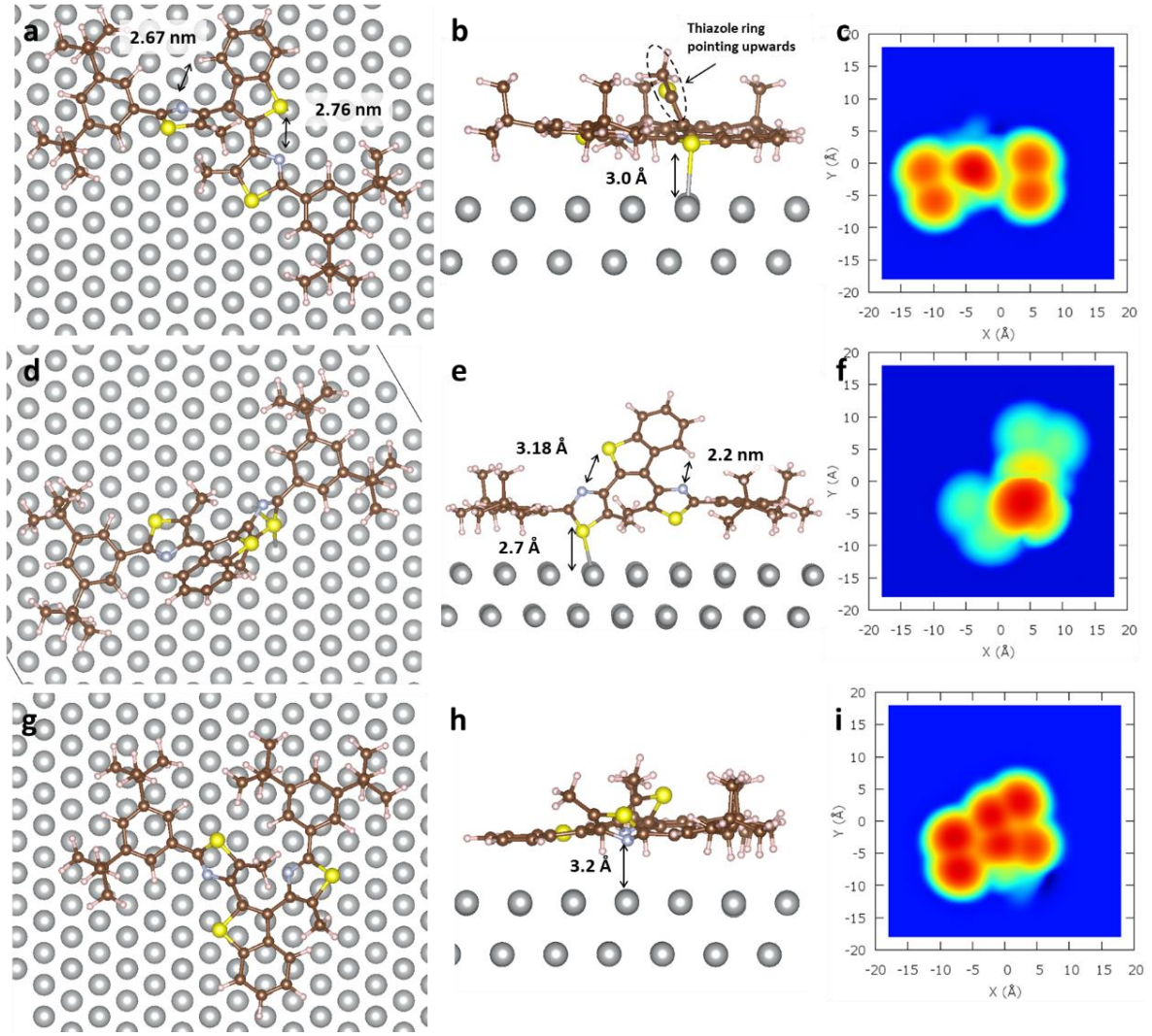

Figure 5.11. DFT-optimized surface geometry of 3 possible conformations of the **3.1*o*** open forms. (a), (d), and (g) show views from the top and (b), (e), (h) show views from the side. ESQC predicted images taken at 0.10 V above the Fermi level are shown on (c), (f),(i). (a), (b), and (c) refer to a *trans* conformation similar to that shown on Figure 5.1b in which all the aromatic rings except one thiazole ring are protruding from the surface (*trans*$_1$). The *trans* attribution refer to the direction of the methyl groups. (d), (e), and (f) is the *trans*$_2$ conformation (Figure 5.1b) in which the benzothiophene moiety is the one protruding from the surface. (g), (h), (i) refer to the C_2 conformation (Figure 3.6) deposited on the surface.

The optimized conformation of **3.3*o*** viewed perpendicular to the Ag(111) surface and from the the side of Ag(111) are shown in Figures 5.11a and 5.11b respectively. This calculated surface conformation is labelled as *trans*$_1$. All aromatic rings bar one thiazole lie on almost the same plane, maximizing the surface area parallel to the Ag(111). The dihedral angle between the benzothiophene moiety and the flat thiazole ring is only 9° (in contrast to 45-55° in the gas phase). Focusing on the *tert*-butyl groups, two of the three methyl groups are on almost the same plane as that of the aromatic rings. Between these methyl groups and the quaternary carbon of the *tert*-butyl group, angles between 108.2-108.7° were calculated, indicating a slight distortion in order to maximize surface contact. These methyl groups present eight hydrogen atoms close to the Ag(111) surface which raise the aromatic plane from the surface by only ~3.0 Å. This is comparable to the calculated distance of flat benzene rings and other methyl-substituted aromatic systems when adsorbed on Ag(111) surface. [9] Due to this planarity, the N-H and S-N bonds which lock the molecule in its reactive conformation in the gaseous

and solution state seem to be stronger as evidenced by lower interatomic distances (Figure 5.11a) compared to those in the gas phase (Figure 5.1d). Optimization also results in the formation of a strong bond between the silver atom and the sulfur atom of the benzothiophene moiety of typical lengths. [10-11] These interactions add up to an adsorption energy of -4.572 eV (Table 5.1), which is five to eight times stronger than that calculated for single aromatic rings with different substitutions.[9] The molecule presents five protrusions on top of the aromatic system: four methyl groups and one thiazole ring with a methyl group (Figure 5.10b) pointing upwards. Aside from the electronic structure of the molecule, these topographical features could also contribute to the STM image calculated on Figure 5.10c which shows one slightly brighter central spot surrounded by four lobes. The arrangement, distances, and size of these lobes correspond well to those observed for Form 1.

We then checked a different surface conformation in which it is the benzothiophene moiety, rather than the thiazole ring, which protrudes from the surface (Figure 5.11d and 5.11e). This surface conformation is labelled as *trans*$_2$ from here on. Optimization found the two phenyl rings parallel to the surface and the methyl groups of the *tert*-butyl arranged as in *trans*$_1$. Further, the thiazole rings are slightly twisted towards the surface so that a bond was found between the sulfur atom of one thiazole group and a silver atom on the surface (with 2.6 Å interatomic distance). The thiazole rings are no longer parallel with the surface, but instead seem to mimic their gas-phase optimized structures skewing around the benzothiophene moiety to avoid direct steric repulsion between the methyl groups. The S-N distance between the benzothiophene sulfur atom and the dihedral angle between these two planes are 3.22 nm and 58^o respectively, which are in agreement with the values obtained in the gas phase. (Figure 5.11e) The benzothiophene moiety is virtually unhindered by the silver surface. It feels attractive forces towards the surface plane, however, due to strong N-H bonding as evidenced by the short N-H distance between the benzothiophene group and the side thiazolyl moiety (2.18 nm). This conformation has an adsorption energy of -5.836 eV. The shorter silver-sulfur bond in *trans*$_2$ than in *trans*$_1$ correlates to this stronger adsorption energy. The aromatic and highly-protruding benzothiophene rings could contribute to the bright STM contrasts relative to the low methyl groups, in accordance with ESQC calculation of the STM image (Figure 5.11f). This calculated image is in good agreement with the geometry of Form 3 in Figure 5.9.

Finally, we also calculated the surface adsorption of **3.3*o*** C_2 (Figure 3.6) on Ag(111). Optimized geometry again shows benzothiophene and phenyl rings on almost the same plane about 3.2 Å away from the surface. (Figure 5.11g,h) The methyl groups of the *tert*-butyl moieties protrude from the surface plane, similar to *trans*$_1$ and *trans*$_2$. Meanwhile, the thiazole rings are angled so that the methyl groups are protruding from the surface. This conformation has a slightly lower adsorption energy of -4.321 eV. The high features of the two methyl groups from thiazole rings and the four methyl groups from the *tert*-butyl functionalities could contribute to the contrast of the calculated STM image on Figure 5.11i. We could not resolve the lobes experimentally but the size and shape of the calculated image corresponds well with that of Form 2.

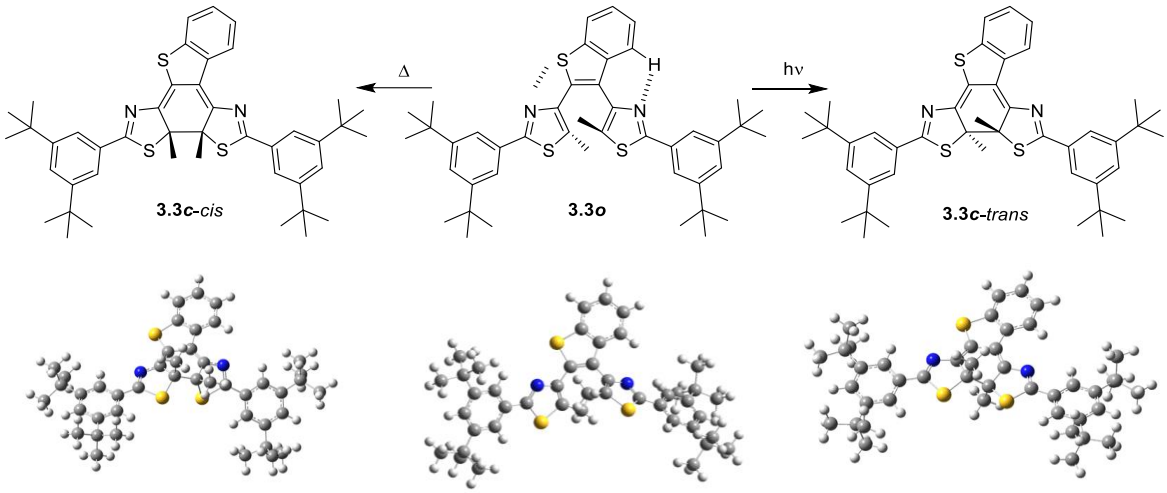

Scheme 5.1. Structures of 3.3*o* and its cyclization products from thermal or photo-induced processes.

Although we performed the deposition of native open forms carefully under dark conditions, the photon-quantitative sensitivity of 3.1*o*[2] may cause unwanted formation of the closed form due to any incident photon that leaks into the sublimation pathway. This closed form has two isomers, a *trans* isomer in which the methyl groups are pointing in opposite directions from the plane of the photoswitching backbone and a *cis* isomer in which the methyl groups are on the same side of the plane. (See Scheme 5.1 for an illustration and the DFT optimized structures of these two products.) The former is the product of photo-induced processes in solution, and probably in the gas phase, while the latter is the result of thermal processes on surfaces.[12,13] We therefore expanded the theoretical studies to a full calculation of both the *cis* and *trans* isomers of the closed form. In both of these isomers, all the rings are locked on the same rigid plane which attempts to approach the surface to maximize adsorption energies despite the steric hindrance due to CH_3 groups. In the *trans* isomer, the methyl group on the reactive carbon coupled with the methyl groups on the *tert*-butyl groups raise the molecule 3.6 Å from the surface (Figure 5.12a,b). This distance is quite far so that a low adsorption energy of -4.187 eV was calculated. This has five protrusions: one methyl group on the thiazole ring that contributes to a bright contrast at the center of the predicted ESQC image and four methyl groups that contribute to a weaker contrast around it (Figure 5.12c). Meanwhile, the conformation of the *cis* form also exhibits all rings on the same plane with sulfur atoms attempting to approach the Ag(111) surface so that one formed a bond with a silver atom (Figure 5.12d,e). Along with van der Waals interactions, these add up to a considerable adsorption energy of -4.620 eV. The ESQC calculated image of close *cis* form is therefore rather similar to that of the close *trans* form except for the brighter central spot due to the additional methyl group protruding at the center of the molecule (Figure 5.12f). These ESQC-calculated images (Figure 5.13c,f) however do not fit with the experimental images as well as those on Figure 5.11c,f,i. As a consequence, we discount the possibility of the images in Figures 3-6 corresponding with any of the closed forms.

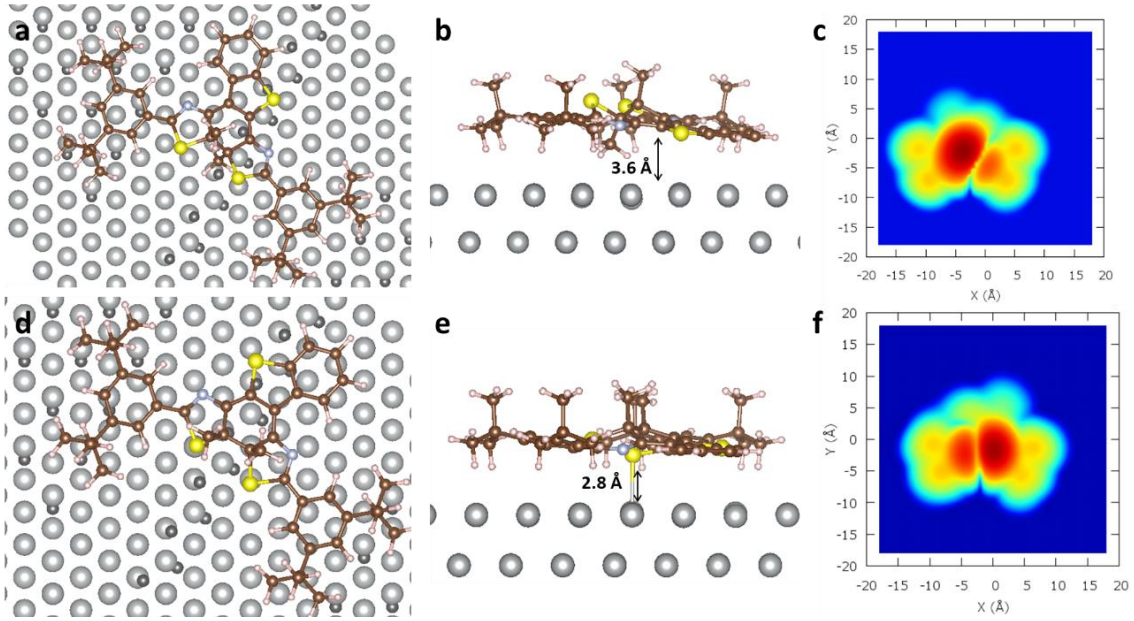

Figure 5.12. DFT-optimized surface geometry of 2 possible conformations of the **3.3*o*** closed forms. (a) and (d) show views from the top and (b) and (e) show views from the side. ESQC predicted images taken at 0.10 V above the Fermi level are shown on (c) and (d), (a), (b), and (c) refer to a *trans*-conformation while (d),(e), and (f) refer to a *cis*-conformation in which the methyl groups point up to the surface.

We further discuss the STS spectrum of **3.3*o*** on Ag(111) based on the calculations. For the open form, we obtained a gap of 2.4 eV between occupied and unoccupied states (Figure 5.13a). The calculated STS for the closed form on the other hand resulted to a gap difference of only 1 V (Figure 5.13b). This lower gap is due to the increased conjugation in the closed form which is well-documented in the literature and is the basis of many of its switching properties and applications. The experimental STS spectra of both Forms 1 and 2 correspond well to the gap calculated for the open forms using the ESQC technique. In all forms experimentally observed, the gap was never reduced to that which could correspond to the closed forms.

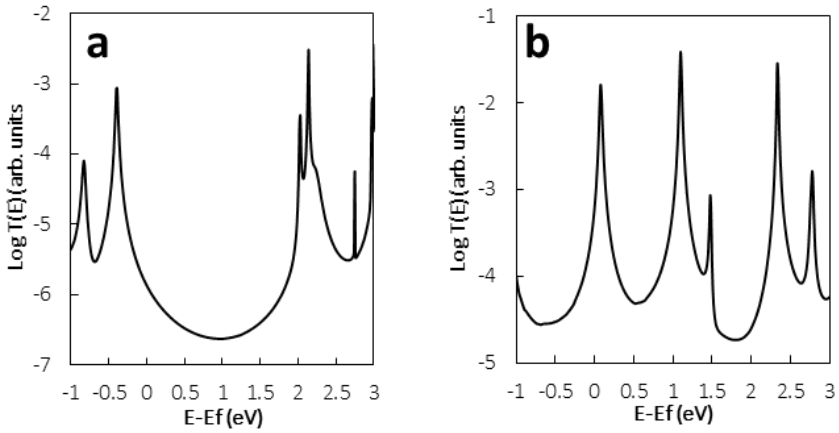

Figure 5.13. Calculated STS spectra of **3.3** (a) ***o*** form and (b) ***c*** form.

To find out the influence of *tert*-butyl groups on the adsorption energy (E_{ads}), we also performed calculations for the derivative without *tert*-butyl groups **3.1*o***. (Table 5.1) For the open forms,

the aromatic rings both lie at almost the same distance (about 3.0 Å) from the surface (Figure 5.13a-d) as that of **3.3*o***. The distance of the *tert*-butyl groups seems large enough to allow some flexibility for the central photochromic core of **3.3*o*** to approach the surface the same distance as that of **3.1*o***.

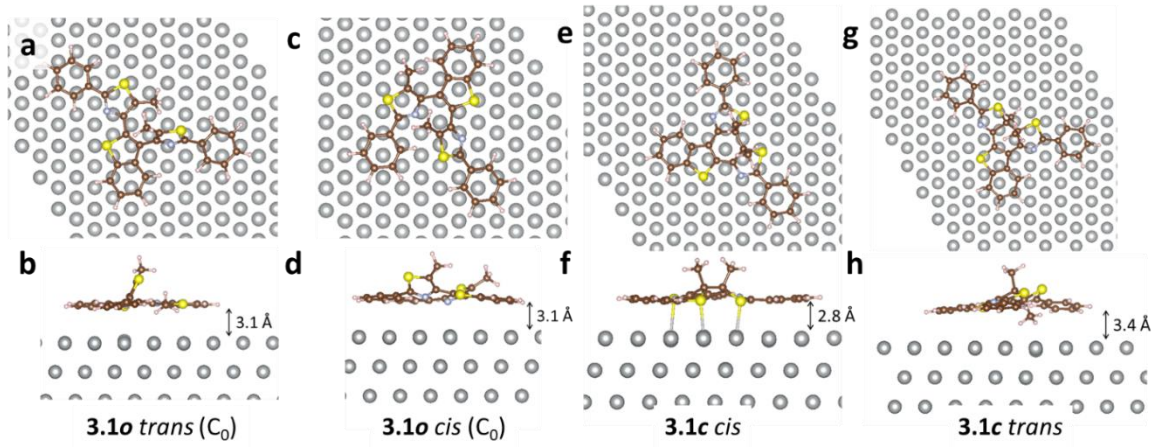

Figure 5.14. Calculated adsorption geometries of different forms of **3.1**. (a,c,e,f) are top views of the Ag(111) surface while (b,d,f,h) are side views.

5.4 Interpretation of STM images *vis-à-vis* calculation results on Ag(111)

The presence of *tert*-butyl groups clearly helped identify the **3.3*o*** molecules on the surface. This is a great improvement compared to a non-modified terarylene (**3.1*o***) deposited on Ag(111) giving only bright symmetric spots (Figure 5.3).

Comparing the experimental images (Figure 5.6) and ESQC calculations (Figure 5.11c), we assign the observed Form 1 to a $trans_1$ (Figure 5.11a,b). Figure 5.11a, however, shows only one of four possible adsorption geometries of this *trans* conformation. Whereas in solution at ambient conditions, with a high thermal energy and with unhindered rotational movements, the difference between molecular conformations may be considered trivial, on a two dimensional surface at a single-molecular level, different conformations of the molecule are expected due to interactions with the substrate.[14] Because of the dissymmetry of the central benzothiophene ring, another possible unique surface conformation may come up from exchanging which thiazole ring lies flat on the surface and which one protrudes from it. Whereas Figure 5.11a shows the thiazole ring attached at the 3-position of benzothiophene protruding from the surface, another possibility is that the thiazole ring at the 2-position of benzothiophene is the one protruding from the surface. Further, the reduction of symmetry elements in two dimensions may induce chirality,[15-16] so that the enantiomers of these two conformations are also expected resulting to four possible surface adsorption geometries. The lack of STM contrast on the central part of the isomer, however, renders calculations to find the adsorption sites of other enantiomeric confirmers unnecessarily costly so that it must be nuanced that the observed Form 1 may correspond to one of four possible conformations. In Figure 5.11, it appears that the two Form 1's are enantiomeric but the question of which thiazole group sticks out of the surface, i.e. which of the four possible conformations it is, seems quite difficult to answer even from the best vertical resolution (typically 2 pm) we could obtain.

Figure 5.11d is similarly one of four possible surface conformations of **3.3*o*** *trans*$_2$. Another possibility is that the sulfur atom from the other side of the thiazole group could be interacting with a silver atom. These two possibilities could have enantiomeric forms, bringing the total number of surface configurations to four. Meanwhile, Figure 5.11g corresponds to **3.3*o*** C_2 (Figure 3.6) deposited on Ag(111). The STM contrast in the ESQC calculated image seems to be mainly due to six methyl groups: two from the thiazole rings and four from the *tert*-butyls. The case would be similar if **3.3*o*** C_1 were instead adsorbed on the surface. Aside from these two, their respective enantiomers would also be possible surface conformers. We are careful, therefore, to say that Form 2 also corresponds to *a* conformation of the **3.3*o*** *cis* adsorbed on the surface.

It is worth noting that, Forms 1 and 3 which have the *trans* conformation contribute to 86 % of the molecules observed while the rest are in the *cis* conformation. Assuming a Boltzmann distribution and using the relative energy differences of the *trans* and *cis* conformations (Figure 3.6), this corresponds well to the expected population of the molecules at 473 K. This implies that when the molecule is heated, the thermal energy was instrumental not only for sublimation but also for allowing the molecule to adapt the other metastable rotational conformers (Figure 3.6 C_1, C_2). Upon landing on the substrate at liquid helium temperature, molecules in the metastable *cis* conformation are frozen and are hindered from rotation by the surface. Matsuda and co-workers reported the observation of assemblies of this *cis* conformation of diarylethenes on the solid-liquid interface,[17] but to the best of our knowledge, this is the first isolation and imaging of the unreactive *cis* isomer at the single-molecular level under ultra-high vacuum conditions.

The central part of the molecule is the main source of dissymmetry of **3.3*o***. Given the low resolution obtained for the central bright part, it is unnecessary to find conformations of other enantiomeric forms by DFT. Instead, we prioritized in our calculations the question of the possibility that these forms may correspond to cyclization products, the closed isomers, which has *cis* and *trans* isomers depending on the direction of the methyl groups on the reactive carbons (Scheme 5.1). Although we performed deposition carefully under dark conditions, the high photosensitivity of the molecule may cause a response from any photon that may leak to the aluminum foil-covered windows of the UHV chamber. In addition to this, Kim and co-workers reported that charge transfer between the metallic surface and classical diarylethenes may reverse the relative stabilities of the open and closed forms so that closed forms may appear when induced thermally.[12] Franke and co-workers on the other hand showed that thermal processes induced by the STM tip result to the formation of the *cis* close isomer.[13] In our system, we discount these possibilities for two main reasons. First, the experimental STM images (Figure 5.9) and STS spectra (Figure 5.10) correspond much better to those calculated for the open than to the closed isomers. Further, the partial induction of closed forms by thermal processes were accomplished upon deposition at room temperature but complete conversion were reported by Kim's group after heating of the substrate at 80 ^{o}C.[12] All our measurements were performed at 4.5 K so that no thermal reaction was expected once the molecule is adsorbed on the cold substrate.

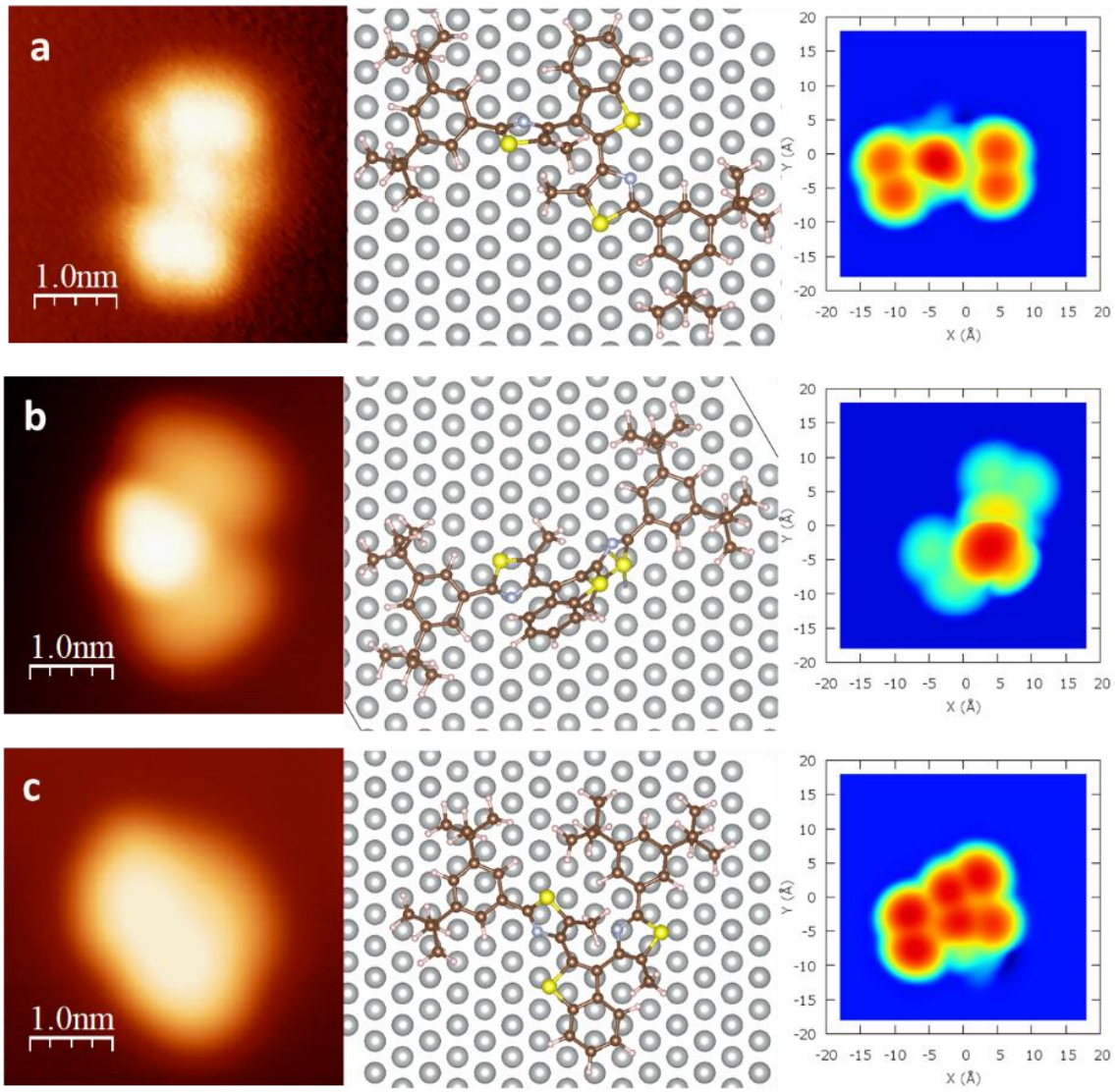

Figure 5.15. With the aid of ESQC calculations, we ascribe form 1 to the **3.3*o*** trans form in (a) while that of form 2 to (b). (c) Form 3 refers to a *cis* isomer of **3.3*o*** deposited on the surface.

Franke's group[13] performed switching using tunneling electrons from the STM tip. We attempted several ways to induce the switching such as bias pulses, electric-field induction, or consecutive scanning at high potentials but no such switching was observed. This may be due to strong hybridization of the molecular orbitals to the metallic state as sulfur atoms may interact strongly with silver atoms. Particularly, Forms 1 and 3 maintain the reactive *trans* conformation but they have strong silver-sulfur interactions. These may have drastically modified the MOs of **3.3*o*** especially that Ag-S bonds were previously shown to have a strong electrostatic character.[10] We also attempted such switching for the molecules found on the NaCl bilayer. Tunneling electrons however caused translation of the molecules due to the weak interactions on the surface. The small amount of molecules on NaCl proves this, as the molecules seem to prefer adsorption on the Ag(111) surface.

The *tert*-butyl groups also prefer a conformation in which two out of three methyl moieties are in contact with the surface favoring van der Waals interactions so that the adsorption energy increases by almost 1 eV in all forms. (Table 5.1). For the open forms of **3.3*o*** (Figure 5.11b,e,h) the *tert*-butyl groups seem to rotate and have enough flexibility to present two methyl groups on the surface implying that their carbon atoms are almost on the same plane as the aromatic rings. These methyl groups could

contribute to the stronger van der Waals interactions with the surface. These strong interactions undoubtedly cause hybridization of the molecular orbitals with the metallic substrate, preventing the switching of the molecule.

The remaining methyl group on the other hand protrudes from the surface and seems to be the main topographical feature that gives *tert*-butyl groups strong contrasts under STM. So that despite the stronger adsorption energy for these compounds, the tip could easily cause translational motion at low voltages due to its proximity to these groups. Meanwhile, high voltages could cause electric-field-induced "jumping" of the molecule either to the tip or on the surface.

For the closed *trans* form, the steric hindrance induced by the methyl group directly on the face of the solid substrate lifts the central part of the ring 3.6 Å from the surface. This seems to be the appropriate conformation in order to lift the molecule from the surface.

It is interesting to note that the calculated E_{ads} for the unsubstituted terarylenes with five aromatic rings are almost five times higher than that calculated for benzene and its derivatives.[9] This could point to possible additive nature of adsorption energies of aromatic rings for future computational studies. Barring synergistic effects, the 1 eV increase in E_{ads} may also be a measure of the attractive forces due to the eight methyl groups from the *tert*-butyl functionalities in contact with the surface.

5.5 Mapping of occupied and unoccupied states on NaCl(001)/Ag(111)

Finally, we look at mapping of electronic states of **3.3*o*** on the surface. Two monolayers of NaCl were shown to be effective in decoupling the molecular orbitals of the compound from the metallic surface to allow access to occupied and unoccupied states.[18-21] The STM of single **3.3*o*** molecules on NaCl(001)/Ag(111) showed similar images adopting a structure similar to Form 1/**3.3*o*** *trans*$_1$. At low voltage, the molecules exhibit the same shape as observed on the metallic surface. No noticeable differences in shape nor contrast were observed from 1.0 to 2.2 V until the voltage was ramped up to 2.4 V (Figure 5.16a). Meanwhile, at negative voltage, no change was seen from -1.8 to -2.4 V until -2.6 V (Figure 5.16b). Above 2.4 V and below -2.6 V, the *tert*-butyl groups lose their influence on the STM image while the central part of the molecule increases in contrast.

Considering that *tert*-butyl groups started to lose their influence on the images at 2.4 V and at -2.6 V on the NaCl surface, we estimated the gap to be around 5 V which is higher than that observe by STS on Ag(111), that predicted by TD-DFT in the gas phase, and that measured when the molecule is in solution.[2] This could be due to the imaging of transient states due to the increased lifetime of electrons/holes on the NaCl layer.[17-20]

Scanning at positive bias voltage means accessing unoccupied states while a negative bias probes occupied states. The loss of contribution from the large *tert*-butyl groups on STM images at very positive and very negative voltages leads us to believe that the measured current at these conditions is mainly due to the unoccupied and occupied states of the compound respectively. Indeed, maps of molecular orbitals (Figure 5.4) clearly show that the *tert*-butyl groups do not have a contribution to the MOs in the gas phase. MO maps from HOMO-2 to LUMO+2 are mainly dominated by the aromatic rings.

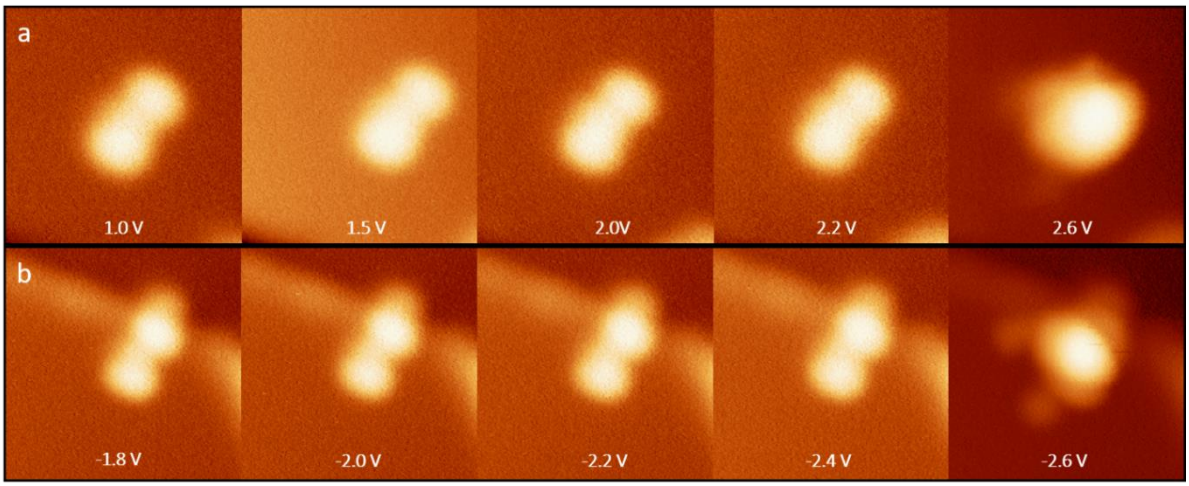

Figure 5.16. Images of **3.3*o*** on NaCl(2)/Ag(111) at (a) increasing positive voltage (image sizes 6 nm x 6 nm) and at (b) increasing negative voltage (image sizes 7 nm x 7 nm). Images were taken at constant current (1 pA).

5.6 Conclusion

In this chapter, we compared the adsorption of a non-functionalized (**3.1*o***) and *tert*-butyl functionalized (**3.3*o***) terarylene on Ag(111) by a combination of STM and DFT studies. STM images reveal three different forms of **3.3*o*** on Ag(111) due to the contrast afforded by *tert*-butyl groups. Such information was not available in the STM imaging of **3.1*o***. Analysis of adsorption geometries reveals that dissymmetry of the central benzothiophene moiety could lead to two pairs of enantiomeric forms of **3.3*o***. The low STM contrast on the central ring, however, render calculation for all the 12 forms unnecessarily costly.

We showed by DFT that despite the size of *tert*-butyl groups, they are not enough to prevent hybridization of the molecular orbitals from the surface, as the distance between the surface and the aromatic rings of the molecule remained almost similar for **3.3*o*** as that of **3.1*o***. Their two methyl groups seemed to adopt a conformation planar to the rest of the molecule, contributing to the surface area that added to stronger van der Waals interactions. Meanwhile, the remaining methyl groups protrude from the surface so that they contribute to bright topographical features when scanned at low bias potentials. We show therefore that when methyl groups are oriented in the right direction, they could be enough to show the contrast expected of *tert*-butyl groups. The contrast is not in itself due to the *tert*-butyl group but due to the orienting effect brought about by the other two methyl groups so that one methyl group protrudes from the surface, as closed forms also have bright contrast due to the central methyl groups not attached to *tert*-butyl groups.

STM images are a combination of topographical and electronic states. At higher bias potentials, (either at > 2.0 V or -2.0 V) the tip-surface distance is high so that the topographical features due to methyl groups started to lose their influence on the STM images, similar to how they do not contribute to the MOs in the gas phase, allowing us to gain access to electronic states. The *tert*-butyl group therefore could serve another purpose of tagging topographical states and ensuring that at some bias potentials, only electronic states could be imaged.

Given the two-dimensional solid substrate is a new medium for new surface-molecule interactions, this study contributes a significant insight to how a functional group may behave on 2D. We detailed the origin of bright contrasts due to *tert*-butyl groups while showing their potential to ensure that only electronic states are imaged.

5.7 Notes and References

[1] T. Nakashima, K. Atsumi, S. Kawai, T. Nakagawa, Y. Hasegawa, T. Kawai, Photochromism of thiazole-containing triangle terarylenes, *Eur. J. Org. Chem.* 2007, *19*, 3212-3218.

[2] J.P.D.C. Calupitan, O. Galangau, O. Guillermet, R. Coratger, T. Nakashima, G. Rapenne, T. Kawai, Synthesis and photochromism of chloro- and tert¬-butyl functionalized terarylene derivatives for surface deposition, *Eur. J. Org. Chem.* 2017, *17*, 2451-2461.

[3] J. K. Gimzewski, C. Joachim, R. R. Schlittler, V. Langlais, H. Tang, I. Johannsen, Rotation of a single molecule within a supramolecular bearing, *Science* 1998, *281*, 531-533.

[4] F. Chiaravalloti, L. Gross, K. H. Rieder, S. Stojkovic, A. Gourdon, C. Joachim, F. Moresco, A rack-and-pinion device at the molecular scale, *Nat. Mater*. 2007, *6*, 30-33.

[5] H.P. Jacquot de Rouville, R. Garbage, R.E. Cook, A.R. Pujol, A.M. Sirven, G. Rapenne, *Chem. Eur. J.* 2012, Rapenne, G. Synthesis of polycyclic aromatic hydrocarbon-based nanovehicles equipped with triptycene wheels, *18*, 3023-3031.

[6] M. Alemani, M. V. Peters, S. Hecht, K. H. Rieder, F. Moresco, L. Grill, Electric field-induced isomerization of azobenzene by STM, *J. Am. Chem. Soc.* 2006, *128*, 14446-14447.

[7] M. Alemani, S. Selvanathan, F. Ample, M. V. Peters, K. H. Rieder, F. Moresco, C. Joachim, S. Hecht, L. Grill, Adsorption and switching properties of azobenzene derivatives on different noble metal surfaces: Au(111), Cu(111), and Au(100), *J. Phys. Chem. C* 2008, *112*, 10509-10514.

[8] We acknowledge J. Echeverria of University of Barcelona for the surface geometry and adsorption energy calculations and X. Bouju of CEMES CNRS (UPR 8011) for the ESQC calculations. For further details and complete citation, please see Section 7.4.

[9] M. Miller, S. Simpson, N. Tymińska, E. Zurek, Benzene derivatives adsorbed to the Ag(111) surface: binding sites and electronic structures, *J. Chem. Phys*. 2015, *142*, 101924.

[10] A. H. Pakiari, Z. Jamshidi, Nature and strength of M–S bonds (M = Au, Ag, and Cu) in binary alloy gold clusters, *J. Phys. Chem. A* 2010, *114*, 9212-9221.

[11] H. Yang, Y. Wang, H. Huang, L. Gell, L. Lehtovaara, S. Malola, H. Häkkinen, N. Zheng, All-thiol-stabilized Ag_{44} and $Au_{12}Ag_{32}$ nanoparticles with single-crystal structures, *Nat. Commun.* 2013, *4*, 2422.

[12] T. K. Shimizu, J. Jung, H. Imada, Y. Kim, Adsorption-induced stability reversal of photochromic diarylethene on metal surfaces, *Chem. Commun.* 2013, 8710-8712.

[13] J. Wirth, N. Hatter, R. Drost, T. R. Umbach, S. Barja, M. Zastrow, R. Rück-Braun, J. I. Pascual, P. Saalfrank, K. J. Franke, Diarylethene molecules on a Ag(111) surface: stability and electron-induced switching, *J. Phys. Chem. C,* 2015, *119*, 4874-4883.

[14] K. S. Mali, N. Pearce, S. De Feyter, N. R. Champness, Frontiers of supramolecular chemistry at solid surfaces, *Chem. Soc. Rev.* 2017, *46*, 2520-2542.

[15] S. De Feyter, P. Iavicoli, H. Xu, Expression of chirality in physisorbed monolayers observed by scanning tunneling microscopy in *Chirality at the Nanoscale*, D. Amabilino (Ed.), Wiley-VCH, Weinheim, 2009, 215-245.

[16] K.-H. Ernst, Supramolecular surface chirality in *Supramolecular Chirality*. M. Crego-Calama, D.N. Reinhoudt (Eds.), Springer, Heidelberg, 2006, 209-252.

[17] N. Maeda, T. Hirose, K. Matsuda, Discrimination between conglomerates and pseudoracemates using surface coverage plots in 2d self-assemblies at the liquid-graphite interface, *Angew. Chem. Int. Ed.* 2017, *56*, 2371-2375.

[18] J. Guo, X. Meng, J. Chen, J. Peng, J. Sheng, X.-Z. Li, L. Xu, J.-R. Shi, E. Wang, Y. Jiang, Real-space imaging of interfacial water with submolecular resolution, *Nature Mater.* 2014, *13* 184-189.

[19] L. Gross, Recent advances in submolecular resolution with scanning probe microscopy, *Nature Chemistry*, 2011, *3*, 273-278.

[20] J. Repp, G. Meyer, S. M. Stojković, A. Gourdon, C. Joachim, Molecules on insulating films: scanning-tunneling microscopy imaging of individual molecular orbitals, *Phys. Rev. Lett.* 2005, *94*, 026803.

[21] C.J. Villagomez, T. Zambelli, S. Gauthier, A. Gourdon, S. Stojkovic, C. Joachim, STM images of a large organic molecule adsorbed on a bare metal substrate or on a thin insulating layer: visualization of HOMO and LUMO, *Surf. Sci.* 2009, *603*, 1526.

Chapter 6

Conclusion and Prospects

This thesis can be summed up as an attempt to control physical and chemical properties, either in the macroscale in solution or in the nanoscale on a 2D surface, of photoswitching terarylenes through a careful understanding of molecular design principles. All throughout the preceding chapters, a constant exchange between understanding and control of molecular properties based on how individual parts of the design of molecules affect the observed properties were evident.

We first gave a background on photoswitching materials with a particular focus on diarylethenes, scanning tunneling microscopy (STM), and STM studies on diarylethenes in the first chapter. We started with a historical background on how photons lighted the way towards the isolation of the *cis* form of azobenzene; this was one of the first photochromic switching materials developed, leading to other photoswitches such as spiropyrans, fulgides, and diarylethenes. Diarylethenes are sought for applications in miniaturized electronics such as memories and switches due to their isomerization between two stable states, the thermal stability of these two isomers, fatigue resistance, high sensitivity, among others. Modification of their central ring to an aromatic ring, to produce the derivative terarylenes, allowed finer tuning of properties and addition of new functions into the compounds. This allowed for more functions to be incorporated into the molecule while at the same time preserving the ***o***-***c*** isomerization of diarylethenes. This was illustrated by enumerating structure-property functions which could be incorporated in the central aromatic ring of these class of molecules.

Given that such functions could promise new advanced functions to molecular electronics, we showed in chapter 1 the need for scanning tunneling microscopy (STM) studies on diarylethenes/terarylenes. By giving a brief history of the major devlopments on STM, we illustrated that it can be a powerful technique to address molecules in the nanoscale. We then showed how different properties observed under the STM either at the solid-liquid interface, ultra-high vacuum, or ambient conditions, could be rationalized by their structures.

Constrained by practical factors such as machine availability, we invested time to carefully choose and develop terarylenes to be prioritized for STM. For this, we chose the criteria of sensitivity as the applications sought require that switching be accomplished with minimum amount of switching stimuli. We showed in Chapter 2 two main strategies to increase the sensitivity of terarylenes to photocyclization and cycloreversion by oxidative electron transfer chain reaction. Such strategies were based on intramolecular forces of attraction and design of electronic states of the molecules. For photocyclization, it suffices to control the ground state geometry of the compounds by intramolecular forces that lock the molecules in their reactive conformations. For cycloreversion, a control of the equilibrium between charged radical states of the ***o*** and ***c*** forms by designing groups that could stabilize/destabilize the charges was necessary. With these, we demonstrated that we could increase oxidative cycloreversion kinetics 1000x and chain reaction efficiency 100x. This chapter therefore illustrated how we can design compounds for highly sensitive switching reactions.

We then proceeded to design these compounds for STM studies. We chose two terarylenes, **3.1*o*** and **3.2*o*** and functionalized them with *tert*-butyl groups (**3.3*o*** and **3.4*o***) and chloro substituents (**3.5*o*** and **3.6*o***). These designs were based on former STM studies cited in Chapter 3. *Tert*-butyl groups were shown to improve STM contrasts while chloro substituents were known to play a function in the

assembly formation through dipole interactions. By a combination of photochemical measurements, spectroscopy, and DFT calculations, we showed that these functionalizations preserved the excellent switching properties of the original compounds. DFT calculations further predicted that several conformations of **3.3*o*** may be observed on the surface due to heating during deposition of the compounds. Initial STM experiments showed that the *tert*-butyl groups did aid in identifying the compound on the surface. In this chapter, we illustrated how we can use molecular design principles to our compounds in order to prepare them for STM studies.

In chapter 4, we studied **3.1*o*** on a Cu(111) surface under ultra-high vacuum (UHV) conditions at 80 K. Initial deposition showed aggregates of molecules with no apparent order, with some molecules moving on the surface. When the tip was retracted and a bias pulse was applied, networks of ordered molecules formed. Between the tip and surface, an electric field induced the alignment of these molecules due to their polarity. These networks were found to be stabilized by π-π interactions for several hours. This presents a new bottom-up approach to construct supramolecular assemblies on 2D surfaces. By applying what we know of the properties of **3.1*o***, we were able to rationalize this phenomenon under ultra-high vacuum conditions.

In the subsequent chapter, deposition of **3.1*o*** on Ag(111) at liquid helium temperature showed bright spots that seem to be a dimeric form of the molecule. Upon application of a bias pulse, the bright spots separate to produce a dark and a triangular spot. Subsequent pulses switched the triangular spot to a dark spot. The lack of information regarding the geometric and electronic structure of the spots led us to investigate **3.3*o*** instead, since its *tert*-butyl groups allowed for the identification of the molecules on the surface. We did observe several conformations of the molecule. With the aid of DFT and ESQC calculations, we ascribed these to a surface adsorption geometry of the molecule. Calculations for the absorption energy further showed that the **3.3*o*** had higher adsorption energy than that of **3.1*o***. The *tert*-butyl groups were also instrumental in ensuring that at some bias voltages, the electronic state of the molecule has the major contribution to the STM image. For the first time, the occupied and unoccupied states of terarylene were mapped on NaCl(001)/Ag(111).

Thus, we showed the importance of molecular design to understand, control, and even rationalize properties and phenomena from the macroscale (e.g. photoisomerization quantum yields and cycloreversion dynamics) down to the nanoscale (e.g. electric-field induced assembly formation and single-molecule adsorption). This power of molecular design should therefore be important in addressing goals to switch molecules on a 2D surface. We did not observe switching for **3.3*o*** on Ag(111) nor on NaCl(001) but by combining our knowledge of how specific molecules interact with surfaces, it should be possible to propose some ideas in order to observe this. To date, only one team managed switching under ultra-high vacuum conditions.[1-2] Even in the solid-liquid interface, switching was shown to happen in the liquid phase instead of the surface.[3] Given that the surface drastically changes the molecular orbitals of the compounds, it should suffice to lift the photoswitching core from the surface. This can be achieved by using structures having a tripodal complex onto which the molecule could be attached[4] or by double-decker designs.[5] Incorporation of sulfur atoms, which have strong interactions with the metal surfaces usually employed for these studies,[2] could also be avoided.

With the combined power of molecular design and STM technique, aspects other than switching of terarylenes may also be investigated. For example, it was illustrated by spectroscopic studies that compounds **1.1**-**1.3** (Chapter 1, Scheme 1.4) switches their electronic conjugation pathway between ***o*** and ***c*** forms. This was proposed to be a molecular rerouter[6] so that it merits conductance

switching experiments at the molecular level. A recently developed STM, having four independent tips, could be instrumental for this as it could measure conductance while imaging molecules.[7] The switching between localization and delocalization of the central imidazole ring in **1.6**[8] could also be investigated. The on-surface synthesis of graphene analogues[9-12] is also a currently booming field in which terarylenes could contribute to. The focus of photorelease of acids or other organic products[13-18] has always been the concept of using the central framework of the ***o*** form to increase the efficiency (quantum yield) of acid release.[14-18] The resulting side-product however, is a flat aromatic network which could be considered as a derivative of sulfur- or nitrogen-doped graphene. Compound **1.9**[13] (Chapter 1, Scheme 1.8) and related compounds[14-18] could therefore be studied by STM as well, but instead of light, inelastic electrons could be used to form the ***c*** form, while the generation of the aromatic analogue could be induced thermally. Lastly, the helicity due to extension of oligomers of thiazoles[19] could be interesting from the viewpoint of chirality in 2D.[20]

From the manipulation of xenon atoms[21] and observation of simple benzene molecules,[22] the field of STM has indeed made significant advances so that now we are manipulating and addressing stimuli-responsive molecules. Whereas a particular stimulus may allow molecular-level access to switch properties of these compounds, the STM may allow control of individual molecules. We were able to show how a proper design of these molecules are important in fine-tuning macroscale properties, rationalizing nanoscale phenomena, and direct engineering of single molecule properties.

This thesis is therefore a humble contribution to the field of molecular design, photochemistry, and surface science. The atomic-scale understanding of light-matter interactions in the start of the 20th century brought us the fundamentals of chemistry and with that, the most powerful tools of molecular design, to influence properties of matter from the bulk down to the nanoscale. We go forward to the 21st century by engineering matter to perform intended functions at the smallest scales, serving as big foundations of revolutionary technologies of the future.

References

[1] J. Wirth, N. Hatter, R. Drost, T. R. Umbach, S. Barja, M. Zastrow, R. Rück-Braun, J. I. Pascual, P. Saalfrank, K. J. Franke, Diarylethene molecules on a Ag(111) surface: stability and electron-induced switching, *J. Phys. Chem. C,* 2015, *119*, 4874-4883.

[2] G. Reecht, C. Lotze, D Sysoiev, T. Huhn, K. J. Franke, Visualizing the role of molecular orbitals in charge transport through individual diarylethene isomers, *ACS Nano*, 2016, *10*, 10555-10562.

[3] R. Arai, S. Uemura, M. Irie, K. Matsuda, Reversible photoinduced change in molecular ordering of diarylethene derivatives at a solution-HOPG interface, *J. Am. Chem. Soc.* 2008, *130*, 9371-9379.

[4] U.G.E. Perera, F. Ample, H. Kersell, Y. Zhang, J. Echeverria, M. Grisolia, G. Vives, G. Rapenne, C. Joachim, S.W. Hla, Controlled clockwise and anticlockwise rotational switching of a molecular motor, *Nature Nanotechnol*. 2013, *8*, 46-51.

[5] Y. Zhang, H. Kersell, R. Stefak, J. Echeverria, V. Iancu, U.G.E. Perera, Y. Li, A. Deshpande, K.-F. Braun, C. Joachim, G. Rapenne, S.-W. Hla, Simultaneous and coordinated rotational switching of all molecular rotors in a network, *Nat. Nanotechnol*., 2016, *11*, 706-712.

[6] T. Kawai, T. Iseda, M. Irie, Photochromism of triangle terthiophene derivatives as molecular re-router, *Chem. Commun.* 2004, 72-73.

[7] J. Yang, D. Sordes, M. Kolmer, D. Martrou, and C. Joachim, Imaging, single atom contact and single atom manipulations at low temperature using the new ScientaOmicron LT-UHV-4 STM, *Eur. Phys. J-Appl. Phys.* 2016, *73*, 107012.

[8] T. Nakashima, M. Goto, S. Kawai, T. Kawai, Photomodulation of ionic interaction and reactivity: reversible photoconversion between imidazolium and imidazolinium, *J. Am. Chem. Soc.* 2008, *130*, 14570-14575.

[9] P. Ruffieux, *et al.* On-surface synthesis of graphene nanoribbons with zigzag edge topology, *Nature*, 2017, *531*, 489-492.

[10] E. Carbonell-Sanromà, *et al.* Doping of graphene nanoribbons via functional group edge modification*, ACS Nano*, 2017, *117*, 7355-7361.

[11] J. Krüger, F. Garcia, F. Eisenhut, D. Skidin, J. M. Alonso, E. Guitián, D. Pérez, G. Cuniberti, F. Moresco, D. Peña, Decacene : on-surface generation, *Angew. Chem. Int. Ed.* **2017**, *56*, 11945-11948.

[12] J. I. Urgel, *et al*. On-surface synthesis of heptacene organometallic complexes, *J. Am. Chem. Soc.* 2017, *130*, 11658-11661.

[13] H. Nakagawa, S. Kawai, T. Nakashima, T. Kawai, Synthesis and photochemical reactions of photochromic terarylene having a leaving methoxy group, *Org. Lett.* 2009, *11*, 1475-1478.

[14] H. Nakagawa, T. Nakashima, T. Kawai, Subsequent chemical reactions of photochromic 4,5-dibenzothienylthiazoles, *Eur. J. Org. Chem.* 2012, 4493-4500.

[15] T. Nakashima, K. Tsuchie, R. Kanazawa, R. Li, S. Iijima, O. Galangau, H. Nakagawa, K. Mutoh, Y. Kobayashi, J. Abe, T. Kawai, Self-contained photoacid generator triggered by photocyclization of triangle terarylene backbone, *J. Am. Chem. Soc.* 2015, *137*, 7023-7026.

[16] R. Li, T. Nakashima, R. Kanazawa, O. Galangau, T. Kawai, Efficient self-contained photoacid generator system based on photochromic terarylenes, *Chem. Eur. J.* 2016, *22*, 16250-16257.

[17] R. Li, T. Nakashima, T. Kawai, A self-contained photoacid generator for super acid based on photochromic terarylene, *Chem. Commun.* 2017, 4339-4341.

[18] O. Galangau, S. Delbaere, N. Ratel-Ramond, G. Rapenne, R. Li, J. P. D. C. Calupitan, T. Nakashima, T. Kawai, Dual photochemical bond cleavage for a diarylethene-based phototrigger containing both methanolic and acetic sources, *J. Org. Chem.* 2016, *81*, 11282-11290.

[19] T. Nakashima, K. Imamura, K. Yamamoto, Y. Kimura, S. Katao, Y. Hashimoto, T. Kawai, Synthesis, structure and properties of α,β-linked oligothiazoles with controlled sequence, *Chem. Eur. J.* 2014, *20*, 13722-13729.

[20] O. Stetsovych, M. Švec, J. Vacek, J. V. Chocholoušová, A. Jančařík, J. Rybáček, K. Kosmider, I. G. Stará, P. Jelínek, I. Starý, From helical to planar chirality by on-surface chemistry, *Nat. Chem.* 2017, *9*, 213-218.

[21] D. M. Eigler, E. K. Schweizer, Positioning single atoms with a scanning tunnelling microscope *Nature*, 1990, *344*, 524-526.

[22] H. Ohtani, R. J. Wilson, S. Chiang, C. M. Mate, Scanning tunneling microscopy observations of benzene molecules on the Rh(111)-(3 × 3) (C_6H_6 + 2CO) surface, *Phys. Rev. Lett.* 1988, *60*, 2398-2401.

Chapter 7

Methods

7.1 Details of Synthetic Procedures

7.1.1 General syntheses, purification, and characterization. 1-bromo-3,5-di-tert-butylbenzene, 2,4-dibromothiazole, thiobenzamide, 4-chlorothiobenzamide, palladium (II) acetate, trimethyl borate, 4,5-Bis-(diphenylphosphino)-9,9-dimethylxanthene (Xantphos), lithium diisopropylamide, iodomethane, tetrakis(triphenylphosphine)palladium, benzothiophene-3-boronic acid, di-tert-butylmethylphosphonium tetrafluoroborate, pivalic acid, potassium phosphate, dioxane, and dry solvents were purchased from Sigma Aldrich and were used without any further treatment. HPLC grade solvent purchased from Sigma Aldrich were used for purification and spectroscopic analyses. ^{1}H and ^{13}C NMR spectra were recorded on a Bruker Avance NMR (300 MHz or 500 MHz) at 25°C. Chemical shifts are defined with respect to TMS = 0 ppm for ^{1}H and ^{13}C NMR spectra and were measured relative to residual solvent peaks. The following abbreviations were used to describe the signals: s for singlet; d for doublet; t for triplet; q for quadruplet; m: for multiplet. Mass spectra were measured using Q TRAP 2000 (Applied Biosystems, High resolution mode), API-365 (Perkin Elmer Sciex), JEOL JMS-Q1000TD and JMS-700 MStation spectrometers. Melting points were measured on a Kofler Heizbank melting point apparatus or with a capillary Melting Point Meter M5000 apparatus. Purifications by automatic flash chromatography were performed with HPLC grade solvents on a Spot ultimate automatic chromatography system (ARMEN Instrument). Two types of prepacked column were used either Versaflash column from Aldrich or Universal column from Yamazen Corporation. High purity grade silica from Fluka (pore size of 60 Å, particle size of 40-63 µm) was used for manual flash chromatography. TLC analyses were achieved on silica gel bought from Fluka (silica gel matrix containing a fluorescent indicator at 254 nm).

7.1.2 Synthesis of compounds in Chapter 2. For studies in section 2.3, compounds **2.2*o***[1] and **2.3*o***[2] were synthesized as previously reported. Synthesis of **2.1*o*** was accomplished as shown in Scheme 2.4. Details are as follows:

4,5-bis(2,5-diphenylthiazol-4-yl)-2-phenylthiazole (2.1*o*). A 100 mL 2-necked flask was charged with 0.11 g of **2.4** (1 eq), bromobenzene (0.090 g, 2.5 eq), di-t-butylmethylphosphine tetrafluoroborate (0.12 g, 0.2 eq), $CsCO_3$ (0.30 g, 4 eq), $Pd(OAc)_2$ (0.010 g, 0.2 eq) and pivalic acid (0.014 g, 0.6 eq) in 4 mL mesitylene. The mixture was refluxed at 150 °C overnight. The mixture was filtered by celite, extracted to ethyl acetate, washed with water, and dried over anhydrous Na_2SO_4. Silica gel column chromatography (9:1 hexane/ethyl acetate) afforded 0.050 g of **2.1*o*** in 34 % yield as colorless powder. ^{1}H NMR (300 MHz, $CDCl_3$, 25 °C, TMS): δ= 8.0 (m, 2 H; ArH), 7.8 (m, 4 H; ArH), 7.4 (m, 10 H; ArH), 7.1 (m, 9 H; ArH); ^{13}C NMR (150 MHz, $CDCl_3$, 25°C, TMS): δ= 147.65, 145.00, 141.76,

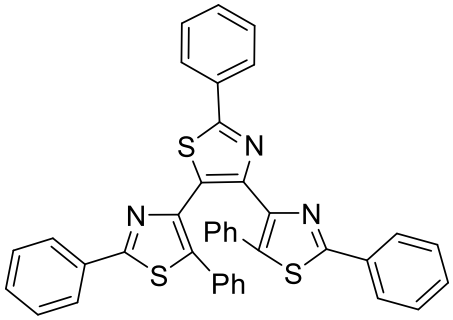

136.11, 133.70, 133.50, 133.35, 131.20, 130.69, 130.56, 130.25, 130.11, 129.82, 128.9, 128.88, 128.85, 128.69, 128.65, 128.36, 128.31, 128.02, 126.85, 126.73, 126.56; ESI-HRMS (m/z) $[M + Na]^+$ calcd. for $C_{39}H_{25}N_3S_3$-Na^+: 654.1108; Found: 654.11083.

4,5-bis(2-phenylthiazol-4-yl)-2-phenylthiazole (2.4). A 100 mL 2-necked flask was charged with 4,4-dibromo-2-phenylthiazole[3] (0.30 g, 0.45 eq), 2-phenyl-4-(4,4,5,5-tetramethyl-1,3,2-dioxaborolan-2-yl)thiazole[4] (0.61 g, 1.0 eq), PPh_3 (0.038 g, 0.07 eq), $Pd(PPh_3)_4$ (0.073 g, 0.03 eq), and 10 mL 2M K_3PO_4 (10 mL) in dioxane (10 mL). The mixture was stirred under N_2 atmosphere at 110 °C for 72 hours. The organic layer was extracted with chloroform, washed with water, and dried over anhydrous Na_2SO_4. The sample was then filtered and concentrated by vacuum evaporation. Silica gel column chromatography (8:2 hexane/ethyl acetate) afforded 0.11 g of product in 25 % yield. ^{1}H NMR (300 MHz, $CDCl_3$, 25 °C, TMS): δ= 8.1 (m, 2 H; ArH), 8.0 (m, 4 H; ArH), 7.5 (m, 6 H; ArH).

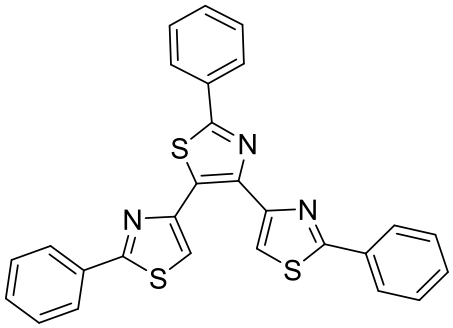

7.1.3 Synthesis of compounds in Chapter 3. Synthetic routes are shown in Schemes 3.1-3.4

Synthesis of 2,3-bis(5-methyl-2-phenylthiazol-4-yl)benzothiophene (3.1*o*). A dry Schlenck flask was charged with 4-bromo-5-methyl-2-phenylthiazole (0.099 g, 1.2 eq, 0.3903 mmol), **3.12** (0.1 g, 1 eq, 0.33 mmol), pivalic acid (0.01 g, 0.3 eq, 0.1 mmol), cesium carbonate (0.21 g, 2 eq, 0.65 mmol), di-tert-butylmethylphosphonium tetrafluoroborate (0.008 g, 0.1 eq, 0.03 mmol), palladium acetate (0.004 g, 0.03 mmol, 0.05 eq, 5mol%), and 1 mL mesitylene under Ar atmosphere. The solution was refluxed at 140 °C overnight and then allowed to cool at room temperature. The solution was then diluted with dichloromethane and ethyl acetate and filtered by celite. The solvents were removed and the crude product was purified by silica gel column chromatography (1:1 CH_2Cl_2:hexane) twice, affording 0.11 g of product (71 % yield). All characterization agreed fully with literature.[5]

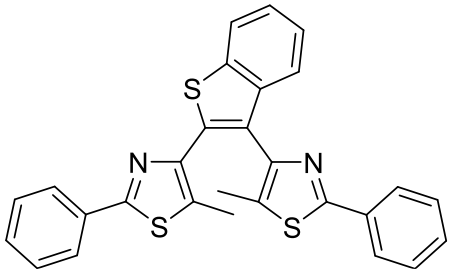

Synthesis of 4,5-bis(5-methyl-2-phenylthiazol-4-yl)-2-phenylthiazole (3.2*o*). 3.2*o* was synthesized by the same procedure as **3.1o** to couple **3.13** and 4-bromo-5-methyl-2-phenylthiazole by C-H direct arylation. From **3.13** (0.18 g, 1 eq, 0.54 mmol), 4-bromo-5-methyl-2-phenylthiazole (0.16 g, 1.2 eq, 0.65 mmol), pivalic acid (0.017 g, 0.3 eq, 0.16 mmol), cesium carbonate (0.35 g, 2.0 eq, 1.1 mmol), di-tert-butylmethylphosphonium tetrafluoroborate (0.014 g, 0.1 eq, 0.054 mmol), palladium acetate (0.006g, 0.05 eq, 0.027 mmol), and 1.7 mL mesitylene, **3.2o** (0.070 g, 26%) was obtained as a white powder. All characterization agreed fully with literature.[2]

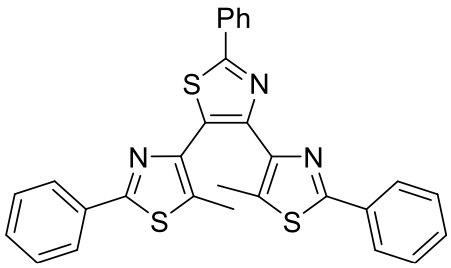

Synthesis of 2,3-bis(5-methyl-2-[3,5-di-tert-butylphenyl]thiazol-4-yl)benzothiophene (3.3*o*). 3.3*o* was

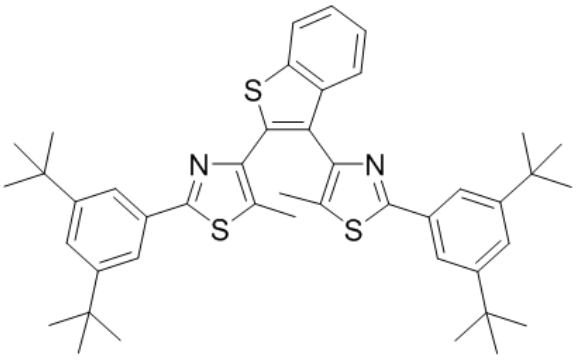

synthesized by the same procedure as **3.1o** to couple **3.14** and **3.8** by C-H direct arylation. From **3.14** (0.25 g, 1.0 eq, 0.59 mmol), **3.8** (0.24 g, 1.1 eq, 0.65 mmol), pivalic acid (0.018 g, 0.3 eq, 0.18 mmol), cesium carbonate (0.39 g, 2 eq, 1.18 mmol), di-tert-butylmethylphosphonium tetrafluoroborate (0.014 g, 0.1 eq, 0.05 mmol), palladium acetate (0.06 g, 0.03 mmol, 0.05 eq, 5 mol%), and 2 mL mesitylene, 0.384 g of product (92 % yield) was afforded. Rf=0.35 (CH_2Cl_2/hexane 1:1) ^{1}H NMR (300 MHz, $CDCl_3$): δ 7.97 – 7.86 (m, 4H, ArH), 7.83 (d, J = 1.8 Hz, 2H, H_a), 7.74 (d, J = 1.8 Hz, 2H, $H_{a'}$), 7.51 (t, J = 1.8 Hz, 1H, H_b), 7.49 (t, J = 1.8 Hz, 1H, $H_{b'}$), 7.47 – 7.33 (m, 3H, ArH), 2.14 (s, 3H, CH_3), 2.06 (s, 3H, CH_3), 1.38 (s, 18H,tert-Bu), 1.36 ppm (s, 18H,tert-Bu); ^{13}C NMR (75 MHz, $CDCl_3$): δ 165.61, 165.55, 151.64, 151.58, 147.11, 145.80, 140.16, 139.92, 136.12, 133.43, 133.05, 131.54, 131.45, 128.69, 124.95, 124.56, 124.47, 124.36, 124.23, 122.07, 120.90, 120.84, 35.12, 35.08, 31.57, 31.54, 12.43, 12.28 ppm; HRMS (EI): m/z calcd for $C_{44}H_{53}N_2S_3$ $[M+H]^+$: 705.3371; found: 705.3370.

Synthesis of 4,5-bis(5-methyl-2-[3,5-di-tert-butylphenyl]thiazol-4-yl)-2-phenylthiazole (3.4*o*). 3.4*o* was

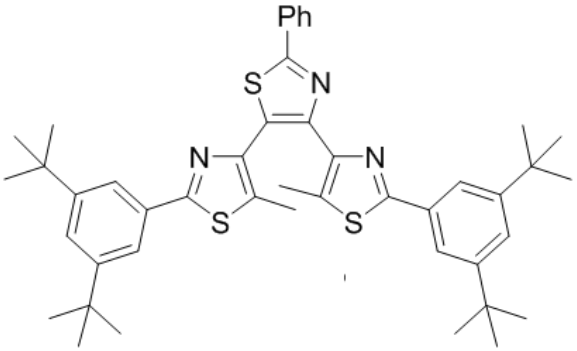

synthesized by the same procedure as **3.1*o*** to couple **3.15** and **3.8** by C-H direct arylation. From **3.15** (0.30 g, 1.2 eq, 0.806 mmol), **3.8** (0.30 g, 1.0 eq, 0.67 mmol), pivalic acid (0.021 g, 0.3 eq, 0.21 mmol), cesium carbonate (0.44 g, 2.0 eq, 1.3 mmol), di-*tert*-butylmethylphosphonium tetrafluoroborate (0.017 g, 0.1 eq, 0.034 mmol), palladium acetate (0.008g, 0.05 eq, 0.034 mmol), and 2.2 mL mesitylene, **3.4*o*** (0.359 g, 66%) was obtained as a white powder. Rf=0.43 (CH_2Cl_2/hexane 1:1) ^{1}H NMR (300 MHz, $CDCl_3$): δ 8.12 – 8.05 (m, 2H, ArH), 7.72 (d, J = 1.8 Hz, 2H, H_a), 7.59 (d, J = 1.8 Hz, 2H, $H_{a'}$), 7.53 – 7.43 (m, 4H), 7.40 (t, J = 1.8 Hz, 1H, $H_{b'}$), 2.65 (s, 3H, CH_3), 2.17 (s, 3H, CH_3), 1.34 (s, 18H,*tert*-Bu), 1.27 (s, 18H,tert-Bu).; ^{13}C NMR (75 MHz, $CDCl_3$): δ 166.78, 165.28, 164.86, 151.46, 151.32, 148.21, 146.29, 143.70, 133.86, 133.20, 133.01, 132.63, 131.81, 130.19, 129.42, 129.04, 126.71, 124.26, 124.01, 120.91, 120.81, 35.06, 34.99, 31.54, 31.49, 12.97, 12.50 ppm; HRMS (EI): m/z calcd for $C_{45}H_{53}N_3S_3$ $[M]^+$: 731.3402; found: 731.3406.

Synthesis of 2,3-bis(5-methyl-2-[4-chlorophenyl]thiazol-4-yl)benzothiophene (3.5*o*). 3.5*o* was

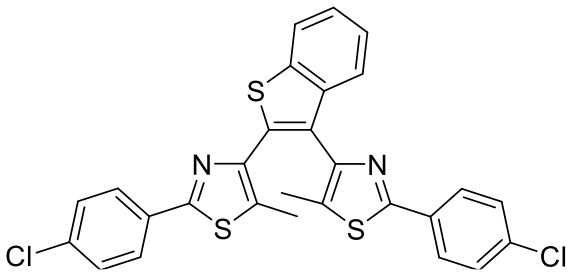

synthesized by the same procedure as **3.1o** to couple **3.16** and **3.11** by C-H direct arylation. From **3.16** (0.20 g, 1.0 eq, 0.69 mmol), **3.11** (0.24 g, 1.0 eq, 0.69 mmol), pivalic acid (0.021 g, 0.3 eq, 0.21 mmol), cesium carbonate (0.46 g, 2.0 eq, 1.39 mmol), di-*tert*-butylmethylphosphonium tetrafluoroborate (0.018 g, 0.1 eq, 0.069 mmol), palladium acetate

(0.008 g, 0.05 eq, 0.035 mmol), and 2.31 mL mesitylene, **3.5o** (0.080 g, 20 % yield) was obtained as a white powder. M.p. 171°C; Rf=0.50 ($CHCl_3$/hexane 1:1) ^{1}H NMR (300 MHz, $CDCl_3$): δ = 7.93-7.82 (m, 6 H, ArH), 7.43-7.37 (m, 6H, ArH), 2.07 (s, 3H, CH_3), 2.03 (s, 3H, CH_3); ^{13}C NMR (75 MHz, $CDCl_3$): δ 163.33, 163.31, 147.42, 146.07, 139.93, 139.88, 135.99, 135.87, 135.86, 132.39, 132.38, 132.04, 129.28, 129.24, 128.40, 127.65, 127.61, 125.25, 124.74, 124.28, 122.21, 12.37, 12.24 ppm; HRMS (EI): m/z calcd for $C_{28}H_{18}Cl_2N_2S_3$ $[M]^+$: 548.0008; found: 548.0003.

Synthesis of 4,5-bis(5-methyl-2-[4-chlorophenyl]thiazol-4-yl)-2-phenylthiazole (3.6o). **3.6o** was

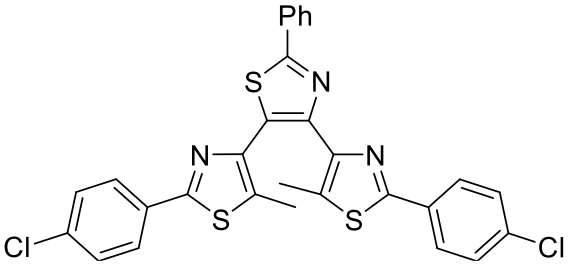

synthesized by the same procedure as **3.1o** to couple **3.16** and **3.11** were coupled by C-H direct arylation. From **3.16** (0.12 g, 1.5 eq, 0.41 mmol), **3.8** (0.1 g, 1.0 eq, 0.27 mmol), pivalic acid (0.008 g, 0.3 eq, 0.081 mmol), cesium carbonate (0.178 g, 2.0 eq, 0.54 mmol), di-*tert*-butylmethylphosphonium tetrafluoroborate (0.007 g, 0.1 eq, 0.027 mmol), palladium acetate (0.003g, 0.05 eq, 0.027 mmol), and 0.9 mL mesitylene, **3.6o** (0.046 g, 31%) was obtained as a white powder. M.p. Rf=0.41 (CH_2Cl_2/hexane 1:1) ^{1}H NMR (300 MHz, $CDCl_3$): δ 8.08 – 8.03 (m, 2H, ArH), 7.91 – 7.82 (m, AA'XX', 2H, ArH), 7.74 – 7.64 (m, AA'XX', 2H, ArH), 7.50 – 7.45 (m, 3H, ArH), 7.43 – 7.36 (m, AA'XX', 2H, ArH), 7.33 – 7.27 (m, AA'XX', 2H, ArH), 2.58 (s, 3H, CH3), 2.13 (s, 3H, CH3); ^{13}C NMR (75 MHz, $CDCl_3$): δ 167.36, 162.94, 162.53, 147.84, 146.55, 144.07, 135.99, 135.66, 133.62, 133.59, 132.83, 132.26, 132.07, 130.42, 129.28, 129.10, 128.82, 128.61, 127.66, 127.53, 126.74, 12.95, 12.50 ppm; HRMS (EI): m/z calcd for $C_{29}H_{19}N_3Cl_2S_3$ $[M]^+$: 575.0018; found: 575.0107.

Scheme 3.1 shows the synthetic route to access the side 2-phenyl-thiazo-5-yl groups (**3.8** and **3.11**) necessary for compounds **3.3*o*** - **3.6*o***. Following are the details:

Synthesis of 4-bromo-2-(3,5-di-tert-butylphenyl)thiazole (3.7). A solution of 1-bromo-3,5-di-tert-

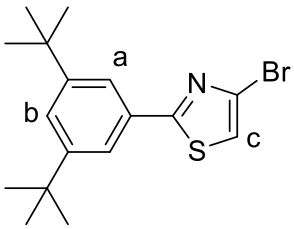

butylbenzene (3 g, 1.68 eq, 11.14 mmol) in 30 mL dry THF was charged with a hexane solution of n-butyllithium (12.26 mmol, 1.1 eq) at -78 °C under Ar atmosphere and stirred for 30 min. Then, trimethyl borate was added (1.9 mL, 16.71 mmol, 2.4 eq) and the solution was slowly heated to room temperature overnight. Then, 5 mL of aq. 6M HCl was added and the solution was stirred for another three hours. 200 mL of water was added and the precipitate was collected, washed with water, and dried in vacuo to generate a white precipitate. The product was used without further purifications. This was then charged with 2,4-dibromothiazole (1.648 g, 1 eq, 6.79 mmol), and potassium phosphate (4.32 g, 3 eq, 20.4 mmol). Meanwhile, a mixture of palladium (II) acetate (0.038 g, 0.025 eq, 0.17 mmol, 2.5mol%) and 4,5-Bis-9,9-dimethylxanthene (Xantphos) (0.098 g, 0.025eq, 0.17 mmol) in 25 mL of dried and degassed THF was stirred and bubbled with Ar gas. A darker color was observed after 15 mins and this was added to the solids above. This resulting mixture was refluxed at 60 °C for 18 hrs. The solids were filtered on celite and the crude was extracted with CH_2Cl_2. The solvent was removed and the product was purified by silica gel column chromatography (CH_2Cl_2) and **3.7** was collected as a yellow oil to yield 1.6 g of product (67% yield). Rf=0.67 (CH_2Cl_2/hexane 1:1); ^{1}H NMR (300 MHz, $CDCl_3$): δ 7.75 (d, J = 1.8 Hz, 2H, H_a), 7.52 (t, J = 1.8 Hz, 1H, H_b), 7.19 (s, 1H, H_c), 1.37 ppm (s, 18H, tert-Bu); ^{13}C NMR (75 MHz, $CDCl_3$): δ

170.38, 151.85, 132.16, 125.90, 125.20, 120.89, 116.21, 35.13, 31.52 ppm; HRMS (ESI): m/z calcd for $C_{17}H_{23}BrNS$ $[M+H]^+$: 352.0735; found: 352.0721.

Synthesis of 4-bromo-2-(3,5-di-tert-butylphenyl)-5-methylthiazole (3.8). 5.08 mmol of a THF solution of lithium diisopropylamide (1.5 eq) was added to a solution of 1.2 g of **3.7** (1 eq, 3.4 mmol) in THF at -78 °C and stirred for 15 mins. Then, iodomethane (0.77 g, 1.6 eq, 5.42 mmol) was added and the mixture was stirred at the same temperature for an additional 2 hours. The solution was then slowly warmed to room temperature before quenching with 20 mL 2M aqueous ammonium chloride. The product was extracted with ether, washed with brine and dried in vacuo. Purification by column chromatography (CH_2Cl_2) afforded 0.905 g of **3.8** (73% yield). M.p. 136 °C; Rf=0.65 (CH_2Cl_2/hexane 1:1); ^{1}H NMR (300 MHz, $CDCl_3$) δ 7.69 (d, J = 1.8 Hz, 2H, H_a), 7.49 (t, J = 1.8 Hz, 1H, H_b), 2.43 (s, 3H, CH_3), 1.36 ppm (s, 18H, tert-Bu); ^{13}C NMR (125 MHz, $CDCl_3$): δ 167.12, 151.84, 132.10, 128.42, 125.05, 124.93, 120.73, 35.15, 31.44, 13.18 ppm; HRMS (EI): m/z calcd for $C_{18}H_{25}BrNS^+$ $[M+H]^+$: 366.0891; found: 366.0876.

Synthesis of 2-(p-chlorophenyl)thiazole (3.9). A solution of *p*-chlorothiobenzamide (5 g, 1 eq, 29 mmol) and 2-bromo-1,1-diethoxyethane (8.59 g, 1.5 eq, 43.6 mmol) in 20 mL of dry ethanol was refluxed overnight. Then, the mixture was allowed to cool to room temperature, diluted with water, extracted with ether, and washed with brine. The combined organic phases were dried over MgSO4, filtered, and dried in vacuo. Purification by column chromatography (or hexane/ethyl acetate 40:1) afforded 3.14 g of **3.9** as yellow oily crystals (65% yield). Rf=0.42 (CH_2Cl_2/hexane 1:1); ^{1}H NMR (300 MHz, $CDCl_3$): δ 7.92 – 7.87 (m, AA'XX', 4H, 2H, H_d), 7.86 (d, J = 3.3 Hz, 1H, H_e), 7.41 (m, AA'XX', 4H, $H_{d,f}$), 7.33 ppm (d, J = 3.3 Hz, 1H, H_g); ^{13}C NMR (75 MHz, $CDCl_3$): δ 167.17, 143.94, 136.04, 132.20, 129.30, 127.88, 119.26 ppm; HRMS (EI): m/z calcd for $C_9H_7ClNS^+$ $[M+H]^+$: 194.9909; found: 194.9915.

Synthesis of 4-bromo-2-(4-chlorophenyl)-thiazole (3.10). A solution of **3.9** (2.00 g, 1eq, 10.2 mmol) and N-bromosuccinimide (2.00g, 1.1eq, 11.2 mmol) in 50 mL DMF was stirred and refluxed overnight. Then, the mixture was allowed to cool to room temperature, diluted with water, extracted with ether and washed with brine. The combined organic phases were dried over $MgSO_4$, filtered and dried in vacuo. Purification by silica-gel column chromatography (hexane/chloroform 8:2) afforded 2.4 g of **3.10** as a white powder (86 % yield). M.p. 103 °C; Rf=0.67 (CH_2Cl_2/hexane 1:1); ^{1}H NMR (300 MHz, $CDCl_3$): δ 7.85 – 7.75 (m, AA'XX', 2H, H_d), 7.72 (s, 1H, H_e), 7.47 – 7.35 ppm (m, AA'XX', 2H, H_f); ^{13}C NMR (75 MHz, $CDCl_3$): δ 168.26, 145.12, 136.55, 131.68, 129.44, 127.51, 109.03 ppm; HRMS (EI): m/z calcd for $C_9H_5BrClNS^+$ $[M]^+$: 272.9015; found: 272.9016.

Synthesis of 4-bromo-2-(4-chlorophenyl)-5-methylthiazole (3.11). Synthesis of **3.11** was accomplished by a halogen-dance reaction from **3.7**. 8.18 mmol of a THF solution of lithium diisopropylamide (1.5 eq) was added to a solution of 1.5 g of **7** (1 eq, 5.45 mmol) in 20 mL of dry THF at -78 °C and stirred for 15 mins under Ar. Then, iodomethane (2.32 g, 3 eq, 16 mmol) was added and the mixture

was stirred at the same temperature for an additional 2 hours. The solution was allowed to warm to room temperature and stirred overnight before quenching with 20 mL of 2M aqueous ammonium chloride. The product was extracted with ether, washed with brine and dried in vacuo. Separation by column chromatography (CH_3Cl/hexane 3:7) afforded 1.45 g of **11** as a white powder (92 % yield). M.p. 98 °C; Rf=0.71 (CH_2Cl_2/hexane 1:1); ^{1}H NMR (300 MHz, $CDCl_3$): δ 7.84 – 7.73 (m, AA'XX', 2H, H_d), 7.43 – 7.32 (m, AA'XX', 2H, H_f), 2.42 ppm (s, 3H, CH_3).; ^{13}C NMR (75 MHz, $CDCl_3$): δ 164.18, 136.32, 131.43, 129.29, 127.27, 125.65 , 13.17 ppm; HRMS (EI): m/z calcd for $C_{10}H_7BrClNS^+$ $[M]^+$: 286.9171; found: 286.9171.

Synthesis of 4-(benzothiophen-3-yl)-2-(phenyl)-5-methylthiazole (3.12). A Schlenck flask was charged

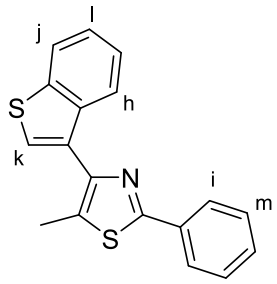

with 4-bromo-5-methyl-2-phenylthiazole[1] (0.476 g, 1 eq, 1.87 mmol), benzothiophene-3-boronic acid (0.596 g, 1.5 eq, 2.81 mmol), potassium phosphate (596 g, 1.5 eq, 2.81 mmol), and tetrakis(triphenylphosphine)palladium (0.064 g, 0.03 eq, 0.056 mmol) under Ar atmosphere. DME (37.5 mL) and water (18.7 mL) were added and the solution was refluxed at 60 °C for 24 hours. The solution was then cooled to room temperature before extracting with ethyl acetate, washed with water, dried over $MgSO_4$ and dried in vacuo. Separation by column chromatography (1:1 CH_2Cl_2:hexane solvent) afforded 0.5 g of the product (87 % yield). M.p. 153 °C; Rf=0.46 (CH_2Cl_2/hexane 1:1); ^{1}H NMR (300 MHz, $CDCl_3$): δ 8.16 – 8.09 (m, 1H, H_h), 8.05 – 7.98 (m, 2H, Hi), 7.95 – 7.90 (m, 1H, H_j), 7.54 (s, 1H, H_k), 7.50 – 7.36 (m, 5H, H_l), 2.56 (s, 3H, CH_3). ^{13}C NMR (75 MHz, $CDCl_3$): δ 164.15, 147.51, 140.15, 138.72, 134.60, 133.89, 130.66, 130.54, 129.86, 129.00, 127.78, 126.42, 125.77, 124.67, 124.50, 124.46, 122.61, 12.81 ppm; HRMS (EI): m/z calcd for $C_{18}H_{13}NS_2$ $[M]^+$: 307.0489; found: 307.0487.

Synthesis of 2-phenyl-5-methyl-4-(2-phenylthiazol-4-yl)-thiazole (3.13). A solution of 4-bromo-5-methyl-

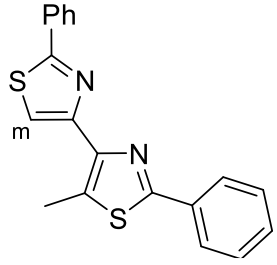

2- phenylthiazole[6b] (0.5 g, 1.5 eq, 1.97 mmol) in dry THF (5.6 ml) under dry Ar conditions was cooled down to -78 °C and then added with 1.8 mL 1.2 M n-butyllithium (1.65 eq, 2.16 mmol). The mixture was stirred for another 15 mins before adding trimethyl borate (1.0 g, 7.5 eq, 9.84 mmol). The mixture was stirred for another two hours at the same temperature before allowing to slowly warm-up to room temperature overnight. Then, the solvents DME (3.3 mL) and water (3.3 ml) were slowly added. Next, 4-bromo-2-phenylthiazole[6b] (0.31 g, 1 eq, 1.31 mmol), potassium phosphate (0.84 g, 3 eq, 3.94 mmol), and tetrakis(triphenylphosphine)palladium (0.09 g, 0.06 eq, 0.079 mmol) were added. The mixture was then refluxed for 24 h at 60 °C, maintaining inert conditions. Then, the reaction was allowed to cool down to room temperature and diluted with water and ether. The product was extracted to ether, washed with brine, dried over $MgSO_4$, and dried in vacuo. Purification by silica gel column chromatography (CH_2Cl_2:hexane 1/1) afforded 0.42 g (96 %) of **3.13**. M.p. 140 °C; Rf=0.15 (CH_2Cl_2/hexane 3:7); ^{1}H NMR (300 MHz, $CDCl_3$): δ 8.08 – 8.01 (m, 2H, ArH), 8.00 – 7.95 (m, 2H, ArH), 7.92 (s, 1H, m), 7.45 (m, 6H, ArH), 2.99 (s, 3H, CH_3); ^{13}C NMR (75 MHz, $CDCl_3$): δ 167.55, 163.94, 152.73, 145.78, 133.96, 133.83, 131.26, 130.08, 129.84, 129.05, 128.98, 126.60, 126.45, 116.64, 13.28 ppm; HRMS (EI): m/z calcd for $C_{19}H_{14}N_2S_2$ $[M]^+$: 334.0598; found: 334.0573.

Synthesis of 4-(benzothiophen-3-yl)-2-(3,5-di-tert-butylphenyl)-5-methylthiazole (3.14). 3.14 was prepared by the same procedure as **3.12** except that 4-bromo-5-methyl-phenylthiazole was replaced by **3.8**. From **3.8** (0.24 g, 1.0 eq, 0.64 mmol), benzothiophene-3-boronic acid (0.17 g, 1.5 eq, 0.96 mmol), potassium phosphate (0.21 g, 1.5 eq, 0.96 mmol), tetrakis(triphenylphosphine)palladium (0.02 g, 0.03 eq, 0.019 mmol, 3mol%) in 12 mL DME and 6 mL water, 0.25 mg (94 % yield) of **3.13** was obtained as a white powder. M.p. 130 °C; Rf=0.63 (CH_2Cl_2/hexane 1:1); ^{1}H NMR (300 MHz, $CDCl_3$) δ 8.16 – 8.07 (m, 1H, H_h), 7.94 – 7.88 (m, 1H, H_j), 7.82 (d, J = 1.8 Hz, 2H, H_a), 7.54 (s, 1H, H_k), 7.51 (t, J = 1.8 Hz, 1H, H_b), 7.43 – 7.37 (m, 2H, H_l), 2.55 (s, 3H, CH_3), 1.38 (s, 18H, tert-Bu). ^{13}C NMR (125 MHz, $CDCl_3$): δ 165.37, 151.63, 147.31, 140.19, 138.83, 133.38, 130.93, 130.13, 130.10, 125.73, 124.62, 124.41, 124.27, 122.60, 120.92, 35.13, 31.57, 12.83 ppm; HRMS (ESI): m/z calcd for $C_{26}H_{30}NS_2$ $[M+H]^+$: 420.1820; found: 420.1808.

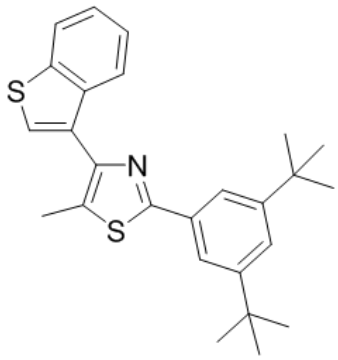

Synthesis of 2-(3,5-di-tert-butylphenyl)-5-methyl-4-(2-phenylthiazol-4-yl)-thiazole (3.15) 3.15 was prepared by the same procedure as **3.13** except that 4-bromo-5-methyl-2-phenylthiazole was replaced by **3.8**. From **3.8** (0.262 g, 1 eq, 1.09 mmol), 4-bromo-2-phenylthiazole (0.261g, 1 eq, 1.09 mmol), n-butyllithium (0.57 mL 2.5 M, 1.3 eq, 1.42 mmol), trimethyl borate (0.86 g, 7.5 eq, 8.19 mmol), potassium phosphate (0.695 g, 3eq, 3.28 mmol), tetrakis(triphenylphosphine)palladium (0.076 g, 0.06 eq, 0.066 mmol, 6mol%), 5.5 mL THF, 2.7 mL DME, and 2.7 mL water, 0.267 mg (55 %) of **3.15** was obtained. M.p. 176 °C; Rf=0.15 (CH_2Cl_2/hexane 3:7); ^{1}H NMR (300 MHz, $CDCl_3$): δ 8.11 – 8.01 (m, 2H, ArH), 7.97 (s, 1H, H_n), 7.81 (d, J = 1.8 Hz, 2H, H_a), 7.54 – 7.50 (t, J = 1.8 Hz, 1H, H_b), 7.49 – 7.41 (m, 3H, ArH), 3.00 (s, 3H, CH_3), 1.41 (s, 18H,tert-Bu). ^{13}C NMR (75 MHz, $CDCl_3$:) δ 167.47, 165.22, 159.80, 152.87, 151.55, 145.58, 134.02, 133.22, 130.83, 130.04, 129.04, 126.59, 124.27, 120.93, 120.77, 116.68, 35.11, 31.58, 13.26 ppm; HRMS (EI): m/z calcd for $C_{27}H_{30}N_2S_2$ $[M]^+$: 446.1850; found: 446.1853.

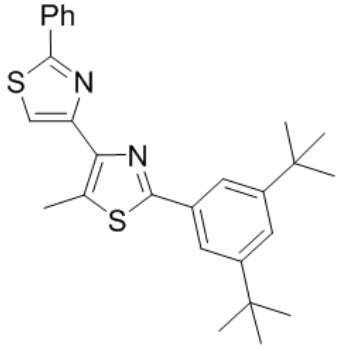

Synthesis of 4-(benzothiophen-3-yl)-2-(4-chlorophenyl)-5-methylthiazole (3.16). 3.16 was prepared by the same procedure as **3.12** except that 4-bromo-5-methyl-2-phenylthiazole was replaced by **3.11**. From **3.11** (0.5 g, 1 eq, 1.73 mmol), benzothiophene-3- boronic acid (0.462 g, 1.5 eq, 2.60 mmol), potassium phosphate (0.552 g, 1.5 eq, 2.60 mmol), tetrakis(triphenylphosphine)palladium (0.06 g, 0.03 eq, 0.05 mmol 3mol%) in 23 mL DME and 12 mL water, 0.490 mg (83 % yield) of **3.13** was obtained as a white powder. M.p. 122 °C; Rf=0.5 (CH_2Cl_2/hexane 1:1); ^{1}H NMR (300 MHz, $CDCl_3$): δ 8.16 – 8.02 (m, 1H, H_h), 8.00 – 7.82 (m, 3H, ArH), 7.53 (s, 1H, H_k), 7.48 – 7.36 (m, 4H, ArH), 2.55 (s, 3H, CH_3). ^{13}C NMR (75 MHz, $CDCl_3$): δ 162.79, 147.71, 140.16, 138.62, 135.73, 132.38, 130.93, 130.43, 129.25, 129.21, 127.59, 125.92, 124.72, 124.54, 124.34, 122.65, 12.81 ppm; HRMS (ESI): m/z calcd for $C_{18}H_{19}ClNS_2$ $[M+H]^+$: 342.0178; found: 342.0175.

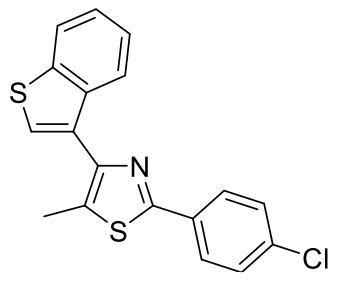

Synthesis of 2-(4-chlorophenyl)-5-methyl-4-(2-phenylthiazol-4-yl)-thiazole (3.17). 3.17 was prepared by

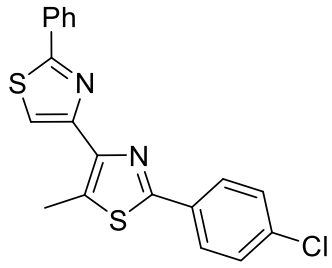

the same procedure as **3.13** except that 4-bromo-5-methyl-2-phenylthiazole was replaced by **3.11**. From **3.11** (0.4 g, 1.2 eq, 1.39 mmol), 4-bromo-2-phenylthiazole (0.276g, 1 eq, 1.16 mmol), n-butyllithium (0.6 mL 2.5 M, 1.3 eq, 1.50 mmol), trimethyl borate (0.91 g, 7.5 eq, 8.66 mmol), potassium phosphate (0.736 g, 3 eq, 3.47 mmol), tetrakis(triphenylphosphine)palladium (0.08 g, 0.06 eq, 0.069 mmol), 5.8 mL THF, 2.89 mL DME, and 2.89 mL water, 97 mg (23 %) of **3.17** was obtained. M.p. 188 °C; Rf=0.58 (CH_2Cl_2/hexane 1:1); ^{1}H NMR (300 MHz, $CDCl_3$): δ 8.08 – 8.01 (m, 2H, ArH), 7.95 – 7.87 (m, 3H, ArH), 7.51 – 7.39 (m, 5H, ArH), 2.98 (s, 3H,tert-butyl). ^{13}C NMR (75 MHz, $CDCl_3$): δ 167.68, 162.56, 152.52, 145.96, 135.73, 133.91, 132.32, 131.61, 130.84, 130.14, 129.19, 129.07, 127.63, 126.61, 116.74, 13.29 ppm; HRMS (EI): m/z calcd for $C_{19}H_{13}ClN_2S_2$ $[M]^+$: 368.0208; found: 368.0208.

7.2 Evaluation of photochemical and switching properties

UV-Vis spectra and quantum yields of photochromic reaction ($\Phi_{c\text{-}o}$ and $\Phi_{o\text{-}c}$) were measured using a JASCO V-660 spectrophotometer and a Shimadzu QYM-01 setup, respectively. For kinetic thermal analyses, the temperature was controlled by a JASCO ETC 505T Temperature controller. Stopped-flow measurements were conducted with a rapid-scan stopped-flow spectroscopic system (Unisoku).

For the oxidative cycloreversion experiments in Chapter 2, kinetics experimeriments were performed by mixing desired amounts of the oxidizing agent tris(4-bromophenyl)ammoniumyl hexachloroantimonate with the closed forms of **2.1**, **2.2**, and **2.3** and monitoring the evolution of absorbance at λ_{max} in the visible region with constant stirring to avoid the effects of diffusion on the electron transfer. Subsequent oxidation could be performed after extraction of the compounds from the oxidation by-products by extraction with dichloromethane (3x), washing with water, and drying over sodium sulfate. Purification by silica-gel column chromatography afforded 100 % yield.

7.3 STM Experiments

STM imaging was performed in an Omicron Low-Temperature Ultra-High Vacuum System working with a base pressure of 1.5×10^{-11} mbar. The Ag(111)/Cu(111) crystal was prepared by repeated cycles of sputtering with Ar^+ ions and subsequent annealing at 750 K. For imaging experiments on insulating bilayers of NaCl(001), NaCl (Sigma Aldrich, reagent grade) was evaporated onto the substrate held at room temperature until a 20 % monolayer coverage was achieved as monitored by a quartz crystal microbalance. The tips were prepared by electrochemical etching and then cleaned by direct current heating on a clean metallic surface until the surface state of the metal was observed and images showed molecular resolution without any multiple tip effects.

Then molecules were then evaporated from a tungsten wire directly onto the substrate held at liquid nitrogen temperature for experiments in Chapter 4. For experiments in Chapter 5, the molecules were deposited from a Knudsen cell directly onto the substrate held at liquid helium temperature. STS

were performed by pointing the STM tip on top of the molecule, turning off the feedback-loop system and recording the tunneling current while scanning over the bias interval at 0.1 V/s.

The software WsXM[6] was used to analyze the images.

7.4 Calculation details

DFT calculations for the optimal geometry of the molecules in the gas phase were accomplished using Gaussian 09[7] with the functional B3LYP with basis set 6-31G(d,p). Calculations of IR spectra showed no negative vibrations ensuring that the geometry corresponded to absolute minima. The reactive anti-parallel conformation was used as input structure.

Torsion angle scans around the relevant dihedral angles were calculated every 20° rotation from the optimized structure of the ***o*** form. Then, the conformations with minimal energy along the scan were further optimized by the same method as above. TD-DFT calculations were performed to calculate the UV-Vis spectra. Excited states up to n = 10 were calculated. Then, HOMO and LUMO maps in the gas phase were generated. Results were visualized by GaussView.[8]

For the molecules adsorbed on the surface,[9] periodic DFT calculations were performed using the numeric atom-centered basis sets all-electron software FHI-aims.[10-11] We used the PBE exchange-correlation functional with inclusion of van der Waals interactions via the Tkatchenko-Scheer procedure [12], and the "tight" settings including the "tier1" basis sets for all atoms. Relativistic effects were taken into account by applying an atomic zeroth-order regular approximation (ZORA). The close-packed Ag(111) surface was modeled by periodic (10 x 10) unit cells containing three atomic layers, separated by 20 Å to avoid undesired interactions of the molecule with the upper metal slab. Both the molecule and the upper layer were relaxed during geometry optimizations while the other two layers were kept frozen. The adsorption energies of the different molecules on the Ag(111) surface were calculated as $E_{ads} = E_{m\text{-}s} - E_m - E_s$, where $E_{m\text{-}s}$ is the total electronic energy of the molecule-surface system and E_m and E_s are the energies of the relaxed Ag slab and of the relaxed gas-phase molecule (both in the same unit cell), respectively.

Then, STM images of relaxed adsorbates were calculated by using the elastic scattering quantum chemistry technique[13-14] (ESQC). Here, the complete STM junction, comprising the surface, the molecular adsorbate, the tip apex and the tip body, is described by a set of molecular orbitals for each atom of this junction at the semiempirically extended Hückel level. The scattering matrix of electrons crossing the tip-surface junction is calculated and the tunneling current is estimated by the Landauer formula.[15] We used Vesta[16] for the visualization of surface conformation.

7.5 References and Notes

[1] G. Gavrel, P. Yu, A. Leaustic, R. Guillot, R. Metivier, K. Nakatani, 4, 4'-Bithiazole-based tetraarylenes: new photochromes with unique photoreactive patterns, *Chem. Commun.* 2012, *48*, 10111-10113.

[2] T. Nakashima, K. Atsumi, S. Kawai, T. Nakagawa, Y. Hasegawa, T. Kawai, Photochromism of thiazole - containing triangle terarylenes, *Eur. J. Org. Chem.* 2007, *19,* 3212-3218.

[3] M. Bergtrup, L. B. L. Hansen*,* New methods for the introduction of substituents into thiazoles, *Acta Chem. Scand.* 1992 *, 46 ,* 372.

[4] J. Hämmerle, M. Schnürch, N. Iqbal, M. Mihovilovic, P. Stanetty, A guideline for the arylation of positions 4 and 5 of thiazole via Pd-catalyzed cross-coupling reactions, *Tetrahedron* 2010, *66*, 8051-8059.

[5] S. Fukumoto, T. Nakashima, T. Kawai, Photon-quantitative reaction of a dithiazolylarylene in solution, *Angew. Chem. Int. Ed.* 2011, *50*, 1565-1568.

[6] I. Horcas, R. Fernandez, J.M. Gomez-Rodriguez, J. Colchero, J. Gomez-Herrero, A. M. Baro, WSXM: A software for scanning probe microscopy and a tool for nanotechnology, *Rev. Sci. Instrum*. 2007, 78, 013705.

[7] Gaussian 09, Revision A.03, M. J. Frisch, G. W. Trucks, H. B. Schlegel, G. E. Scuseria, M. A. Robb, J. R. Cheeseman, G. Scalmani, V. Barone, G. A. Petersson, H. Nakatsuji, X. Li, M. Caricato, A. V. Marenich, J. Bloino, B. G. Janesko, R. Gomperts, B. Mennucci, H. P. Hratchian, J. V. Ortiz, A. F. Izmaylov, J. L. Sonnenberg, D. Williams-Young, F. Ding, F. Lipparini, F. Egidi, J. Goings, B. Peng, A. Petrone, T. Henderson, D. Ranasinghe, V. G. Zakrzewski, J. Gao, N. Rega, G. Zheng, W. Liang, M. Hada, M. Ehara, K. Toyota, R. Fukuda, J. Hasegawa, M. Ishida, T. Nakajima, Y. Honda, O. Kitao, H. Nakai, T. Vreven, K. Throssell, J. A. Montgomery, Jr., J. E. Peralta, F. Ogliaro, M. J. Bearpark, J. J. Heyd, E. N. Brothers, K. N. Kudin, V. N. Staroverov, T. A. Keith, R. Kobayashi, J. Normand, K. Raghavachari, A. P. Rendell, J. C. Burant, S. S. Iyengar, J. Tomasi, M. Cossi, J. M. Millam, M. Klene, C. Adamo, R. Cammi, J. W. Ochterski, R. L. Martin, K. Morokuma, O. Farkas, J. B. Foresman, and D. J. Fox, Gaussian, Inc., Wallingford CT, 2016.

[8] GaussView, Version 6, Roy Dennington, Todd A. Keith, and John M. Millam, Semichem Inc., Shawnee Mission, KS, 2016.

[9] The author acknowledges J. Echeverria of University of Barcelona, Barcelona, Spain for the surface geometry and adsorption energy calculations and X. Bouju of CEMES CNRS (UPR 8011), Toulouse, France for the ESQC calculations of the predicted STM images.

[10] V. Blum, R. Gehrke, F. Hanke, P. Havu, X. Ren, K. Reuter, M. Scheffler, *Ab initio* molecular simulations with numeric atom-centered orbitals, *Comput. Phys. Commun*. 2009, *180*, 2175-2196.

[11] V. Havu, V. Blum, P. Havu, M. Scheffler, Efficient O(N) integration for all-electron electronic structure calculation using numeric basis functions, *J. Comput. Phys.* 2009, *228*, 8367-8379.

[12] A. Tkatchenko, M. Scheffler, Accurate molecular van der Waals interactions from ground-state electron density and free-atom reference data, *Phys. Rev. Lett.* 2009, *102*, 073005

[13] P. Sautet, C. Joachim, Calculation of the benzene on rhodium STM images, *Chem. Phys. Lett*. 1991,*185* ,23–30.

[14] P. Sautet, C. Joachim, Electronic transmission coefficient for the single-impurity problem in the scattering-matrix approach, *Phys. Rev. B: Condens. Matter Matter. Phys.* 1988, 38, 12238-12247.

[15] R. Landauer, Electrical resistance of disordered one-dimensional lattices, *Philos. Mag.* 1970, *21*, 863-867.

[16] K. Momma, F. Izumi, VESTA 3 for three-dimensional visualization of crystal, volumetric and morphology data. J. Appl. Crystallogr. 2011, 44, 1272-1276.

Scientific Production

Publications

1. Fast and Efficient Oxidative Cycloreversion Reaction of a π-Extended Photochromic Terarylene

   J.P.D.C. Calupitan, T. Nakashima, Y. Hashimoto, T. Kawai, *Chem. Eur. J.* 2016, *29*, 10002-10008. (Cover)

2. Dual photochemical bond cleavage for a new diarylethene-based phototrigger containing both methanolic and acetic sources

   O. Galangau, S. Delbaere, N. Ratel-Ramond, G. Rapenne, R. Li, J.P.D.C. Calupitan, T. Nakashima, T. Kawai, *J. Org. Chem*. 2016, *81*, 11282-1120.

3. Synthesis and photochromism of chloro and tert-butyl functionalized terarylenes derivatives for surface deposition

   J.P.D.C. Calupitan, O. Galangau, O. Guillermet, R. Coratger, T. Nakashima, G. Rapenne, T. Kawai, *Eur. J. Org. Chem.,* 2017, *17*, 2451-2461.

4. Scanning Tunneling Microscope Tip Induced Formation of a Supramolecular Network of Terarylene Molecules on Cu(111)

   J.P.D.C. Calupitan, O. Galangau, O. Guillermet, R. Coratger, T. Nakashima, G. Rapenne, T. Kawai, *J. Phys. Chem. C* 2017, *121*, 25384-25389.

5. Adsorption of Terarylenes on Ag(111) and NaCl(001)/Ag(111): a Scanning Tunneling Microscopy and Density Functional Theory Study

   J.P.D.C. Calupitan, O. Guillermet, O. Galangau, M. Yengui, J. Echeverria, X. Bouju, J. Echeverria, R. Coratger, T. Nakashima, G. Rapenne, T. Kawai, *J. Phys. Chem. C* 2018, DOI:10.1021/acs.jpcc.7b11122.

6. Triangle terarylene as possible photoactivatable hydride donor

   C. J. Martin, M. Minamide, J.P.D.C. Calupitan, T. Nakashima, G. Rapenne, T. Kawai, *submitted*.

Conference oral presentations

1. Photochromic terarylenes with highly-sensitive cycloreversion capability and their STM investigations

   Annual Meeting of the Japanese Photochemistry Association Tokyo, Japan (6-8 september 2016)

2. Single-molecule STM images and switching of terarylenes on metallic surfaces

   IAS Focused Program on Advanced Microscopy and Spectroscopy of Supramolecular and Macromolecular Systems on Surfaces, Hong Kong (12-15 december 2016)

3. Highly sensitive terarylenes and their STM studies

   12th Phenics International Network Symposium, Strasbourg, France (22 july 2017)

4. STM studies of highly-sensitive photoswitching terarylenes

   5th ITO International Research Conference, Forefront of Molecular Dynamics at Surfaces: From a single molecule to catalytic reaction, Tokyo, Japan (20-23 november 2017)

5. STM-study on Photochromic Triangle Terarylenes; Electric Field-induced Formation of 2D-self-organized Structure

   7th Photosynergetics Symposium*,* Osaka, Japan (26-27 january 2018)

Conference poster presentations

1. Ultra-efficient oxidative cycloreversion of terarylenes

   Inter'l Symposium for Photo- & Electro-Molecular Machines, Toulouse, France (6-7 october 2015)

2. Switching terarylenes with varying stimuli

   Forum sondes-locale, Montbeliard, France (21-25 march 2016)

3. Highly sensitive terarylenes and their STM studies

   Int'l Conference on Photochemistry, Strasbourg, France (16-22 july 2017)

Acknowledgements

I would like to thank Prof. Tsuyoshi Kawai and Prof. Gwénaël Rapenne, who not only served as my research supervisors but mentors as well. Their invaluable guidance were most instrumental in my formation as a scientist. I would have not entered NAIST if it were not for Prof. Masao Tanihara and Dr. Mime Kobayashi who welcomed and introduced me to this institution. I thank Dr. Takuya Nakashima, Dr. Yoshiyuki Nonoguchi, and Dr. Olivier Galangau for their contribution to my formation. Special thanks to the examination committee members Prof. Elena Ishow, Dr. Michel Sliwa, Prof. Eric Benoist, Prof. Kenji Matsuda, and Prof. Hisao Yanagi for reading and giving constructive comments to the manuscript. Prof. Hiroko Yamada is also acknowledged for serving as a supervisor during my studies in NAIST.

To members of the Photonic Molecular Science, past and present, I thank you for making this journey memorable. To Shunsuke Iijima, Rui Kanazawa, Ruiji Li, Motohiro Nakano, Ramarani Sethy, Yuki Taniguchi, Takafumi Nakagawa, Tan Yan Bing, Keita Kojiyama, Naoya Takeuchi, Takuya Kitano, Ami Takada, Shiori Matsuoka, Ryo Mizutsu, Hajime Yamamoto, Hiroto Yoshida, Dr. Jatish Kumar, and Dr. Colin Martin, thank you very much. To Yuichiro Hashimoto, Takao Takishita, Yu Iihara, Yuki Kita, Akiko Hayashide, Tommohiro Ikeda, Kouhei Fujiwara, Ryosuke Asato, Junpei Kuno, Kasumi Shigekawa, Miho Minamide, and Daiya Shimizu, who are some of the reasons why Japan is memorable to me, for the laughter and the friendship, thank you very much. I would also like to acknowledge the technical staff Ms. Chigusa Goto and Ms. Miku Yamada who helped me. Ms. Kyoko Kato, Ms. Toko Hishikawa, and Ms. Mami Miyamoto (who is now a dear friend), current and former staff who made administrative procedures in a foreign language accessible to me, thank you. I would also like to thank the NAIST International Student Office. ありがとうございました.

To the NAIST Filipino community, thank you.

To all members of the Groupe Nanosciences in CEMES especially: Dr. Erik Dujardin, the head of the group; the chemists Dr. Andre Gourdon, Dr. Claire Kammerer, Dr. Jacques Bonvoisin, Christine Viala, Dr. Andrej Jancarik, Lenka Pallova, Guillaume Erbland, Gaspard Levet, and Theo Guerin, with whom I shared many memorable lunchtimes; and Prof. Roland Coratger and Dr. Olivier Guillermet who trained me in STM, thank you very much. Dr. Xavier Bouju and Dr. Jorge Echeverria are also acknowledged for their contributions.

I also thank Prof. Saw Wai-Hla for accommodating me in Argonne National Laboratory, USA.

I will never forget my mentors in Ateneo de Manila University: Prof. Erwin P. Enriquez, Dr. Nina Rosario L. Rojas, Prof. Ma. Assunta Cuyegkeng, Prof. Agustin Martin Rodriguez, Padre Roque Ferriols, S.J., Dr. Corazon Lalu-Santos, and Sir Eddieboy Calasanz. Their views and perspectives in science, literature, philosophy, life, and the greater scheme of things shaped me in several ways. I owe a huge part of my formation to the scholarship grant from Ateneo that allowed me to pursue chemistry. For all that Ateneo has given to me, I am forever grateful.

Sa aking pamilya, Nanay Caring, Tatay Thon, Ate Atchell, Kuya Archie, Ate Azenith, Niña, Mama Sonia, Papa, Mama, Ate Kat, Ate Kaye, Klarisse, at Nanay Ceiling, salamat sa lahat-lahat.

Kay Gian na laging nandyan, salamat.

Justin at Janine, salamat.

Kay Nanay, salamat sa inspirasyon para magpatuloy. Lahat ng ito, para sa iyo.

J.P.D.C. Calupitan